KAIQUE MOREIRA MATOS MAGALHÃES

Investigations on critical load and strain regime in very slender RC columns by dynamic mathematical approach

São Paulo

2023

KAIQUE MOREIRA MATOS MAGALHÃES

Investigations on critical load and strain regime in very slender RC columns by dynamic mathematical approach

Corrected version

Thesis presented to the Polytechnic School of the University of São Paulo, in partial fulfillment of the requirements for the degree of Doctor of Science in the Graduate Program in Civil Engineering (PPGEC).

Subject area: Structural Engineering

Advisor: Prof. Dr. Reyolando Manoel Lopes Rebello da Fonseca Brasil (USP)

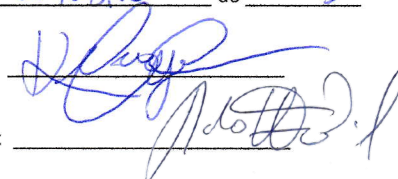Co-Advisor: Prof. Dr. Alexandre de Macêdo Wahrhaftig (UFBA)

SÃO PAULO

2023

Este exemplar foi revisado e corrigido em relação à versão original, sob responsabilidade única do autor e com a anuência de seu orientador.

São Paulo, _02_ de ___OUTUBRO___ de _2023_

Assinatura do autor: _____

Assinatura do orientador: _____

Catalogação-na-publicação

ACKNOWLEDGEMENT

structural engineering. Your assistance, starting from the internship period, has been invaluable in helping me gain expertise in the professional realm.

To the esteemed Engineer, boss, and friend **Carlos Roberto Cardoso** (RC Engenharia), for all the encouragement and support in my formation as an Engineer. Your competent technical expertise has become a significant reference, allowing me to pursue a career in structural engineering with even greater enthusiasm.

To my girlfriend, best friend, and partner of many years, **Bianca Barreto**, I am grateful for all your love, patience, care, and encouragement throughout this journey. This achievement would not have been possible without your significant contribution and understanding during difficult times. I am certain that we will celebrate many more accomplishments together. Having you by my side made this period of dedication and effort lighter and more achievable.

To my sister, **Kelly Magalhães**, for all the support and warmth over the years while being away from home. Your care and love were essential for the success of this journey. We have experienced joyful and challenging moments together, and we will continue to do so forever. To my siblings, **João Guilherme** and **Júlia Moreira**, for all the affection and encouragement.

To my grandparents**, Naguimar Martins** and **Orlando Martins** (in memoriam), for their unconditional love throughout my life's journey. You are the main contributors to shaping my character. You will always be my greatest love.

To my mother, **Érica Magalhães**, for your parental love and protection over the years. Your words of encouragement have fueled my progress.

To my father, **José Luiz Magalhães** (in memoriam), for all the love and sacrifices made throughout your life so that my dreams could one day become a reality. Unfortunately, you are no longer physically present to witness and celebrate this great achievement, but I am certain that you have remained by my side in some way and will continue to do so.

"We only do better what we repeatedly insist on improving. The pursuit of excellence should not be a goal, but a habit."

(Aristoteles)

ABSTRAC

An analytical investigation was developed based on the concepts of deformable solid dynamics to determine the critical buckling load and induced strain behavior in very slender reinforced concrete (RC) columns. The elements of structural dynamics were taken into consideration in the analysis. Construction imperfections and/or second-order effects were linearized using the negative component of geometric stiffness, the physical nonlinearity of concrete was accounted for by reducing the flexural stiffness product, and the viscoelastic behavior of concrete was considered according to the criteria outlined in NBR 6118:2014 from the Brazilian Association of Technical Standards (ABNT).This investigation was further supported by the publication of two articles in high-impact international journals. The initial article evaluated the deformation behavior of concrete induced by axial compressive force, including the contribution from material creep, using two distinct mathematical approaches. The first mathematical procedure adopted the stress-strain curve of concrete standardized by ABNT NBR6118:2014 and compared it to the method of integrating the differential displacement relationships along the length of the structure. In the second published work, the mathematical development was applied to a practical real case, generalizing the formulation's applicability to highly slender RC columns. It also assessed the influence of concrete's rheological properties on the critical buckling load, considering the possibility of implementing the structure in different regions of Brazil with varying temperature and humidity conditions. Ultimately, a maximum reduction of over 70% in the column's load capacity was observed in the most unfavorable region of the analysis.

Keywords: Mathematical model; critical buckling load; slenderness; creep; reinforced concrete; dynamic analysis.

RESUMO

Foi desenvolvida uma investigação analítica, baseada nos conceitos da dinâmica dos sólidos deformáveis, para determinação da carga crítica de flambagem e do regime de deformações induzidos em colunas extremamente esbeltas de concreto armado. Os elementos da dinâmica estrutural presentes na análise foram levados em consideração. As imperfeições construtivas e/ou efeitos de segunda ordem foram linearizadas por meio da parcela negativa da rigidez geométrica, a não linearidade física do concreto foi considerada por meio da redução do produto de rigidez à flexão e o comportamento viscoelástico do concreto foi levado em conta pelos critérios da NBR 6118:2014 da Associação Brasileira de Normas Técnicas (ABNT). A presente investigação foi consolidada com a publicação de dois artigos em periódicos de alto impacto internacional. O artigo inicial avaliou, por meio de duas abordagens matemáticas distintas, o regime de deformações do concreto induzido pela força normal de compressão, incluindo a parcela devida à fluência do material. No primeiro procedimento matemático, foi adotado a curva de tensão-deformação do concreto, padronizada pela ABNT NBR6118:2014, que foi comparado ao método de integração das relações diferenciais de deslocamentos ao longo do comprimento da estrutura. Em relação ao segundo trabalho publicado, o desenvolvimento matemático foi aplicado à um caso prático real, generalizando a validade da formulação em colunas extremamente esbeltas de concreto armado, além de avaliar a influência das propriedades reológicas do concreto, na carga crítica de flambagem, considerando-se a possibilidade de implantação da estrutura em diferentes regiões do Brasil, com índices de temperatura e umidade variáveis. Ao fim, contatou-se uma redução máxima de mais de 70% da capacidade de carga da coluna, na região mais desfavorável da análise.

Palavras-chave: Modelo matemático; carga crítica de flambagem; esbeltez; fluência; concreto armado; análise dinâmica.

LIST OF PUBLICATIONS

PAPER 01

Magalhães KMM, Wahrhaftig AM and Brasil RMLRF. Strain regime induced by axial compression in slender reinforced concrete columns using different mathematical approaches. Structures 2023,49,655-665.

PAPER 02

Magalhães KMM, Brasil RMLRF, Wahrhaftig AM, Siqueira GH, Bondarenko I and Neduzha L. Influence of Atmospheric Humidity on the Critical Buckling Load of Reinforced Concrete Columns. Int. J Struct Stab Dyn 2022; 22: 2250011-1–225011–24.

LIST OF FIGURES

GENERAL INTRODUCTION

PAPER 01

PAPER 02

LIST OF TABLES

GENERAL INTRODUCTION

PAPER 01

PAPER 02

SUMMARY

1   GENERAL INTRODUCTION

This thesis, written in English, is a compilation of two articles published in high-impact international journals, preceded by this introduction about their context.

The design of slender structures presents a formidable challenge to modern-day structural engineers due to the intricate interplay of nonlinear effects stemming from the structure's geometric configuration and material characteristics, notwithstanding the remarkable progress achieved in structural analysis technologies. Notably, reinforced concrete structures exhibit distinctive attributes owing to the behaviors of their constituent materials, namely concrete and steel. The inherent nonlinear behavior of such structures primarily arises from the inherent heterogeneity of concrete, which imparts diverse properties contingent upon its composition and may even manifest distinct chemical compositions contingent upon the locale of manufacture.

Concrete's time-dependent response, intricately linked to rheological principles, encompasses the interplay of solid particles (aggregates) and a fluid component (hydrated cement paste). To capture the viscoelastic behavior of concrete more accurately, engineers employ rheological models incorporating interconnected springs and dampers, enabling the prediction of comprehensive deformations while considering crucial factors such as the duration, type, and timing of applied loads.

Practically speaking, the technical codes guiding the analysis and design procedures of reinforced concrete structures account for influential phenomena like creep and shrinkage. These standards encompass two pivotal considerations in the dimensional design of construction systems. Firstly, they incorporate a reduction in the member's stiffness coefficient, and secondly, propose a strength reduction coefficient based on the duration of load application and the environmental conditions to which the member is exposed. For the design of reinforced concrete structures, typically three main analyses are conducted: deformation analysis, stress analysis, and stability verification. In the case of slender structures specifically, the primary safety concern is their stability, as the structure may collapse due to loss of stability before reaching the

material's ultimate strength. This investigation can be evaluated from different perspectives, either through static concepts (without considering inertial forces) or dynamically.

The traditional and conventionally used procedure for this verification establishes the maximum force that can be applied to the structure near its collapse, which is defined as the critical buckling load. The first investigation of critical buckling load was conducted by Euler [1] in 1774, who established formulations based on statics. His studies were further complemented by Greenhill [2] in 1881, who included the self-weight in the stability analysis of columns. According to Timoshenko [3], Euler buckling occurs only within the elastic range of the material. It is defined as the phenomenon in which a structural element loses its equilibrium under the action of a sufficiently large compressive axial force, causing it to deviate from its initial straight configuration.

Although the initial postulations were statically solved by considering the forces developed in the most stressed section of a column after assuming a certain deflected configuration, the solution of buckling simultaneously enters the field of structural dynamics.

In this regard, Wahrhaftig et al. [4] investigated analytical solutions to incorporate the self-weight in determining the critical load of columns. In this study, the complexity of including the self-weight lied in the fact that the mathematical formulation relied on integral solutions related to the differential equations of the problem. Ultimately, the authors compared the analytical results with computational methods and experimental procedures, demonstrating good agreement between the results. This validation supported the development of the presented analytical-approach.

When it comes to analytical methods for determining the fundamental frequency of structures, one of the most widely used methods was developed by Rayleigh [5]. This method stands out as a simple and effective technique based on the principles of energy conservation in a system, considering its oscillation in free vibration. Therefore, the determination of the frequency corresponds to the equality between the maximum potential energy and kinetic energy terms for the adopted vibration configuration. In

other words, to obtain the final response, it is necessary to assume a deformed configuration of the structure during vibration, typically described by a function called the shape function. This function must exclusively satisfy the essential boundary conditions of the structure. Such a procedure can be employed for analyzing a wide range of problems related to structural stability.

The procedure suggested by Rayleigh [5] can be applied both for calculating the frequency and determining the critical buckling load. In this analysis, all components of structural stiffness should be taken into account, including the conventional stiffness, which depends on the material behavior such as elasticity, viscoelasticity, or even plasticity, as well as the geometric stiffness, which depends on the axial force acting on the structure. Some mathematical approaches related to these analytical developments based on the method proposed by Rayleigh [5] can be found in the works of Wahrhaftig et al. [6]-[8].

In this regard, this research has been consolidated as a continuation of investigations based on the concepts established by Rayleigh [5], in which a mathematical investigation was developed to predict the variation of critical buckling load and induced deformation in extremely slender reinforced concrete columns using structural dynamics.

The investigations conducted in this research were consolidated writing–two articles published in high-impact international journals, which present the methods used and the obtained results. In the initial article, Magalhães et al. [9] evaluated, via two distinct mathematical approaches, the deformation behavior of concrete induced by compressive normal force (up to the critical buckling load), including the contribution of material creep. In the second article, Magalhães et al. [10] applied the mathematical development to a real practical case, generalizing the validity of the formulation for extremely slender reinforced concrete columns. The influence of the rheological properties of concrete, based on variations in relative humidity, on the critical buckling load was assessed.

2 CONTEXTUALIZATION OF INVESTIGATIONS

A mathematical-model was developed to assess the critical buckling load and induced stresses in extremely slender reinforced concrete columns, taking into account the concrete rheological properties. The chosen method of analysis involves a mathematical modeling based on the principles of deformable solid dynamics, which will be presented in this chapter.

It is known that the natural vibration frequencies of reinforced concrete structures undergo changes influenced by several factors, such as: (a) the intensity and nature of applied loading, meaning they depend on the level and type of internal stresses; (b) variations in the material's elastic modulus due to creep; and (c) geometry, including the cross-sectional inertia that depends on the level of cracking experienced by the element. Thus, the mathematical procedure incorporates all these aspects to evaluate the changes in natural frequencies, deformations, and also to verify the load capacity of the columns under different usage scenarios.

Thus, this thesis comprises a collection of two articles (Chapter 03 and Chapter 04), published in international journals, which address the applicability and validation of the concepts developed throughout this research. In summary, the first article titled "Strain regime induced by axial compression in slender reinforced concrete columns using different mathematical approaches" assessed the strain regime of concrete induced by axial compression, including the component attributed to material creep, through different mathematical approaches. Two mathematical procedures were employed: the first one adopted the standardized stress-strain curve of concrete, while the second procedure involved the integration of differential equations along the length of the structure at intervals defined by its geometry. In essence, this comparison aimed to validate the use of Hooke's law for the material's deformation region initially considered as linear.

In the second article, "Influence of Atmospheric Humidity on the Critical Buckling Load of Reinforced Concrete Columns," the mathematical development for determining the critical buckling load was expanded and applied to slender reinforced concrete columns, using a real case study as a reference to generalize the applicability of the formulation. Furthermore, the influence of the concrete's rheological properties on the variation of the critical load was investigated, considering the possibility of implementing the structure in different regions of Brazil, subjecting it to different temperature and humidity conditions. These factors had a significant impact on the obtained results, confirming the need for such verification in assessing the long-term load capacity of this type of structure.

Next, a more detailed presentation will be given regarding the developed mathematical formulation in the studies, the analysis methodology applied to the two published articles, and the normative procedure provided by ABNT NBR6118:2014 [12] for predicting the behavior of concrete due to creep and shrinkage.

2.1 GENERALIZED MATHEMATICAL FORMULATION

The analytical method developed in this research is based on the concepts of mechanical vibration theory, specifically the determination of the natural frequencies of vibration of reinforced concrete columns. It considers that the element is influenced by gravitational forces resulting from the distributed mass due to its own weight and a concentrated mass at the upper free end. The hypothesis of undamped free vibration was adopted, considering only the horizontal degree of freedom at the top of the column and the assumption of small displacements.

While it is well-known that single-degree-of-freedom (SDOF) systems may not always provide adequate modeling of a real structure, often requiring the use of multiple-degree-of-freedom systems for a more comprehensive qualitative and quantitative description of their behavior, they are important for preliminary investigations as they offer greater ease of interpretation in terms of physical results. Such models are highly valuable within a hierarchical modeling philosophy of structures, where the primary

objective is to obtain an efficient model that represents the behavior closest to reality while considering a minimum number of degrees of freedom.

To approximate the analyzed motion using a SDOF system, it is assumed that the element deforms in a single mode, which is appropriately chosen to represent the vibratory motion of the first buckling mode. The shape function that describes this deflection is defined as $\varphi(x)$, where x is an independent variable representing the location along the height of the structure (in this specific case, the column), and the amplitude of the motion is represented by the generalized coordinate q(t).

The shape function was obtained using Equation (1):

$$\varphi(x) = \frac{v(x,t)}{q(t)} \, , \qquad\qquad (1)$$

where $v(x,t)$ represents the equation for the deflected shape of the element. By applying the Principle of Virtual Work (PVW) and its derivatives, considering the properties described in Figure 1, we have:

$$\delta W_{Ext} = \delta W_{Int} \, , \qquad\qquad (2)$$

where W_{Ext} represents the work of the external forces performed by the inertia forces, given by Equation (3), and W_{Int} represents the work of the internal forces performed by the deflection, defined by Equation (4).

Figure 1 – Mathematical model of a column with one degree of freedom.
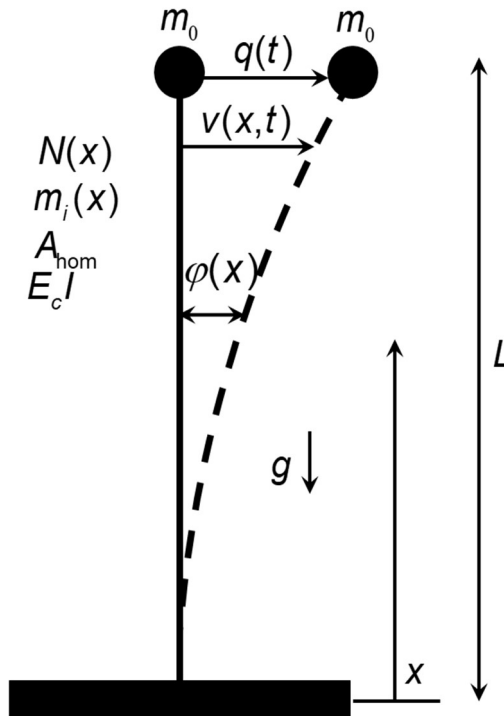
Source: Author

In Figure 1, g represents the acceleration due to gravity, L is the total length of the element; m_0 is a concentrated mass at the top of the structure; x is the independent variable of the problem, with its origin at the base of the column; $N(x)$ is the axial force; E_c is the longitudinal elastic modulus of the concrete; I is the second moment of area (moment of inertia) of the cross-section; A_{hom} is the homogenized cross-sectional area, accounting for the presence of steel rebars; and $m_i(x)$ is the distributed mass component, which includes its own weight and additional masses.

$$W_{Ext} = -\int_0^L m_i(x)\frac{\partial^2 v(x,t)}{\partial t^2}\delta v(x,t)dx + m_0\frac{\partial^2 v(x,t)}{\partial t^2}\delta v(x,t)dx + \int_0^L \left(m_0 g + N(x)\right)\left(\frac{\partial \varphi(x)}{\partial x}\right)^2 \quad (3)$$

and

$$W_{Int} = \int_0^L M(x,t)\left(\frac{\partial^2 v(x,t)}{\partial x^2}\right)dx \; , \quad (4)$$

where $M(x,t)$ is the bending moment.

Substituting Equations (3) and (4) into Equation (2):

$$-\int_0^L m_i(x)\frac{\partial^2 v(x,t)}{\partial t^2}\delta v(x,t)dx + m_0\frac{\partial^2 v(x,t)}{\partial t^2}\delta v(x,t)dx + \int_0^L \left(m_0 g + N(x)\right)\left(\frac{\partial \varphi(x)}{\partial x}\right)^2 dx +$$

$$\int_0^L M(x,t)\left(\frac{\partial^2 v(x,t)}{\partial x^2}\right)dx = 0.$$

(5)

Given that:

$$M(x,t) = \frac{\partial^2 v(x,t)}{\partial x^2}E_c I,$$

(6)

and, by Equation (1), it is known that:

$$\varphi(x) = \frac{v(x,t)}{q(t)} \therefore v(x,t) = \varphi(x)q(t),$$

$$\frac{\partial v(x,t)}{\partial x} = \frac{\partial \varphi(x)}{\partial x}q(t), \quad \frac{\partial^2 v(x,t)}{\partial x^2} = \frac{\partial^2 \varphi(x)}{\partial x^2}q(t),$$

$$\frac{\partial v(x,t)}{\partial t} = \varphi(x)\frac{\partial q(t)}{\partial t}, \quad \frac{\partial^2 v(x,t)}{\partial t^2} = \varphi(x)\frac{\partial^2 q(t)}{\partial t^2},$$

(7)

Rearranging Equation (5):

$$\left[\left(\int_0^L m_i(x)\varphi(x)^2 dx + m_0 g dx\right)\frac{\partial^2 q(t)}{\partial t^2} + \left(\int_0^L E_c I\left(\frac{\partial^2 \varphi(x)}{\partial x^2}\right)^2 dx\right)q(t) - \left(\left(\int_0^L m_0 g + N(x)\right)\left(\frac{\partial \varphi(x)}{\partial x}\right)^2 dx\right)q(t)\right]\delta q(t) = 0.$$

(8)

Since the variation, $q(t)$, can take any value, the term within brackets becomes zero and Equation (8) can be rewritten as:

$$[M]\frac{\partial^2 q(t)}{\partial t^2} + [K(m_0,t)]q(t) = 0 \therefore [M]\ddot{q}(t) + [K(m_0)]q(t) = 0 \tag{9}$$

where [M] represents the generalized mass matrix of the system (Equation (10)) and [K(m_i)] represents the generalized total stiffness matrix of the problem (Equation (12)).

The total generalized mass of the system, M(m_0), is calculated using Equation (10):

$$M(m_0) = \int_0^L \bar{m}\varphi(x)^2 dx + \sum_{i=1}^n m_0 g \tag{10}$$

where $\varphi(x)$ is the shape function that characterizes the vibratory motion and depends on the boundary conditions of the problem, which in the case under investigation can be given by Equation (11):

$$\varphi(x) = 1 - \cos\left(\frac{\pi x}{2L}\right). \tag{11}$$

Different shape functions that satisfy the boundary conditions of the problem can be applied to obtain the structural response [11].

The dynamic properties of the model can be obtained, i.e., the total generalized stiffness of the system, considering the weight force as positive, using Equation (12).

$$K(m_i) = K_0 - K_g(m_0), \tag{12}$$

where K_0 represents the conventional stiffness, given by Equation (13), and $K_g(m_i)$ represents the geometric stiffness, as given by Equation (14), in a general form.

$$K_0 = \int_0^L E_c I\left(\frac{d^2\varphi(x)}{dx^2}\right)^2 dx , \text{ e} \tag{13}$$

$$K_g(m_0) = \int_0^L N(x)\left(\frac{d\varphi(x)}{dx}\right)^2 dx + \int_0^L m_0 g\left(\frac{d\varphi(x)}{dx}\right)^2 dx \quad \text{(14)}$$

where $E_c I$ is known as the flexural stiffness product, m_0 is the mass applied at the top of the structure, and g is the acceleration due to gravity. The axial force component, $N(x)$, included in the analysis for the consideration of geometric stiffness, is determined by Equation (15).

$$N(x) = \bar{m}(L - x)g \quad \text{(15)}$$

where $\bar{m}$ represents the mass per unit length and L is the total length of the element.

In order to determine the moment of inertia of the homogenized section, it is necessary to consider the presence of reinforcing bars in slender reinforced concrete columns. Assuming that there are a number of bars, n_b, distributed along the cross-sectional area S, with a diameter D and cover depth c, and each bar (b_i) has a diameter d_{bi} located at position i defined by R_{bi} and θ_i, as shown in Figure 2.

Figure 2 – Determination of the homogenization factor
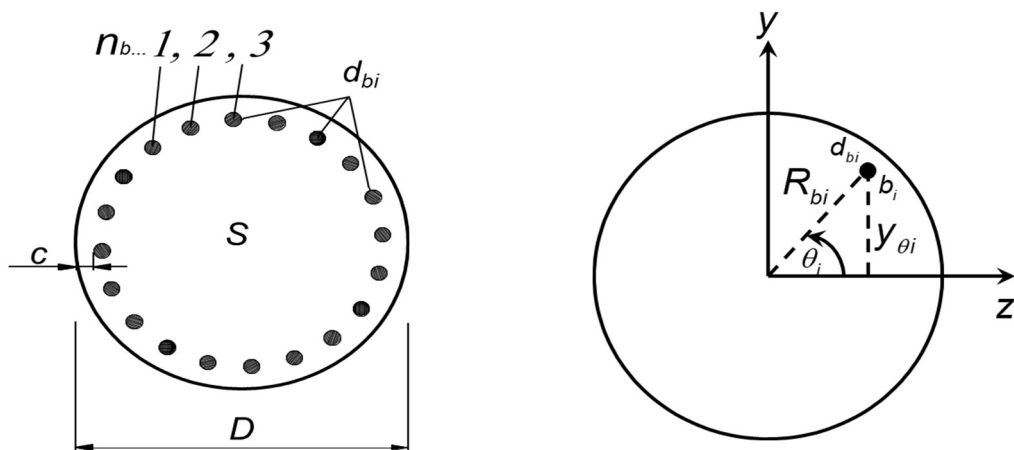
Souce: author

Therefore, based on Figure 2:

$$R_{bi} = \frac{D}{2} - c - \frac{d_{bi}}{2} .$$
(16)

The distance between the centroid of each bar and the axis of the cross-section can be calculated, considering θ_i as an independent variable that takes values between 0 and 2π, by Equation (17):

$$y(\theta_i) = \sin(\theta_i) R_{bi} .$$
(17)

The spacing between the bars, *esp*, is determined by:

$$esp = \frac{2\pi R_{bi}}{n_b} ,$$
(18)

where the angular phase displacement, Δθ, between two adjacent bars is given by Equation (19):

$$\Delta\theta = \frac{esp}{R_{bi}} .$$
(19)

Thus, the moment of inertia of each bar about the centroid of the cross-section, applying the Parallel Axis Theorem, can be calculated as follows:

$$I_i(\theta_i) = \frac{\pi d_{bi}^4}{64} + y(\theta_i)^2 \frac{\pi d_{bi}^2}{4} .$$
(20)

Therefore, the homogenization of the moment of inertia is calculated using the following relation:

$$I_{hom} = I(\theta)(\Psi - 1) ,$$
(21)

where Ψ is the ratio between the longitudinal deformation moduli (steel, E_a, and concrete, E_c) given by Equation (22):

$$\Psi = \frac{E_a}{E_c}.$$ (22)

To calculate the total (homogenized) moment of inertia of the cross-section, it is necessary to consider the non-homogenized moment of inertia, given by:

$$I_s = \frac{\pi}{64} D^4.$$ (23)

Added to the term from Equation (21), resulting in:

$$I_h = I_s + I_{\text{hom}}.$$ (24)

Finally, Equation (25) represents the frequency, in Hertz, as a function of the level of cracking and the generalized mass of the system:

$$f(m_0) = \frac{1}{2\pi} \sqrt{\frac{K(m_0)}{M(m_0)}}.$$ (25)

Considering concrete as a time-dependent material, as discussed earlier, the variation of frequency becomes a temporal quantity, since the longitudinal modulus of elasticity of concrete is also time-dependent. Therefore, the longitudinal modulus of elasticity of concrete may be described as follows:

$$E_c(t) = \frac{1}{\dfrac{1}{E_c} + \dfrac{\phi(t)}{E_c}},$$ (26)

where $\phi(t)$ represents the creep coefficient, which can be estimated using different mathematical formulations. In the specific case of this research, the behavior due to concrete creep and shrinkage will be considered following the normative provisions presented by ABNT NBR6118 [12].

In the creep and shrinkage calculation model of ABNT NBR6118 [12], for cases where the stress in the concrete does not vary significantly, the following simplifying assumptions are made: creep deformation varies linearly with applied stress, and the effects of stress increments at different times can be superimposed (the principle of superposition is adopted).

Assuming no restriction on concrete deformation and considering a constant stress, the total deformation of concrete over time is given by:

$$\varepsilon_c(t) = \varepsilon_c(t_0) + \varepsilon_{cc}(t) + \varepsilon_{cs}(t),$$

(27)

where $\varepsilon_c(t_0)$ is the immediate deformation at time t_0, $\varepsilon_{cc}(t)$ is the creep deformation, and $\varepsilon_{cs}(t)$ is the shrinkage deformation, both as a function of time t.

In a reinforced concrete element, the determination of deformations due to the creep component, $\varepsilon_{cc}(t)$, is calculated by applying Equation (28):

$$\varepsilon_{cc}(t) = \left(\frac{\sigma_c(t_0)}{E_{c28}} \right) \phi(t,t_0) \therefore \varepsilon_{cc}(t) = \frac{\sigma_c(t_0)}{E_c(t)},$$

(28)

where $\sigma_c(t_0)$ is the normal stress at the time t_o (in days) when the structure is loaded, and E_c is the modulus of elasticity of concrete, defined in Equation (29):

$$E_c(t) = \frac{1}{\dfrac{1}{E_{c0}} + \dfrac{\phi(t,t_0)}{E_{c28}}},$$

(29)

where E_{c0} is the modulus of longitudinal deformation of the concrete at the time of structure loading; E_{c28} is the modulus of longitudinal deformation at 28 days (in MPa). The determination of the modulus of longitudinal deformation at time i is given by Equation (30) or Equation (31) depending on the characteristic compressive strength (f_{ck}) of the concrete, and $\phi(t,t_0)$ is the concrete creep coefficient at time t for loads applied at time t_0, given by Equation (32):

$$E_{ci} = \alpha_E 5600\sqrt{f_{ck}} \ ,$$

(30)

where E_{ci} is the initial modulus of deformation of the concrete, in this case considered for concretes f_{ck} ranging from 20 MPa (C20) to 50 MPa (C50), or,

$$E_{ci} = 21{,}5 \times 10^3 \alpha_E \left(\frac{f_{ck}}{10} + 1{,}25 \right)^{\frac{1}{3}} \ ,$$

(31)

for concretes f_{ck} ranging from 55 MPa (C55) to 90 MPa (C90), where f_{ck} (in MPa) is the characteristic compressive strength of the concrete and α_E is a coefficient that depends on the type of aggregate used in the concrete. For basalt and diabase aggregate, the coefficient is 1.2; for granite and gneiss aggregate, the coefficient is 1.0; for limestone aggregate, the coefficient is 0.9; and for sandstone aggregate, the coefficient is 0.7. These values apply to both strength classes.

$$\phi(t,t_0) = \phi_a + \phi_{f\infty}[\beta_f(t) - \beta_f(t_0)] + \phi_{d\infty}\beta_d(t) \ ,$$

(32)

ϕ_a is the coefficient of rapid deformation, which depends on the compressive strength class of the concrete (C20 to C45 or C50 to C90) given by Equation (33) or Equation (34); $\phi_{f\infty}$, Equation (36), is the final value of the irreversible slow deformation coefficient, dependent on the relative humidity of the environment (U), the consistency of the concrete at casting, age of the concrete at the time of load application (t_0), and the time considered for analysis (t), for concrete with compressive strength classes up to 50 MPa. For concrete with compressive strength between 50 MPa and 90 MPa, a reduction factor of 0.45 is applied; β_f at t and t_0 are coefficients related to the irreversible slow deformation, depending on the age of the concrete; $\phi_{d\infty}$ is the final value of the reversible slow deformation coefficient, considered constant with a value of 0.4, and $\beta_d(t)$ is the coefficient related to the slow reversible deformation as a function of time elapsed after the start of loading (Equation (41)). Therefore:

$$\phi_a = 0,8\left[1 - \frac{f_c(t_0)}{f_c(t_\infty)}\right],$$
(33)

for concrete compressive strength classes between 20 MPa and 45 MPa (C20 to C45), or,

$$\phi_a = 1,4\left[1 - \frac{f_c(t_0)}{f_c(t_\infty)}\right],$$
(34)

for concrete compressive strength classes between 50 MPa and 90 MPa. The relationship $f_0(t_0)$ and $f_c(t_\infty)$ corresponds to the increase in concrete strength and can be calculated using Equation (35):

$$\beta_1 = e^{\left\{s\left[1-\left(\frac{28}{t}\right)^{1/2}\right]\right\}},$$
(35)

where s is a factor related to the type of concrete: s = 0.38 for CPIII and CPIV cement; s = 0.25 for CPI and CPII cement; s = 0.20 for CPV-ARI cement.

$$\phi_{f\infty} = \phi_{1c}\phi_{2c},$$
(36)

where:

$$\phi_{1c} = 4.45 - 0.035U,$$
(37)

U is the relative humidity in percentage. It is worth noting that the coefficient ϕ_{1c}, given by Equation (37), is valid for slump values determined according to the recommendations of NBR 16889 (2020), in the range of 5 cm to 9 cm, and with $U \le$ 90%. For a humidity of 100%, the value suggested by the Brazilian standard is 0.8. Parameter ϕ_{2c} is calculated using Equation (38):

$$\phi_{2c} = \frac{42 + h_{fic}}{20 + h_{fic}},$$
(38)

where h_{fic} is the fictitious thickness of the element expressed in centimeters, which is a parameter calculated based on the dimension and shape of the element, expressed as a single quantity in terms of the theoretical or effective thickness. This thickness is obtained by dividing the area of the section, A_c, by the semi-perimeter in contact with the atmosphere, D_c, calculated using Equation (39):

$$h_{fic} = \frac{2\gamma A_c}{\pi D_c},$$
(39)

where the parameter γ is the coefficient dependent on the relative humidity of the environment, obtained using Equation (40):

$$\gamma = 1 + e^{(-7.8 + 0.1U)}.$$
(40)

It is worth noting that there is a limit to the use of this coefficient, which is restricted to relative humidities between 40% and 90% (40% ≤ U ≤ 90%). When ambient humidity exceeds the upper limit of the range, up to U = 100%, the value of the coefficient becomes fixed at 30 (γ = 30). The coefficient $\beta_d(t)$ is given by:

$$\beta_d(t) = \frac{t - t_0 + 20}{t - t_0 + 70}.$$
(41)

Another quantity dependent on the relative humidity conditions of the environment is the coefficient $\beta_f(t)$, which is determined by Equation (42):

$$\beta_f(t) = \frac{t^2 + At + B}{t^2 + Ct + D},$$
(42)

where parameters A, B, C, D and E are given by Equations (43) to (47):

$$A = 40;$$
(43)

$$B = 116h_{fic}^3 - 282h_{fic}^2 + 220h_{fic} - 4.8;$$
(44)

$$C = 2.5h_{fic}^3 - 8.8h_{fic} + 40.7; \tag{45}$$

$$D = -75h_{fic}^3 + 585h_{fic}^2 + 496h_{fic} - 6.8; \tag{46}$$

$$E = -169h_{fic}^4 + 88h_{fic}^3 + 584h_{fic}^2 - 39h_{fic} + 0.8, \tag{47}$$

It is worth noting that in this case, the fictitious thickness should be expressed in meters.

Once the parameters of interest have been obtained, the portion related to shrinkage deformation can be calculated using equation:

$$\varepsilon_s^{cs}(t) = \varepsilon_s^{cs\infty}[\beta_s(t) - \beta_s(t_0)], \tag{48}$$

where $\varepsilon_s^{cs}(t)$ is the final value of shrinkage, which is related to the consistency of the concrete and the relative humidity of the environment, determined by Equation (49), and $\beta_s(t_0)$ is the coefficient related to concrete shrinkage at times t and t_0, given by Equation (52). Thus,

$$\varepsilon_s^{cs\infty} = \varepsilon_{1s}\varepsilon_{2s}, \tag{49}$$

where ε_{1s} is the coefficient dependent on the relative humidity of the environment and the consistency of the concrete, obtained by Equation (50):

$$\varepsilon_{1s} = \left(-8.09 + \frac{U}{15} - \frac{U^2}{2284} - \frac{U^3}{133765} + \frac{U^4}{7608150}\right)10^{-4}, \tag{50}$$

It is worth noting that the coefficient ε_{1s}, given by Equation (50), is valid for concrete slump values between 5 cm and 9 cm, with relative humidity percentages between 40 and 90. For a relative humidity of 100%, the deformation suggested by the standard is a fixed value of -1×10^4 cm. The coefficient ε_{2s} is a function of the fictitious thickness of the element, and depends, among other factors, on the relative humidity of the environment, and is calculated by Equation (51):

$$\varepsilon_{2s} = \frac{32 + 2h_{fic}}{28.8 + 3h_{fic}} \cdot$$

(51)

Finally, the coefficient $\beta_s(t)$ is given by:

$$\beta_s(t) = \frac{\left(\dfrac{t}{100}\right)^3 + A\left(\dfrac{t}{100}\right)^2 + B\left(\dfrac{t}{100}\right)}{\left(\dfrac{t}{100}\right)^3 + C\left(\dfrac{t}{100}\right)^2 + D\left(\dfrac{t}{100}\right) + E} \cdot$$

(52)

According to ABNT NBR6118 [12], in cases where high precision is not required in determining the final values of the creep coefficient and specific shrinkage deformation, the values can be obtained relatively easily through a simple linear interpolation from Table 1. This allows for a simplified estimation of the time-dependent behavior of concrete.

Table 1 – Creep and shrinkage of ABNT NBR6118 [12]

Environment	Humidity (%)	Creep			Shrinkage ($\times 10^4$)			γ
		Slump according to ABNT NBR NBR 16889 [13]						
		0 - 4	5 - 9	10 - 15	0 - 4	5 - 9	10 - 15	
In water	-	0,6	0,8	1,0	1,0	1,0	1,0	30,0
In a very humid environment, immediately above water	90	1,0	1,3	1,6	- 1,6	- 2,5	- 3,1	5,0
Outdoors, generally	70	1,5	2,0	2,5	- 3,8	- 5,0	- 6,2	1,5
In a dry environment	40	2,3	3,0	3,8	- 4,7	- 6,3	- 7,9	1,0

Source: adapted from ABNT NBR6118 [12].

It should be noted that, according to the normative recommendations, the values presented in Table 1 are considered valid for plastic and ordinary Portland cement concretes, subjected to temperatures between 0°C and 40°C.

The coefficient related to irreversible slow deformation, $\beta f(t)$, which is a function of concrete age and given by Equation (42), can also be obtained, in a simplified manner, through a graphical analysis, considering the fictitious thickness of the element and the fictitious age of the concrete in days. Figure 3 shows the variation of the coefficient $\beta_f(t)$

Figure 3 – Graphical variation of the coefficient $\beta_f(t)$
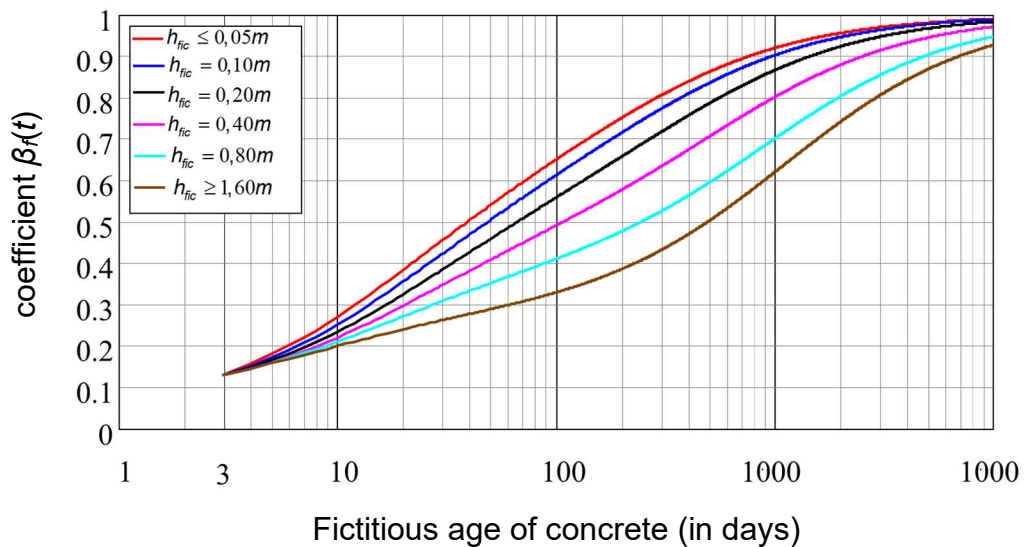
Source: Author

Similarly, the coefficient $\beta_s(t_0)$ (for shrinkage) can be determined through graphical analysis using Figure 4.

Figure 4 – Graphical variation of the coefficient $\beta_s(t_0)$

Fictitious age of concrete (in days)
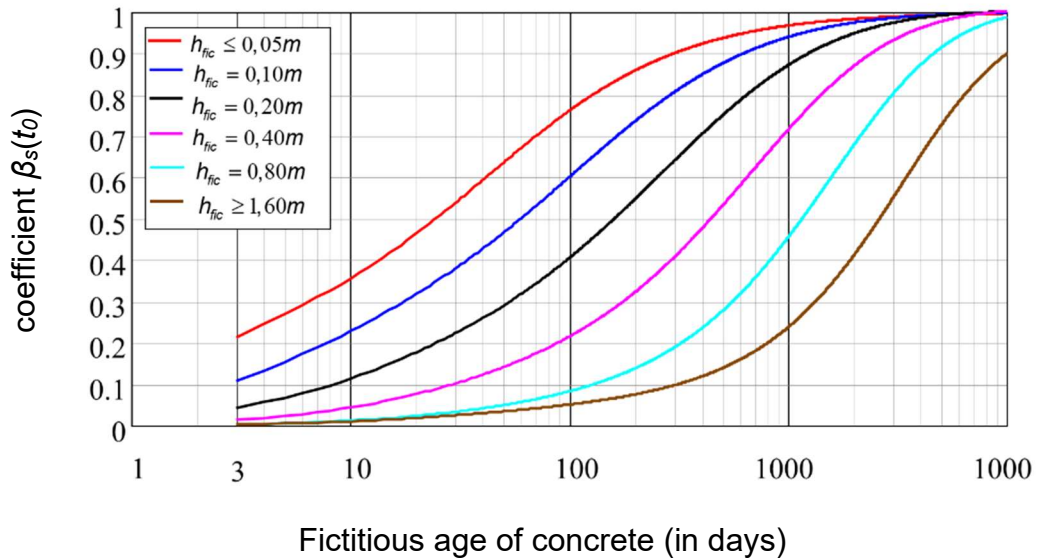
Source: Author

It is also possible to determine, for the same concrete, the curves of irreversible slow strain as a function of time, corresponding to different initial loading application times, by shifting the strain axis parallelly, as shown in Figure 5.

Figure 5 – Variation of irreversible slow deformation
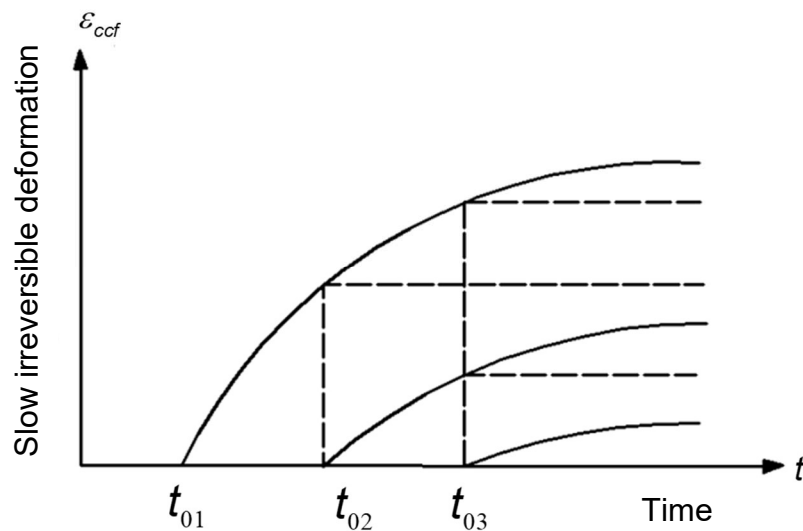
Source: adapted from ABNT NBR6118 [12]

Therefore, Equation (25) can be extended in its final form as:

$$f(m_0,t) = \frac{1}{2\pi}\sqrt{\frac{K(m_0,t)}{M(m_0)}} \; . \tag{53}$$

where it is possible to determine the variation of the structure's frequency as a function of the value of concentrated mass, varying at the top of the structure, and time, as the total generalized stiffness component will take into account some rheological properties of the concrete, namely, creep and shrinkage.

Therefore, by expressing the frequency in terms of the concentrated mass at the free end and time, the critical buckling force is established as a certain value that causes the frequency to become zero. This value, when multiplied by the acceleration due to gravity, defines the force corresponding to the collapse of the system.

2.2 STRAIN REGIME INDUCED BY AXIAL LOADING

In the field of structural engineering, the assessment of a structure's behavior and performance under axial loading necessitates the consideration of its overall strain. This strain encompasses two primary components: elastic strains and inelastic strains. Elastic strains manifest immediately upon the application of the axial load and exhibit reversibility, governed by the material's elastic properties. Conversely, inelastic strains accrue over time and are irretrievable, attributed to phenomena like creep and shrinkage. To accurately anticipate the entirety of strains, engineers meticulously analyze both instantaneous elastic strains and time-dependent inelastic strains, thereby ensuring that the design adheres to performance criteria and adequately accounts for enduring structural modifications.

In the case of slender reinforced concrete columns, the strain encompassing them entails an initial deformation complying with Hooke's Law, as well as a gradual augmentation of time-dependent strain rate. The determination of total strains assumes paramount significance in the design of these columns, as it guarantees their safety and performance throughout their service life. Mathematical models,

incorporating approaches grounded in stress-strain diagrams and the foundational principles of linear elastic behavior articulated by Robert Hooke [14], are employed to evaluate these deformations.

These deformations can be evaluated using various mathematical models. However, two distinct mathematical methods will be presented, which were used in the investigations and are part of the collection of published articles that constitute this thesis. One method is based on the stress-strain diagram provided by ABNT NBR6118 [12], which is directly dependent on the compressive strength curve of the concrete, i.e., its f_{ck}. The second method is based on the premise of linear elastic behavior, following the law established by Robert Hooke in 1678 [14].

Thus, assuming that the same stress levels are used in both analyses and considering the validity of the linear elastic regime, the expected result is that the strain behavior obtained by the two different mathematical methods will exhibit similar values.

The method based on the stress-strain diagram of the Brazilian standard is related to the behavior depicted in Figure 6. It can be observed that there is an elastic and linear phase characterized by a supposedly straight and inclined segment, where the deformations are assumed to be completely recoverable after unloading, with the limits defined at positions $0{,}50f_{cd}$ (half of the concrete compressive design strength) and ε_{c1}. This is followed by a nonlinear elastic phase, characterized by a curved and parabolic segment, which ends at the pair of points $0.85f_{cd}$ and ε_{c2}. Finally, there is a plastic phase, represented by a horizontal line, where the induced deformation cannot be completely recovered after unloading. After that, the stresses remain unchanged even for increasing strains, which continue to progress for further loading until reaching the ultimate value, εcu, indicating failure due to the exhaustion of the structural section resistance.

Figure 6 – Idealized stress-strain diagram
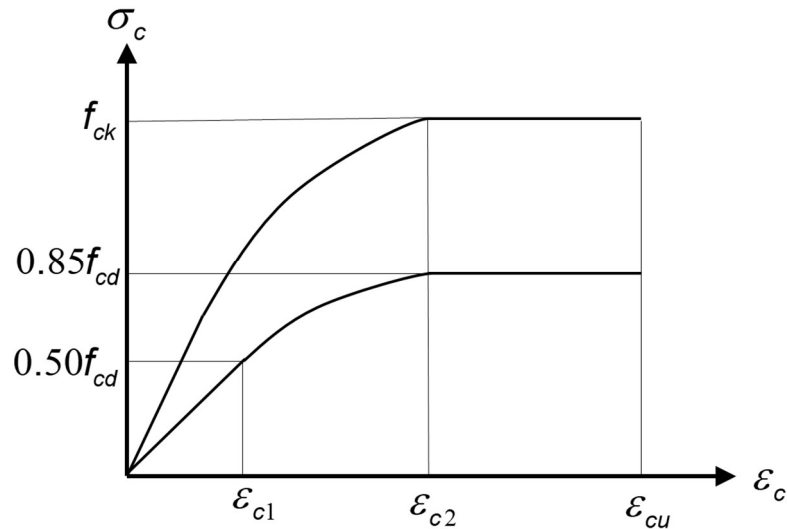
Source: Author

The calculation of the compressive design strength of concrete (f_{cd}) is determined according to the guidelines of ABNT NBR6118 [12] using equation (54):

$$f_{cd} = \frac{f_{ck}}{\gamma_c}.$$

(54)

where γ_c is the safety factor related to material uncertainties, which is a value specified by the standard, and f_{ck} is the characteristic strength assumed in concrete structure designs and should be verified using a standardized procedure after 28 days of material production.

Equation (55) is the relationship between stress and strain of concrete, which can be used in various analyses, including the ultimate limit state.

$$\sigma_c = 0{,}85 f_{cd} \left[1 - \left(1 - \frac{\varepsilon_c}{\varepsilon_{c2}} \right)^n \right].$$

(55)

In equation (55), $n = 2$ is adopted for concretes with f_{ck} less than or equal to 50 MPa ($f_{ck} \leq 50$ MPa). In this case, the adopted values for the specific shortening strain of

concrete at the beginning of the linear section (ϵ_{c1}), at the start of the plastic plateau (ϵ_{c2}), and at the rupture strain (ϵ_{cu}) are ϵ_{c1} = 0.10%, ϵ_{c2} = 0.20%, and ϵ_{cu} = 0.35%, respectively.

To obtain the concrete strain, equation (55) can be inverted with respect to the strain component ε_c, as follows:

$$\varepsilon_c = -\left[\sqrt[n]{\frac{\sigma_c}{0,85f_{cc}}+1}+1\right]\varepsilon_{c2}. \tag{56}$$

As the investigation will be carried out in a temporal manner, the concrete creep strain was incorporated into equation (56), following equation (27). Thus, the stress-strain diagram becomes time-dependent, as follows:

$$\varepsilon_c = -\left[\sqrt[n]{\frac{\sigma_c}{0,85f_{cc}}+1}+1\right]\varepsilon_{c2}\left[1+\phi_f(t)\right]. \tag{57}$$

Figure 7 – Stress-strain diagram with concrete creep
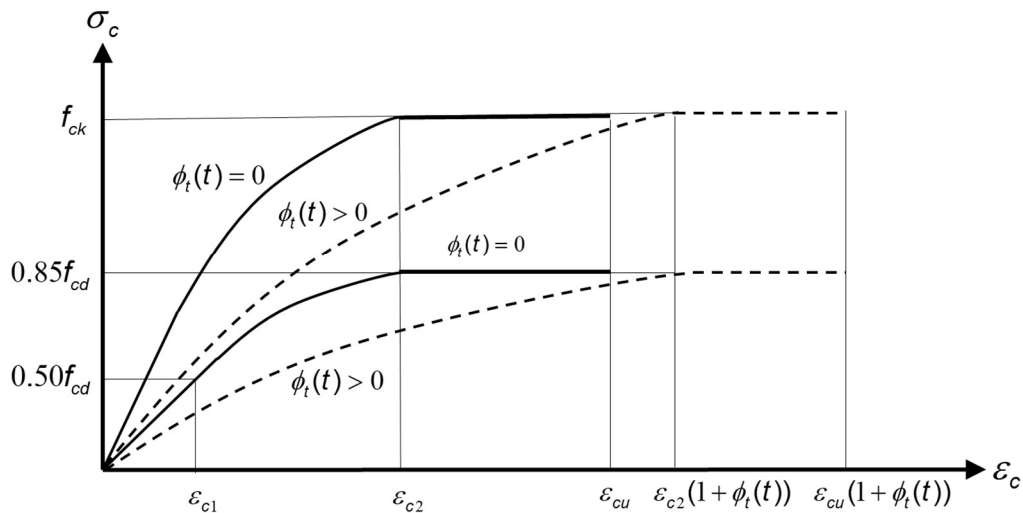
Source: Author

For the second mathematical model, the approach was based on the assumption of elastic-linear behavior of concrete, a concept established by the English

mathematician and physicist Robert Hooke, who in 1678 presented a way to calculate the elongation in bars subjected to axial load, that, in modern notation, may be given by equation (58).

$$d\delta = \frac{N(x)dx}{EA(x)}.$$

(58)

where $N(x)$ and $A(x)$ are the normal force and the cross-sectional area varying in the differential element dx, and E is the modulus of elasticity of the material. Therefore, integrating equation (58) over the length of the bar will provide the total displacement induced by that force, thus:

$$\delta(t) = \int_0^L \frac{N(x)dx}{EA(x)}.$$

(59)

To incorporate the rheological behavior of concrete, we simply replace E with $E_c(t)$, where the creep of concrete follows the assumptions described in equation (29).

The present investigation focuses on the study of slender columns made of reinforced concrete. Figure 8 illustrates a generalized mathematical model of a non-prismatic bar under compression, which is adopted in the approaches to determine the critical load and the final deformation behavior of the column.

As can be observed, the proposed model pertains to a column fixed at the base and free at the top, with a concentrated mass set at the free end. The column may or may not have variable geometry along its length. In this case, the column is subjected to gravitational forces originating from the concentrated mass distributed along its length.

Figure 8 – Mathematical model of a non-prismatic bar under compression
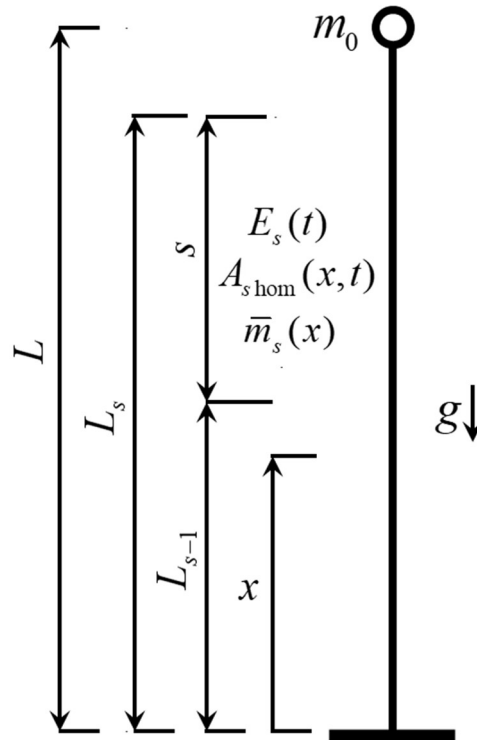
Source: Author

In Figure 8, g represents the acceleration due to gravity, L is the total length, L_s and L_{s-1} are the positions above and below a segment s; m_0 is a concentrated mass fixed to the top of the structure; x is the independent geometric variable of the problem, with its origin at the base of the column. With respect to a particular segment, $E_s(t)$ is the longitudinal modulus of elasticity, which takes into account the viscoelastic behavior of the material; $A_{shom}(x,t)$ is the cross-sectional area, assumed to vary with x, representing the interpolation of the upper and lower sections at the considered segment, both homogenized over time to include the presence of steel reinforcement bars; and $\bar{m}_s(x)$ is the portion of the distributed mass along the segment, which includes its own weight and other masses per unit length added to it.

Thus, by adopting equation (59), it can be rewritten considering the variation of a mass (m_0):

$$\delta_s(t,m_0) = \int_{L_{s-1}}^{L_s} \left[\frac{\left[\left(N_0(m_0) + \sum_{s+1}^{n} N_{s+1} + \overline{m}_s(L_s - x)g \right) \right]}{E_c(t)A_{s\,\text{hom}}(x,t)} \right] dx \,. \tag{60}$$

By definition, it is known that the strain associated with the total elongation produced by axial forces related to a certain segment is obtained by summing the displacements of the segments located above, and including itself, under the conditions established in equation (61):

$$\delta_s(t,m_0) = \varepsilon_{cc2}(t,m_0) = \frac{\sum_{s=1}^{n} \delta_s(t,m_0)}{\sum_{s=1}^{n} L_s} \,. \tag{61}$$

where δ_s represents the elongation of segment s and n is the number of segments considered in the analysis. In this context, the normal stress can then be calculated at section S considering the accumulated strain up to and including the strain of the segment under consideration, taking into account the modulus of elasticity of the material at the instant of interest, as follows:

$$\sigma_{cS}(t,m_0) = \varepsilon_{cc2}(t,m_0)E_c(t) \,. \tag{62}$$

Once the stress at a concrete section S is defined using equation (62), equation (57) should be written in terms of the same independent variables, leading to its rewriting in the form of equation (63):

$$\varepsilon_{cc1}(t,m_0) = -\left[\sqrt[n]{\frac{\sigma_{cS}(t,m_0)}{0,85 f_{cd}}} + 1 + 1 \right] \varepsilon_{c2}(1 + \phi_f(t)) \,. \tag{63}$$

Therefore, equations (61) and (63) should yield identical results for the same analysis when the assumption of linear elastic behavior of concrete is valid.

3 PAPER 01

3.1 COMPLETE CITATION FORMAT

Magalhães KMM, Wahrhaftig AM and Brasil RMLRF. Strain regime induced by axial compression in slender reinforced concrete columns using different mathematical approaches. Structures 2023,49,655-665.

3.2 ABOUT THE JOUNAL AND IMPACT FACTOR

The article that will be presented in this chapter was published by the Research Journal of the Institution of Structural Engineers, called Structures. According to your website: "Structures aims to publish internationally leading research across the full breadth of structural engineering. Papers for Structures are particularly welcome in which high-quality research will benefit from wide readership of academics and practitioners such that not only high citation rates but also tangible industrial-related pathways to impact are achieved". Its impact factor is 4.01.

3.3 TITLE

Strain regime induced by axial compression in slender reinforced concrete columns using different mathematical approaches.

3.4 ABSTRACT

A mathematical investigation to determine the strain regime induced by normal compression force in concrete, including the portion due to material creep, was presented. The consideration of creep suggests the possibility of changing the constitutive law of the material since it introduces a temporal variation, hence the need

to use different mathematical paths to evaluate the imposed strains. The analysis was conducted on a real reinforced concrete column, with variable geometry and high slenderness ratio, on which two different approaches were considered. In the first one, a concrete stress-strain curve, standardized by a technical norm, was used. In the second one, the integration of differential relations of displacements along the length of the structure was adopted. The analysis was performed by considering the structural system loaded by just its self-weight to the critical buckling load.

3.5 KEYWORDS

Temporal strains; Normative stress-strain diagram curve; Differential relations of deformation; Linear behavior; Hooke's law; Axial compression.

3.6 DIGITAL OBJECT IDENTIFIER (DOI)

3.7 INTRODUCTION

The design of reinforced concrete structures must be done in such a way as to guarantee performance, durability, and safety. In this sense, there are normative regulations that aim to systematize the calculation procedures for the dimensioning and verification of structural elements built using concrete, presenting analytical-mathematical formulations to be considered in the analysis process. The Brazilian technical standards (Brazilian Association of Technical Standards - ABNT) for projects using reinforced concrete structures is ABNT NBR 6118:2014 - Design of structural concrete - Procedure [1], which has a technical quality standard that is compatible with

international standards, such as ACI [2] and Eurocode [3], and is even ISO 9000 certified. ABNT NBR6118 [1] presents criteria for evaluating concrete structures in relation to their Ultimate Limit State (ULS), which concern the dimensioning of these systems, the calculation of stresses and deformation, and verification of structural collapse conditions, for which the stress-strain curve of concrete is a central parameter of reference.

In particular, the verification of the ULS of slender reinforced concrete columns has been a subject of constant investigation in the scientific environment, since it reaches an ULS defined by the loss of stability, which occurs without the column having exhausted the resistance capacity of its cross sections. It is noteworthy that advanced methods exist to assess the ULS of slender columns, although there are still some gaps in relation to their time-dependent behavior [4]-[5] However, it is important to be highlighted that the more slender a column, the lower its axial loading capacity due to aspects related to its stability [6]-[16].

For axially loaded reinforced concrete parts, the displacements resulting from the applied force gradually increase with the level of induced stress, passing through values that define the behavior of the stress-strain curve of the material. If the stress level remains unchanged over time, a solid made of concrete may show increased strain, even under these conditions, which are caused by the rheology of the material. This property changes the stress-strain curve of concrete as originally presented. Rheology is understood to be the study of deformation and flow of matter [17]-[18] which is a phenomenon that is directly related to the viscoelastic behavior of concrete [19]. When observed in the context of continuum mechanics, the basic assumptions associated with rheology admit that the response of a Hookean solid in terms of stress can be considered linearly proportional to the strain rate in time [20].

For reinforced concrete columns, part of the strain of the structure occurs instantaneously, at the moment of application of the load (initial strain) and this obeys Hooke's law. Another time-dependent portion (strain rate) tends to gradually increase, resulting in much higher values, when compared to the initial ones [21]. Thus, during

the design and/or verification of axially stressed slender columns, it is necessary to evaluate the total imposed strains, both instantaneous and temporal, to verify the suitability of the design for safety, in-service performance and durability [22]-[28].

With respect to the temporal strains of reinforced concrete structures, it should be noted that these are characteristic of the rheology of the material, called creep. Creep is defined as the temporal and gradual increase in the deformation of concrete, even under constant stress [29]. It is a phenomenon influenced by a series of factors such as, for example, the age of the concrete, when the loading takes place, atmospheric conditions and dimensions of the structural element [30]-[32]. Creep interferes with induced strains in concrete [33]-[39]. For this reason, in the calculation of strains due to creep, ABNT NBR6118 [1] recommends that a mathematical procedure be adopted, to determine the coefficient to be assigned to the modulus of elasticity of the material and that depicts, in a temporal way, the behavior of the material in terms of creep. This behavior is reflected in the entire course of the stress-strain curve, including the region of linear behavior.

In the context of what was previously described, this study sought to investigate, through the assumption of two distinct analytic-mathematical processes, the total deformations induced by axial loading, which includes the portion due to creep. For this, a reinforced concrete column, real, prefabricated, and of variable cross-section was adopted. It is noteworthy that the investigated element has a high slenderness ratio, which potentiates the strains due to the creep of the concrete [40], resulting in reason of this characteristic its choice. The first process was developed based on the stress-strain diagram for concrete proposed by ABNT NBR6118 [1], which is a curve that is dependent on the characteristic compressive strength of concrete. In the second process, the differential relation of deformations of segments related to each cross section subject to concrete creep, were considered and conceptualized according to the principle established by Robert Hooke in 1678 [41]. As a premise, since the stress level is identical in both analyses within the linear regime, the expected result is that the strains obtained by the two processes present the same values. This is, therefore, the investigated hypothesis.

3.8   IDEALIZED STRESS-STRAIN DIAGRAM

ABNT NBR 6118 [1] established that, for stresses acting lower than 50% of the compression strength of concrete, f_c, a linear relationship between stresses and strains can be assumed. The strength of concrete is a quantity that consolidates as the material ages. In that sense, f_{ck} is the standard resistance assumed in the design of concrete structures, which must be verified by a standardized procedure when an age of 28 days is reached since the material was produced. Within the design scope, it is necessary to apply an adjustment factor to f_{ck} for safety, so that the design value of concrete cylinder compressive strength, f_{cd}, is established in accordance with Equation (1):

$$f_{cd} = \frac{f_{ck}}{\gamma_c},$$

(1)

where γ_c is the partial safety factor related to the uncertainties of the material, which is a value foreseen in the standard. In the analysis of the ULS, the stress-strain diagram shown in Figure 1 can be used, which represents the dependence of stress on the strain of the concrete established by Equation (2) and valid for the range of strains, including the linear elastic, non-linear elastic and plastic regions of behavior (extending to the limit allowed for concrete failure).

As can be seen in Figure 1, there is a typically elastic and linear phase, characterized by a supposedly straight inclined line, where the deformations presented are assumed to be completely recoverable after unloading. Their limits define the position $0.50\sigma_c$, i.e., $0.42f_{cd}$, and ε_{c0}; another stretch of non-linear elastic behavior, where the diagram is characterized by a curved, parabolic segment that ends at the pair of points $0.85f_{cd}$ and ε_{c2}; and another plastic, horizontal segment, where the portion of the induced strain cannot be more completely recovered after the solid is unloaded. After yielding, the stresses remain unchanged, even for increasing values of strains, which continue advancing for new loadings up to the last possible value, ε_{cu}.
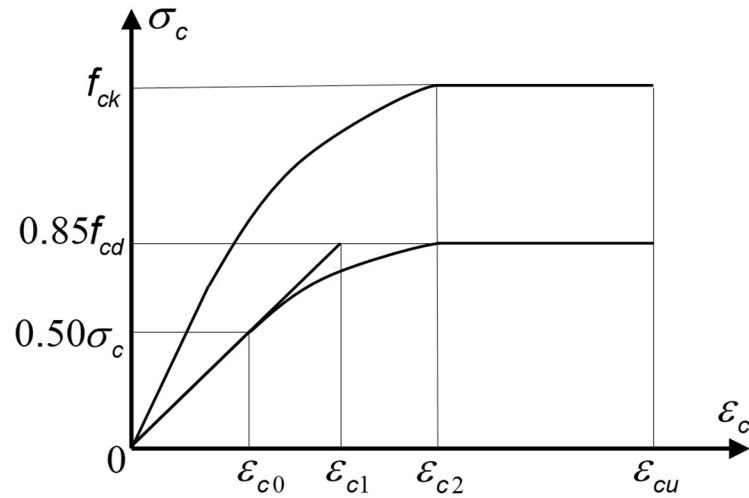
Figure 1 – Idealized stress-strain diagram for concrete in axial compression [1]

$$\sigma_c(\varepsilon_c) = 0.85 f_{cd} \left[1 - \left(1 - \frac{\varepsilon_c}{\varepsilon_{c2}} \right)^n \right].$$

(2)

In Equation (2), $n = 2$ is adopted for concretes with f_{ck} less than or equal to 50 MPa ($f_{ck} \leq 50$ MPa). In this case, the adopted value for the strain of shortening the concrete at the limit of the linear stretch, ε_{c0}, is proportional to $\varepsilon_{c1} = 0.10\%$; at the beginning of the plastic plateau, it is $\varepsilon_{c2} = 0.20\%$; and for the strain of the shortening of the concrete at rupture, it is $\varepsilon_{cu} = 0.35\%$.

Equation (3) presents the terms for determining the total strain in compression, ε_c, including the immediate one, ε_{ci}, and the creep of concrete, ε_{cc}, according to the definition of the technical reference standard,

$$\varepsilon_c = \varepsilon_{ci} + \varepsilon_{cc}.$$

(3)

For the implementation of creep deformations in concrete, ε_{cc}, in the stress-strain diagram of the material, it is necessary to consider the two terms that contribute to the phenomenon, one referring to the slow deformation, ε_{ccf}, and the other to the fast, ε_{cca}. Rapid deformation is irreversible and occurs during the first twenty-four hours after the

structure is subjected to loading. The slow strain is composed of two other parts, the slow irreversible strain, ε_{ccf}, and the slow reversible strain, ε_{ccd},

$$\varepsilon_c = \varepsilon_{ci} + \left(\varepsilon_{cca} + \varepsilon_{ccf} + \varepsilon_{ccd} \right).$$

(4)

As can be seen, there is an important change in the constitutive relation of the concrete after including the creep, which modifies the stress-strain curve of the material, in addition to imposing the concept of irreversibility of strain, even after the body has been unloaded, which occurs regardless of the stress level that is induced. With this, it is understood that, if the material flows, the part related to this strain cannot be fully recovered even if the total discharge of the solid occurs.

In turn, creep strain can be conveniently described as a function of a coefficient, $\phi_{f(t)}$, which is a quantity that incorporates time dependence into the calculation process. For its calculation, ABNT NBR 6118:2014 considers that: (1) creep strain varies linearly with applied stress; (2) for stress additions applied at different time steps, the respective creep effects obey the superposition principle; (3) the fast strain portion is constant over time; (4) the irreversible slow strain is a function of time depending on the concrete strength at the loading instant and its final strength in time; (5) the coefficient of slow reversible strain depends only on the duration of loading, being its final value and growing independents of the concrete age at the time of load application; (6) the irreversible slow strain depends on the relative humidity of the environment, concrete slump, the member thickness, the age of the concrete at the loading time application, and the instant considered in the analysis; (7) the irreversible slow strain curve is a function of time which depends on the concrete age at the time of loading.

In this way, it is possible to state that the time-dependent strain of the concrete, considering the basic assumptions contained in ABNT NBR 6118 [1], is given by the following set of equations, which was already experimentally validated [42].

$$\varepsilon_c = \varepsilon_{ci} \left[1 + \phi_f(t) \right],$$

(5)

where the coefficient $\phi_{f(t)}$ represents the sum of the coefficients of fast deformation, ϕ_a, irreversible slow deformation, $\phi_{f\infty(t)}$, and reversible slow deformation, $\phi_{d\infty(t)}$:

$$\phi_f(t) = \phi_a(t) + \phi_{f\infty}(t) + \phi_{d\infty}(t).$$

(6)

The determination of the coefficient of fast, slow irreversible and slow reversible deformation is given by Equations (7), (9) and (18), respectively.

$$\phi_a(t) = 0.8\left[1 - \frac{f_c(t_0)}{f_c(t)}\right],$$

(7)

where $f_c(t_0)$ represents the strength of the concrete at the beginning of the external loading and $f_c(t)$ is the strength of the concrete at time, t, when the analysis is performed. Both obey an exponential law that corrects the strength of concrete in relation to the design standard, which must be verified 28 days after the production of the material, and is given by:

$$f_c(t) = e^{0.38\left(1 - \sqrt{\frac{t_{28}}{t}}\right)} f_{ck},$$

(8)

where t represents days and t_{28} means 28 days. It is easy to verify that $f_c(28$ days$)$ = f_{ck}. Therefore, it can be said that the relationship between $f_c(t_0)$ and $f_c(t)$ represents the growth function of concrete strength. Observing Equation (8), it is possible to verify that the strength of concrete advances with time, surpassing the value of f_{ck}, the limit established in the stress-strain diagram for design purposes.

The portion of irreversible slow deformation, as already mentioned, is defined by:

$$\phi_{f\infty}(t) = \phi_{1c}\phi_{2c}\left[\left(\frac{t^2 + At + B}{t^2 + Ct + D}\right) - \left(\frac{t_0^2 + At_0 + B}{t_0^2 + Ct_0 + D}\right)\right],$$

(9)

where ϕ_{1c} and ϕ_{2c} are calculated by Equations (10) and (11), respectively; t represents the total time, and t0 is the initial time when the load is applied. The coefficients A, B,

C and *D* are calculated, in that order, by the Equations from (13) to (17). Therefore, the first coefficient of irreversible strain, ϕ_{1c}, is given by:

$$\phi_{1c} = 4.45 - 0.035U,$$

(10)

where *U* represents the relative humidity of the environment, expressed as a percentage. In turn, the coefficient ϕ_{2c} can be obtained by Equation (11):

$$\phi_{2c} = \frac{42 + h_{fic}}{20 + h_{fic}},$$

(11)

where h_{fic} is the fictitious thickness of the part (in cm) given by:

$$h_{fic} = \frac{21 + e^{(-7.8 + 0.1U)} A_S}{\pi D_S},$$

(12)

where A_S and D_S are the area and perimeter of the cross-section *S*, under consideration. Then,

$$A = 40,$$

(13)

$$B = 116(h_{fic})^3 - 282(h_{fic})^2 + 220h_{fic} - 4.8,$$

(14)

$$C = 2.5(h_{fic})^3 - 8.8h_{fic} + 40.7,$$

(15)

$$D = -75(h_{fic})^3 + 585(h_{fic})^2 + 496h_{fic} - 6.8,$$

(16)

$$E = -169(h_{fic})^4 + 88(h_{fic})^3 + 584(h_{fic})^2 - 39h_{fic} + 0.8.$$

(17)

In turn, the coefficient $\phi_{d\infty}(t)$ is calculated by:

$$\phi_{d\infty}(t) = 0.4\left[\frac{t - t_0 + 20}{t - t_0 + 70}\right].$$

(18)

In this way, the longitudinal deformation modulus of concrete, $E_c(t)$, can be calculated, adding the material creep, by:

$$E_c(t) = \frac{1}{\dfrac{1}{E_{c0}}} + \frac{1}{\dfrac{\phi_f(t)}{E_{c28}}},$$

(19)

where E_{c0} is the longitudinal deformation modulus of the concrete at the moment when loading is applied, and E_{c28} is the value of this same parameter 28 days after its production. For the definition of E_{c28}, it was considered the slope of the elastic-linear regime. Thus, according to the graph in Figure 1, it is possible to write that:

$$E_{c28} = \frac{0.85 f_{cd}}{0.001}.$$

(20)

Therefore, incorporating the temporal variation of the strains to the behavior of the concrete, Equation (2) is now written as:

$$\sigma_c(\varepsilon_c, t) = 0.85 f_{cd} \left[1 - \left(1 - \frac{\varepsilon_c}{\varepsilon_{c2}[1 + \phi_f(t)]} \right)^n \right],$$

(21)

allowing the introduction of the creep to the stress-strain diagram of the concrete in compression. The portion of the deformation due to the creep of the material influences all the limits of the original diagram. Figure 2 represents the idealized stress-strain diagram after considering the creep of the concrete.
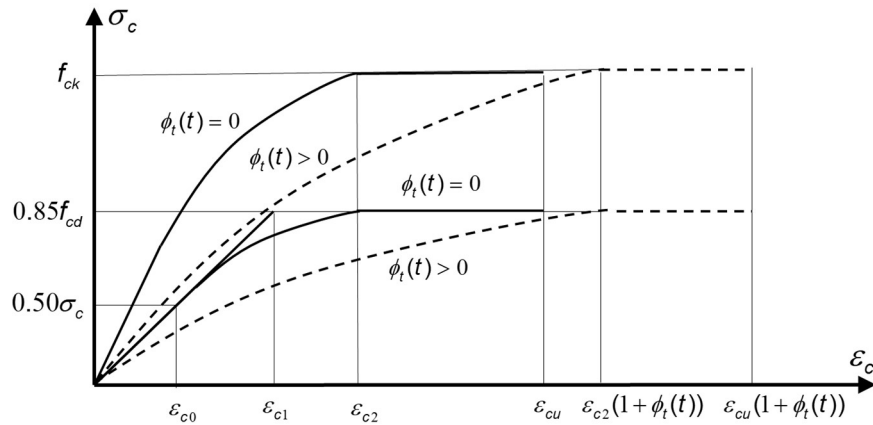
Figure 2 – Stress-strain diagram of concrete in compression considering creep [1]

On the other hand, it is possible to rewrite Equation (2) inversely, to obtain strains in terms of concrete stress. Therefore:

$$\varepsilon_c(\sigma_c,t) = -\left[\sqrt[n]{\frac{\sigma_c}{0.85f_{cd}}+1}+1\right]\varepsilon_{c2}\left[1+\phi_f(t)\right].$$

(22)

3.9 DIFFERENTIAL DEFORMATION RELATIONSHIPS

Determination of the deformation of solids characterized as longitudinal bars goes back to the work of the English mathematician and physicist Robert Hooke. In 1678, Hooke established the law that allows calculating the elongation (positive or negative) of a bar subjected to normal forces, represented by Equation (23):

$$d\delta = \frac{N(x)}{EA(x)}dx.$$

(23)

$N(x)$ and $A(x)$ are the normal stress and the cross-sectional area, which vary in the differential element dx, and E is the modulus of elasticity of the material or Young's modulus. Therefore, the integral of Equation (23) in the length of the bar will give the total displacement induced by that effort. If the material constituting the solid exhibits viscoelastic behavior, such as concrete, this affects the modulus of elasticity and the

cross-sectional area, since it is normally formed by the junction of concrete with another material, usually steel reinforcement bars. So, the previous equation can be written in the following form:

$$d\delta(t) = \frac{N(x)}{E_c(t)A_{hom}(x,t)}dx ,$$

(24)

where $A_{hom}(x,t)$ is the homogenized cross-section area of concrete, and the integral in the element domain (i.e., from 0 to L) leads to temporal displacements because the modulus of elasticity defines different values at different instants of time:

$$\delta(t) = \int_0^L \frac{N(x)}{E_c(t)A_{hom}(x,t)}dx .$$

(25)

If a column as indicated in Figure 3 is considered, the application of Equation (25) in this case must be restricted to the domain of each segment of the solid. So, the total deformation must represent the accumulation of displacements of all segments under consideration, i.e., a summation. The model described in Figure 3 concerns a column clamped at the base and free at the top, with a lumped mass applied to the free end, which may or may not have variable geometry along its length. In this case, the column is under the action of gravitational forces originating in the concreted and distributed mass, along its length.
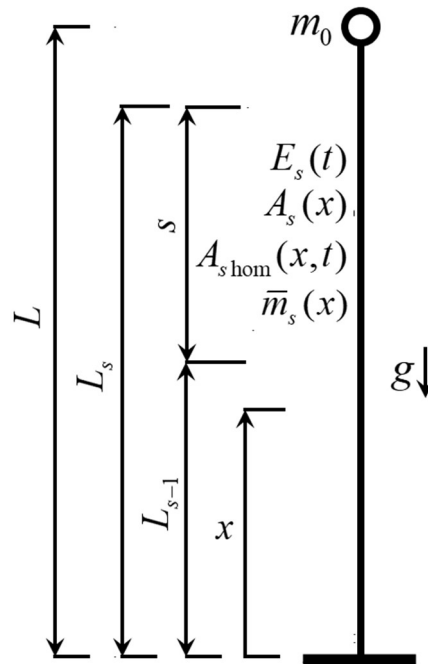
Figure 3 – Mathematical model of a non-prismatic bar in compression

In Figure 3, g is the acceleration due to gravity, L_s and L_{s-1} are the positions above and below a segment s, m_0 is a concentrated mass applied to the top of the structure, and x is the geometric independent variable of the problem, having its origin at the base of the column. Relative to a given segment s, $E_s(t)$ is the longitudinal deformation modulus, which considers the viscoelastic behavior of the material. If this is not the case, it will be a time-independent parameter, E_s. $A_s(x)$ the nominal area varying geometrically in the segment, and $A_{shom}(x,t)$ is the concrete homogenized cross-section area, admitted variable with x and which represents the interpolation of the upper and lower sections of the considered segment. The homogenization of the cross-section is done to include the presence of steel reinforcement bars. After homogenizing, the sections formed by the viscoelastic modulus passe to be also a temporal function. In Figure 3, $\bar{m}_s(x)$ is the portion of the distributed mass along the segment, which includes its own weight and other masses per unit length that are added to it. The dependence of x on the previous or forward parameters disappears if the segment is prismatic.

If it is assumed that the mass m_0 can vary independently, the displacement $\delta_s(t,m_0)$ presented by each segment s, depends on both time and this parameter, which can be written (in terms of what was established in Equation (25)) as:

$$\delta_s(t,m_0) = \int_{L_{s-1}}^{L_s} \left[\frac{\left[\left(N_0(m_0) + \sum_{s+1}^{n} N_{s+1} + \bar{m}_s(L_s - x)g \right) \right]}{E_c(t)A_{s\,\text{hom}}(x,t)} \right] dx \,, \tag{26}$$

With

$$N_0(m_0) = m_0 g \,, \tag{27}$$

and

$$N_s = \int_{L_{s-1}}^{L_s} \bar{m}_s(x)g dx \,, \text{ with } \bar{m}_s(x) = A_s(x)\rho_s + \bar{m}_s^a \,. \tag{28}$$

For the segment s, ρ_s is the density of the material (concrete plus reinforcement in the present case); $A_s(x)$ is the gross cross-section area, which varies with x in said segment, as previously stated, if not, it will just be A_s; and $\bar{m}_s^a$ is a mass per unit length, representative of the external masses added to the segment. It can be written that:

$$A_s(x) = \frac{A_s - A_{s-1}}{L_s - L_{s-1}}(x - L_{s-1}) + A_{s-1}, \tag{29}$$

where A_S is the nominal not-homogenized cross-sectional area (steel reinforcement bar and concrete) provided by the structural arrangement. In Equation (26), the homogenized area of the segment s, which geometrically varies with x is found by:

$$A_{s\,\text{hom}}(x,t) = \frac{A_{\text{hom}S}(t) - A_{\text{hom}S-1}(t)}{L_s - L_{s-1}}(x - L_{s-1}) + A_{\text{hom}S-1}(t), \tag{30}$$

considering that $A_{hom S}(t)$ is the homogenization of A_S, it can be obtained by:

$$A_{\text{hom}S}(t) = A_S^c + A_S^{st}\xi(t), \text{ with } \xi(t) = \frac{E_S^{st}}{E_c(t)}, \tag{31}$$

where A_S^c and $E_c(t)$ are the net area and the viscoelastic modulus of concrete, which is already defined in Equation (19). A_S^{st} and E_S^{st} are the area and modulus of elasticity of the steel reinforcement bar of a section S, with s and S having the same counter, n, in the summation. $\xi(t)$ is the homogenizing factor. By definition, the strain, $\varepsilon_{cc2}(t,m_0)$, associated with the total elongation related to a given segment s is obtained by the sum of the displacements of the segments located above, and, even, under the conditions established in Equation (32):

$$\varepsilon_{cc2}(t,m_0) = \frac{\sum_{s=1}^{n}\delta_s(t,m_0)}{\sum_{s=1}^{n}L_s}, \tag{32}$$

where n is the number of segments considered in the analysis. In this context, the normal stress, $\sigma_{cS}(t,m_0)$, can then be calculated in section S considering the accumulated strain up to and including that of the segment under consideration, taking the temporal modulus of the material at the instant of interest, by:

$$\sigma_{cS}(t,m_0) = \varepsilon_{cc2}(t,m_0)E_c(t). \tag{33}$$

Once the stress in a concrete section S is defined through Equation (33), Equation (22) must be written as a function of the same independent variables, which leads to rewriting it in the form of Equation (34):

$$\varepsilon_{cc1}(t,m_0) = -\left[\sqrt[n]{\frac{\sigma_{cS}(t,m_0)}{0.85f_{cd}}+1}+1\right]\varepsilon_{c2}(1+\phi_f(t)). \tag{34}$$

Thus, if the behavior established by the equation of the normative of reference correctly describes the linear stretch as such, the results obtained by Equations (32) and (34) must coincide.

3.10 APPLICATION

For the present investigation, a slender, real, reinforced concrete post, with variable geometry along its height, was chosen. The column selected for the study was 46 m high, including the superstructure. It comprised a 40 m hollow circular section, a foundation of caisson type (with a base diameter of 140 cm and a length of 20 cm) and a shaft with a diameter of 80 cm and length of 580 cm, see Figure 4(a). Table 1 presents the geometric parameters of the structure, where D is the external diameter; th represents the wall thickness of hollow structural sections; d_b and n_b are the diameter and number of reinforcement bars, respectively; c' is concrete cover; L are the heights relative to the segment s; and S indicates a specific cross section.

Table 1 – Geometric parameters of the structure

Parameter	Section				
	S1	S2	S3	S4	S5
D (cm)	140	80	80	70	70
th (cm)	-	-	15	13	13
d_b (mm)	12.5	12.5	12.5	12.5	12.5
n_b (und)	20	20	20	20	20
c' (mm)	25	25	25	25	25
L (cm)	0-20	20-600	600-1200	1200-1900	1900-4600

D = external diameter; th = thickness; d_b = diameter of reinforcement bars, n_b = number of reinforcement bars; c' = concrete cover; L = height; S = cross section.

In Figure 4(b), the geometric characteristics of the column are described. In Figure 4(c), photographs of the real system selected for study can be seen, in which the

existence of devices attached to its top can be observed, representing a concentrated mass applied to the free end of the column, whose value will be allowed to vary independently from zero until the force associated with that mass reaches the critical buckling load. With this strategy, it is possible to go through the entire possible range of stresses until the column reaches the ULS defined by the proximity of the loss of its stability. Additional devices are also installed along the entire structure, featuring a distributed mass of 40 kg/m which is added to the column's self-weight. The density, ρ, of reinforced concrete is considered equal to 2600 kg/m³ for the superstructure and 2500 kg/m³ for the foundation.

To include the creep of the concrete, the following hypotheses were considered: (a) the structure was loaded after 28 days of its production (t_0 = 28 days); (b) the relative humidity of the environment admitted was 70%; (c) the characteristic compressive strength of concrete, defined for the superstructure, was 45 MPa (f_{ck} = 45 MPa). Thus, E_{c0} = E_{c28} = 27321.43 MPa. For the foundation, the strength of the concrete was assumed to be equal to 20 MPa (f_{ck} = 20 MPa). Therefore, for this part of the structure E_{c0} = E_{c28} = 12142.86 MPa.
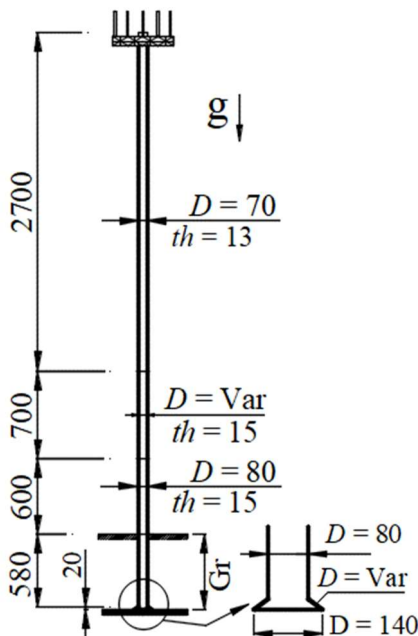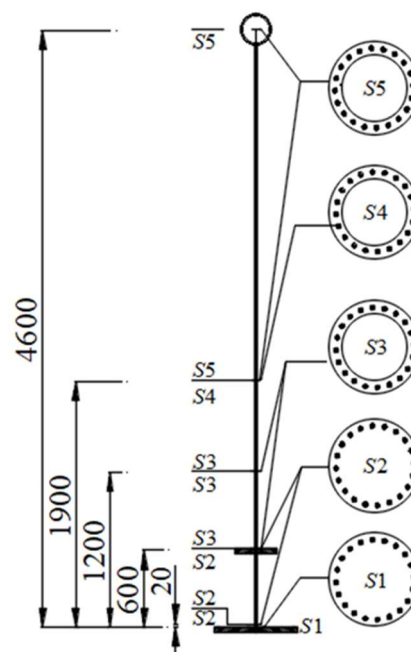
(a) Geometric parameters   (b) Cross-sections   (c) Photographs

Figure 4 – The investigated structure. All dimensions are given in cm.

3.11 RESULTS AND DISCUSSION

The calculation of strain in these cross sections was exclusively aimed at sections *S3*, *S4*, and *S5*, and was performed assuming homogenization over time, in accordance with Equation (31). Using the parallel axis theorem [43]-[44], the values found at the beginning of the loading of the structure for the homogenization factors were: 1.066, 1.079 and 1.084 for sections 3 to 5, in that order. At the end of the investigated period (7500 days), these values became 1.245, 1.298 and 1.318. It is noteworthy that sections S1 and S2 are part of the foundation and, therefore, do not incorporate creep in the proposed mathematical investigation, being unusual their verification in the present context.

Table 2 summarizes the results obtained, where ε_{cc2} and ε_{cc1} are the strains obtained by the differential relations of displacements and by the stress-strain diagram of the concrete, calculated for the time periods of 0, 90, 500, 1000, 2000, 3000, 4000, 5000, and 7500 days, all of them chosen for mere convenience. In Table 2, Δ indicates variation. A_{homS3}, A_{homS4} and A_{homS5} represent the homogenized sections *S3*, *S4* and *S5*. The following considerations were made in the performed analyses: (a) the modulus of elasticity of steel reinforcement was equal to 205 GPa; (b) the concrete was produced under standard conditions; (c) the acceleration of gravity was 9.807 m/s^2; and (d) the normal force of compression was positive and applied to the geometric center of the section.

Table 2 – Strains in time

t	ε_{cc2} (x 10^{-3})			ε_{cc1} (x 10^{-3})			Δ (%) ε_{cc1} , ε_{cc2}		
(day)	A_{homS3}	A_{homS4}	A_{homS5}	A_{homS3}	A_{homS4}	A_{homS5}	A_{homS3}	A_{homS4}	A_{homS5}
0	0.0723	0.0719	0.0697	0.0737	0.0732	0.0709	1.94*	1.81	1.72
90	0.1008	0.0971	0.0859	0.1022	0.0984	0.0869	1.39	1.34	1.16
500	0.1212	0.1151	0.0972	0.1226	0.1163	0.0981	1.16	1.04	0.93
1000	0.1285	0.1215	0.1012	0.1299	0.1228	0.1021	1.09	1.07	0.89
2000	0.1340	0.1263	0.1042	0.1355	0.1276	0.1051	1.12	1.03	0.86

3000	0.1364	0.1284	0.1055	0.1379	0.1297	0.1063	1.10	1.01	0.76
4000	0.1377	0.1295	0.1062	0.1392	0.1308	0.1070	1.09	1.00	0.75
5000	0.1385	0.1303	0.1066	0.1400	0.1316	0.1075	1.08	1.00	0.84
7500	0.1397	0.1313	0.1072	0.1412	0.1326	0.1081	1.07	0.99	0.84
Δ(%)	**48.25**	**45.24**	**34.98**	**47.80**	**44.80**	**34.41**	-	-	-

e_{cc2} = strains obtained by the differential relations of displacements, Eq. (32); e_{cc1} = strains obtained from the stress-strain diagram of concrete, Eq. (34); Δ = difference, * = maximum value.

The values of strains for each instant of time, t, were calculated through Equations (32) and (34), respectively, considering the lowest positions of sections *S3*, *S4* and *S5* in their respective segments, after the lumped mass was set at the critical buckling load, $m_{cr}(t)$, according to Equation (35):

$$m_{cr}(t) = \frac{N_{cr}(t)}{g}.$$

(35)

$N_{cr}(t)$ is the critical buckling load at the instant analyzed. $N_{cr}(t)$ is defined in accordance with Figure 5, which is the model of Figure 3 that can have segments of varying inertia, $I(x,t)$, with the addition of lateral springs that characterize the soil-structure interaction and a function $\phi(x)$, which represents the first buckling mode of the column, see Equation (40). Under the conditions already established, the generalized stiffness [45] of the problem is calculated by considering the following equations. The conventional stiffness is found by:

$$K_0(t) = \sum_{s=1}^{n} k_{0s}(t), \text{ with } k_{0s}(t) = \int_{L_{s-1}}^{L_s} E_s(t)I_s(x,t)\left(\frac{d^2\phi(x)}{dx^2}\right)^2 dx,$$

(36)

while the geometric stiffness is obtained by:

$$K_g(m_0) = \sum_{s=1}^{n} k_{gs}(m_0),$$

(37)

With

$$k_{gs}(m_0) = \int_{L_{s-1}}^{L_s} \left[N_0(m_0) + \sum_{s+1}^{n} N_{s+1} + \bar{m}_s(x)(L_s - x)g \right] \left(\frac{d\phi(x)}{dx} \right)^2 dx \,. \tag{38}$$

The third part of the stiffness is that which results from the soil-structure interaction, being calculated by:

$$K_{So} = \sum_{s=1}^{n} k_s \,, \text{ with } k_s = \int_{L_{s-1}}^{L_s} k_s^{so}(x)\phi(x)^2 dx \text{ and } k_s^{so}(x) = S_s D_s(x), \tag{39}$$

where $k_s^{so}(x)$ is a factor that depends on the lateral dimension, $D_s(x)$, of the foundation and of an elastic parameter, S_s, inherent to the soil type, in each layer s. Equation (40) describes the considered buckling mode:

$$\phi(x) = 1 - \cos\left(\frac{\pi x}{2L} \right). \tag{40}$$
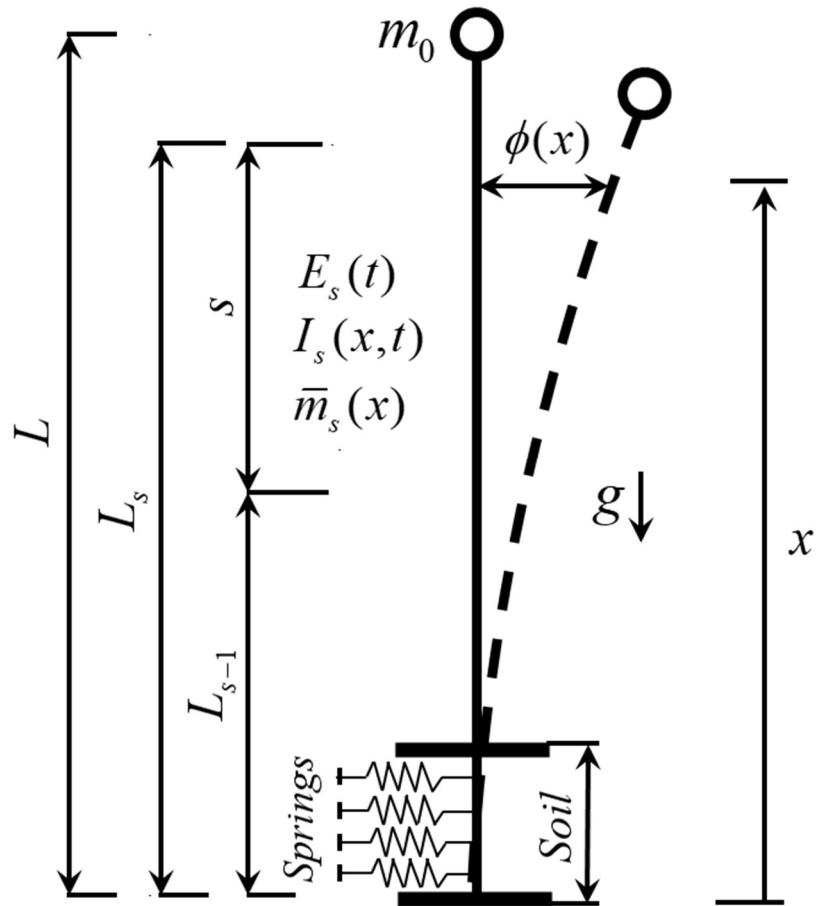
Figure 5 – Mathematical model for defining the critical buckling load.

The final stiffness of the column, *K(m₀,t),* is obtained by the sum of the previous components, resulting in:

$$K(m_0,t) = K_0(t) - K_g(m_0) + K_{So}.$$

(41)

In this context, the critical buckling load is established for the condition of zero stiffness, at each instant, *t*, of interest, according to Equation (42):

$$N_{cr}(t) = N_0(m_0)\big|_{K(m_0,t)=0}.$$

(42)

Once the instants of interest are defined, it is possible to follow the correlation of structural stiffness, Equation (41), with the force at the free end of the column, Equation

(27), and the corresponding $N_{cr}(t)$ definition (Figure 6). The results consider the soil represented by an elastic parameter equal to 2699 kN/m³.
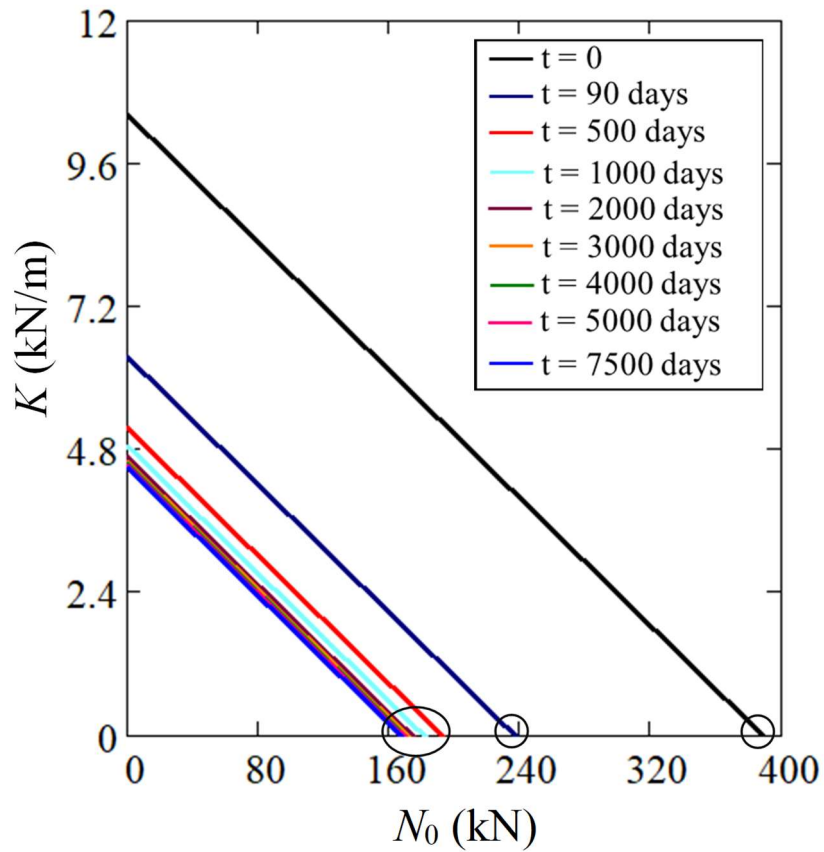
Figure 6 – Correlation of structural stiffness with the force at the free end

The comparative analysis of the results for the segments related to each cross section, assuming the loading condition at the critical buckling load, is shown in Figure 7(a) - Section *S3*; Figure 7(b) - Section *S4*, and Figure 7(c) - Section *S5*.

(a) Section *S*3

(b) Section *S*4
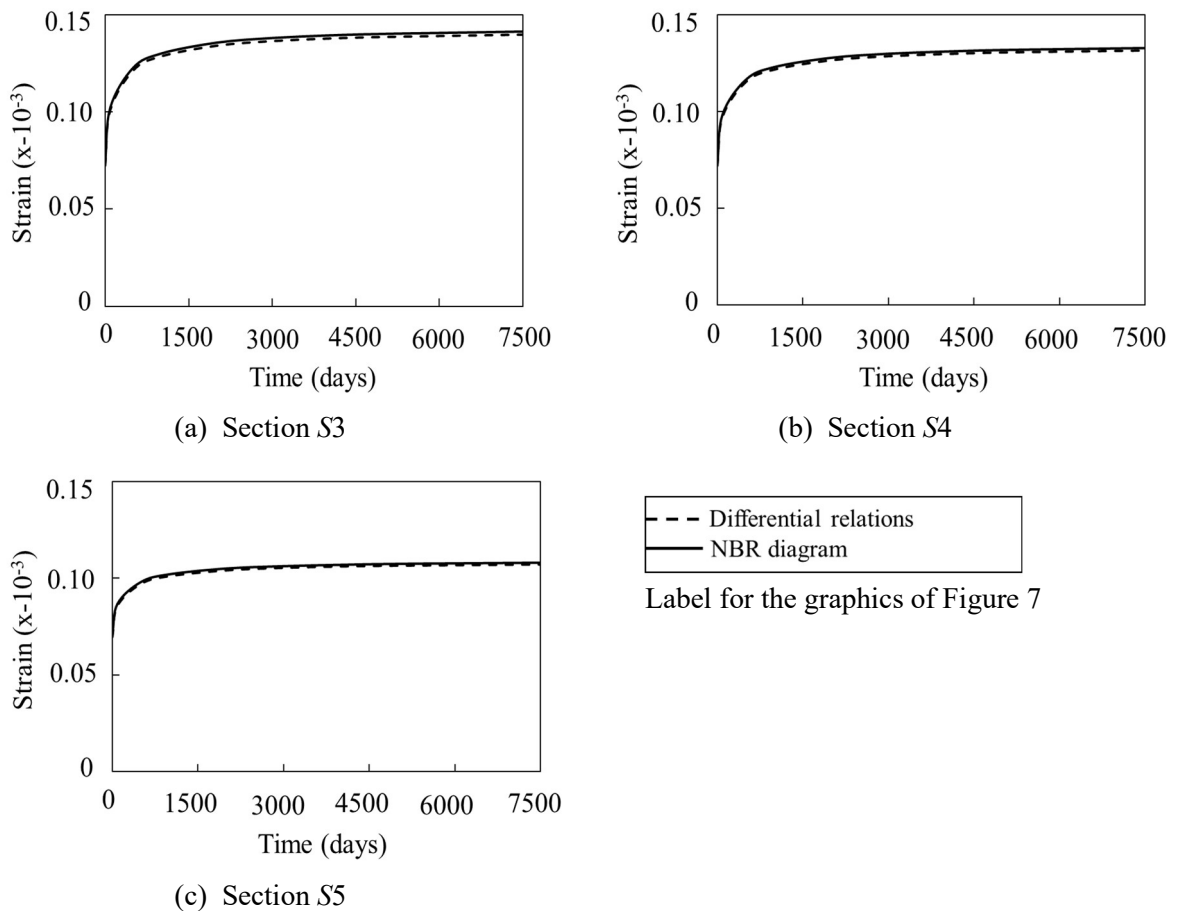
(c) Section *S*5

Figure 7 – Strains by using the stress-strain diagram and differential relations.

On the other hand, following the precepts contained in Equation (21), the stress and strain pairs for the referred sections can be determined. Figure 8 presents the stress-strain diagram for the moments of interest already defined. In the graphs in Figure 9, the upper dashed line (dash-dash) indicates the stress corresponding to 0.42f_{cd}, a value that delimits, by hypothesis, the linear behavior of concrete. The lower dashed line (dash-two dots-dash) indicates the maximum stress, σ_{max}, induced by vertical loading in the respective homogenized concrete sections.

(a) Section *S*3

(b) Section *S*4
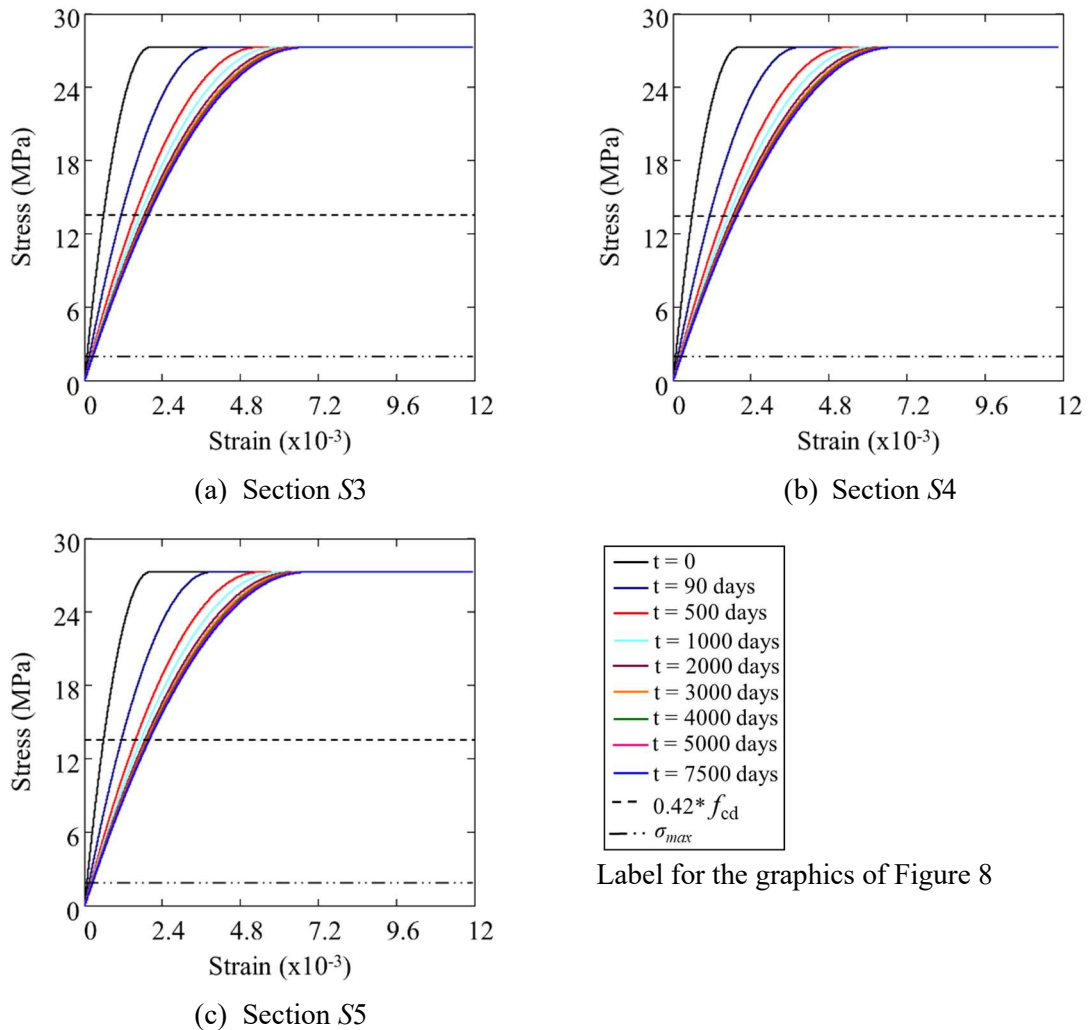
(c) Section *S*5

Figure 8 – Stress-strain diagram for different time instants in sections *S*3-*S*5

Using Equations (32) and (34), it is possible to evaluate the deformation regime for the set of forces applied at the end of the column, which varies from zero up to the load limit established by the critical buckling load. The results are presented for the initial and final time of the analysis. With this, it can be seen that there is a slight difference between both mathematical processes used for stress values close to the end of the loading.

The simple observation of the graphs in Figure 9 can lead to the assumption that there is a perfect correspondence with a straight line, either for results obtained by the stress-strain diagram or by the differential relations of displacements. However, this only holds for analyses performed by differential relations which, in fact, are linear, since

they obey Hooke's law. When the results obtained by the stress-strain diagram are carefully observed, it can be seen that the region conceptually defined to be linear is more properly characterized as a smooth curve, of long radius. This observation can be easily proven by calculating the relationships between stresses and strains for different pairs of values. In doing that, it is possible to verify the lack of a constancy of results, even for positions well below $0.42f_{cd}$.
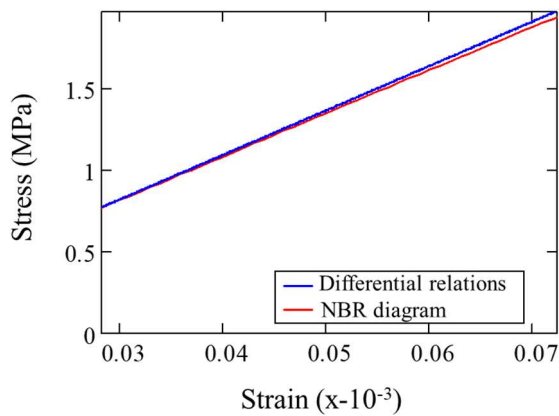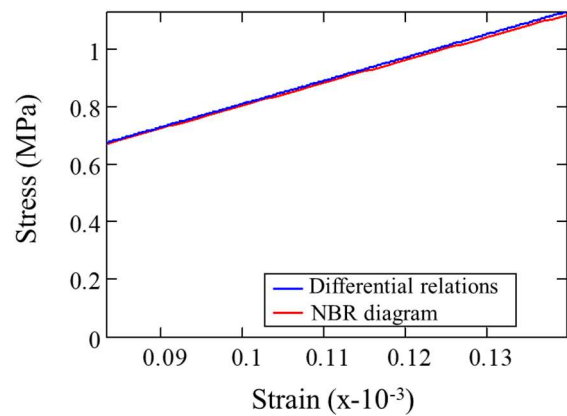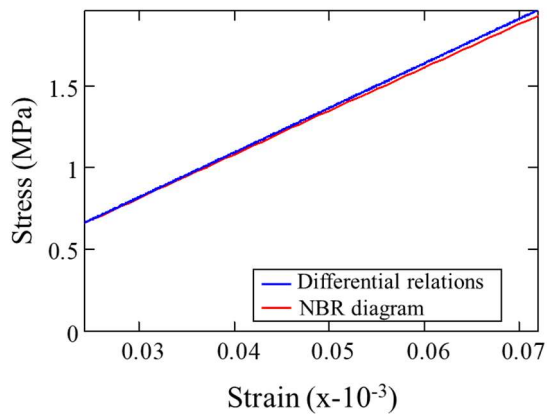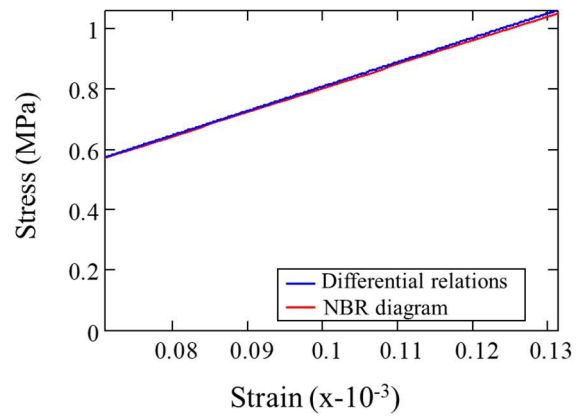
(a) Section $S3$

(b) Section $S4$

(c) Section *S5*
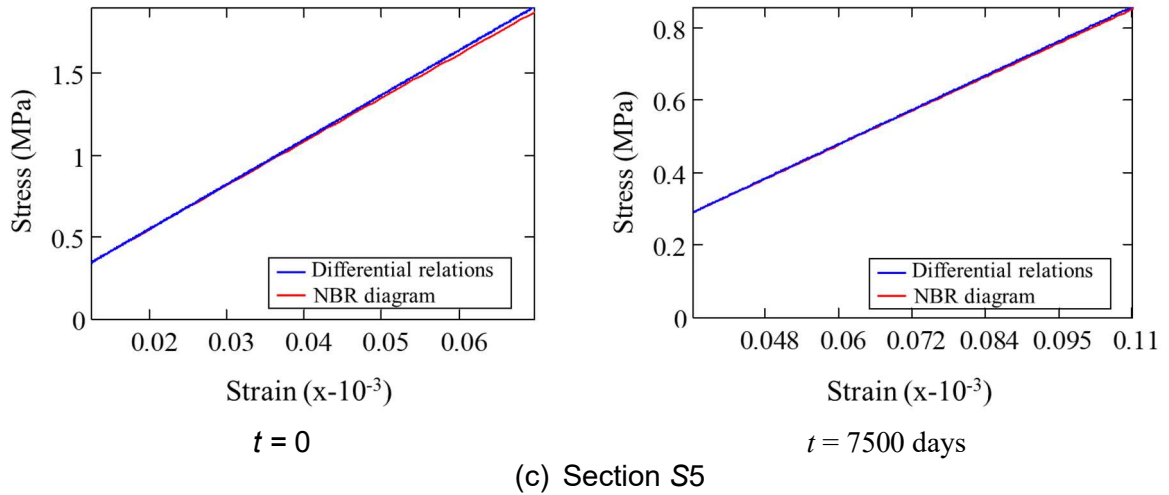
Figure 9 – Stress-strain relationship at critical buckling load

As it is imperative to verify the stress levels in the concrete, this can be done for the limit value of the loading, established by the critical buckling load, $N_{cr}(t)$, according to Equation (43), where $m_{cr}(t)$ is the mass associated with the critical buckling load, already defined in Equation (35), and $\sigma_{cS}(t)$ is the normalized stress in the concrete homogenized section:

$$v_{cS}(t) = \frac{\sigma_{cS}(t, m_{cr}(t))}{0.85 f_{cd}}.$$

(43)

The values of $N_{cr}(t)$ and $v_{cS}(t)$ in the analyzed sections, are shown in Table 3. They were calculated using the concrete modulus defined in the terms of Equation (20), with ω indicating the reinforcement ratio of each section. The graph in Figure 10 represents the advance of the normalized stresses in the homogenized concrete sections at the selected time instants. The maximum stress was found to have a value slightly higher than 7% and corresponds to the *S3* section at the initial moment of loading.

Table 3 – Critical buckling load and normalized stress in concrete

t	N_{cr}	ΔN_{cr}	v_{cS} (%)		
			A_{homS3}	A_{homS4}	A_{homS5}
(day)	(kN)	(%)	($\omega = 0.83\%$)	($\omega = 0.99\%$)	($\omega = 1.10\%$)
0	388.96	-	7.23*	7.19	6.97
90	237.33	38.98	5.22	5.03	4.42
500	192.82	18.75	4.56	4.32	3.62
1000	181.69	5.77	4.38	4.13	3.41
2000	174.38	4.03	4.26	4.00	3.27
3000	171.54	1.63	4.21	3.95	3.21
4000	170.03	0.88	4.18	3.92	3.18
5000	169.09	0.55	4.17	3.91	3.17
7500	167.78	0.77	4.14	3.88	3.14
Δ (%) =	**-56.86**	-	**42.74**	**46.04**	**54.95**

Δ = variation; N_{cr} = critical buckling load; v = normalized stress in the concrete homogenized section; ω = steel ratio; A_{homS3}, A_{homS4}, A_{homS5} are the homogenized cross-sections 3, 4, 5; * = maximum value.
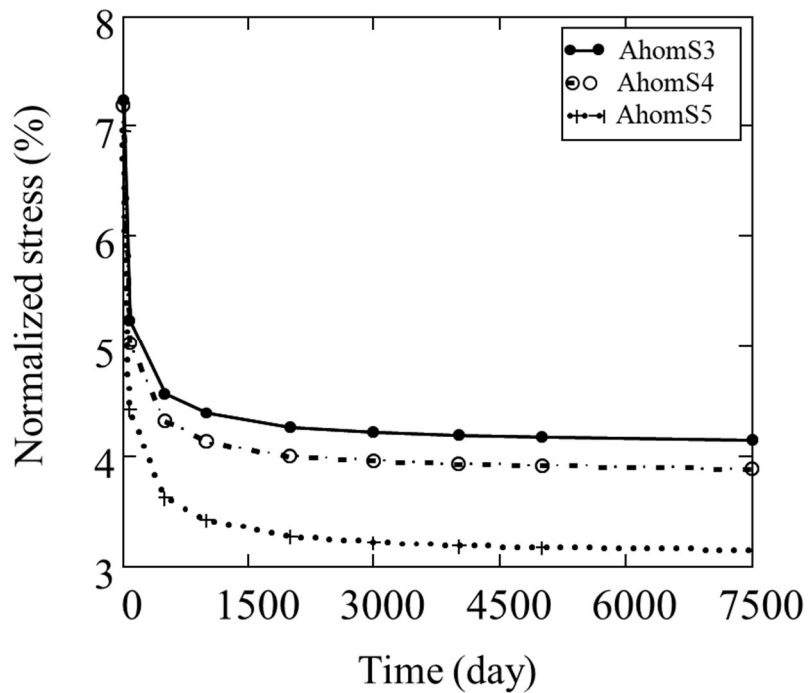
Figure 10 – Normalized stress in the concrete homogenized section in time

Through direct observation of the graph in Figure 10, it is possible to see that the stress in the concrete tends to decrease with time due to the creep of the material, that is, as the strains in the concrete increase, the stresses in the homogenized sections decrease with time. The portion of the stress that is no longer resisted by the concrete is transferred to the steel of the reinforcement [47]-[48].

In addition to the previous analyses, the absolute stress levels for each section evaluated, with the normal force applied to the top of the structure, are presented in Figure 11. The inflection points represent the imminence of collapse of the system by bifurcation of the equilibrium, which assume different values according to each instant considered.

(a) Section $S3$

(b) Section $S4$

(c) Section $S5$

Label for the graphics of Figure 11
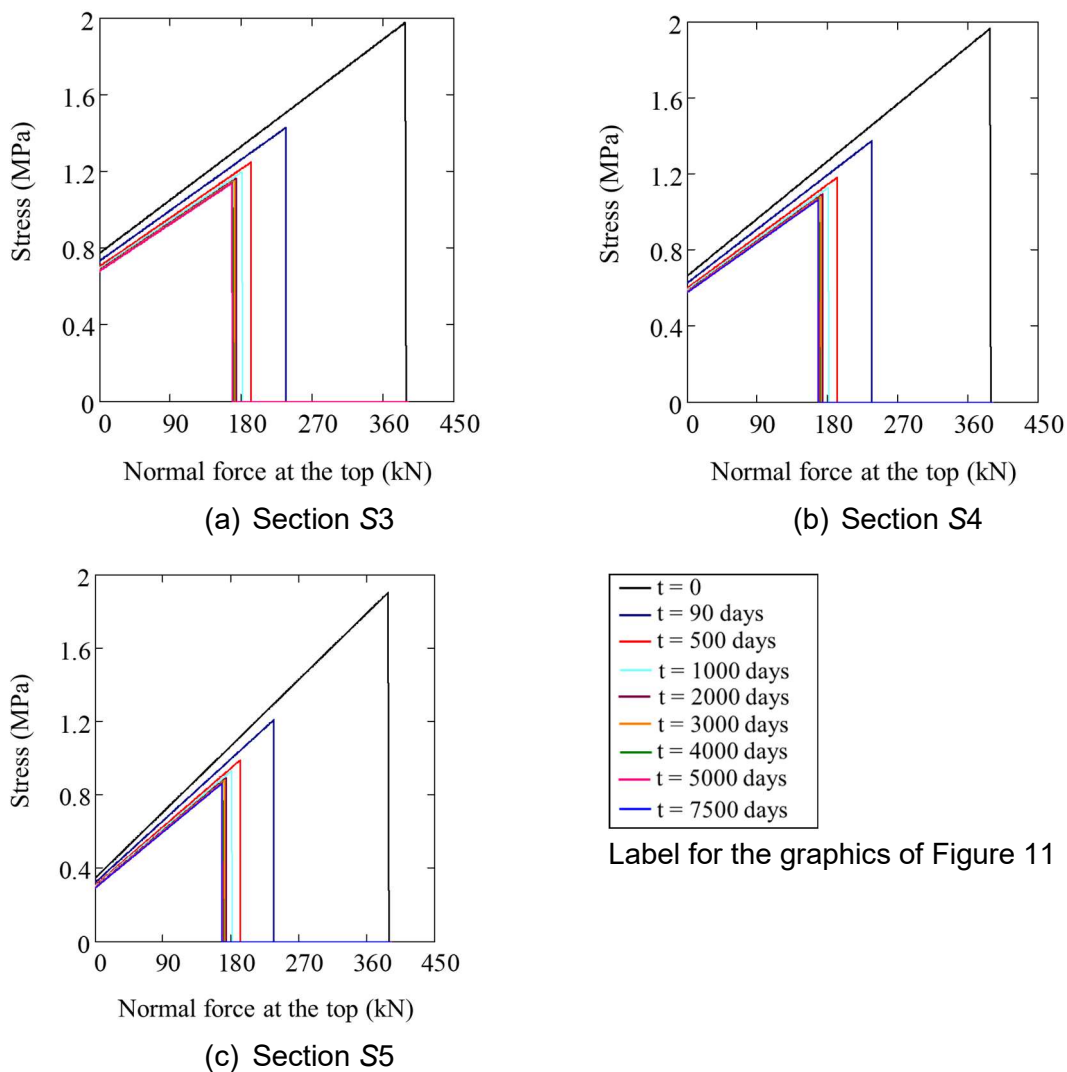
Figure 11 – Stresses with the axial force at the column end

3.12 CONCLUSIONS

In this work, two mathematical approaches were carried out to determine the strain regime imposed by axial loading, including the additional portion by creep that characterizes the rheological behavior of the material. The inclusion of creep modifies the constitutive law of the material and makes the analysis a time-dependent one. In the investigation, a slender column made of reinforced concrete, with a geometry varying along its length, was adopted for study. It was considered at a time interval of 7500 days after the system was loaded. In the end, the following conclusions can be presented:

- The maximum final strain refers to the segments above the section S3. Its value is equal to 0.141×10^{-3}, when obtained by the stress-strain diagram of the concrete, and 0.139×10^{-3}, when calculated through the differential relations of deformation: a difference of 1.07%.

- The strain variations in the segments related to sections *S3*, *S4*, and *S5*, were 47.8%, 44.8% and 34.4%, respectively, for the total time investigated when the stress-strain diagram was used. The previous percentages are situated at 48.2%, 45.2% and 34.9% when the differential relationship method is utilized. This means that, in terms of the temporal variation of strains, the initial and final values is practically the same when observed by one or the other method.

- Comparing the two mathematical procedures with each other, the time at which the analysis is performed is an intervening factor. Considering the period of 90 days, the percentage difference between the methods is 1.39%, 1.34% and 1.16%, for sections *S3*, *S4* and *S5*, respectively.

- The maximum stress level found corresponds to a little more than 7% of the design value of concrete cylinder compressive strength, revealing that the stresses induced by the maximum vertical loading, in the analyzed case, remained in the region assumed to be linear elastic behavior of the concrete.

- The comparative study of the results, points to a good agreement between the normative stress-strain curve of the concrete and the calculations made with the

differential relations of displacements for the entire set of forces analyzed, whose value extends to the critical buckling load. This evidence suggests the authorization of the use of Hooke's law for the deformation region of the material considered as linear.

- However, it is important to point out that, although the normative reference defines the existence of a linear region of strains, the equation suggested to describe this behavior cannot accurately associate it with a straight line; it is more appropriately characterized as a smooth curve.

3.13 REFERENCES

[1]   Brazilian Association of Technical Standards. NBR 6118: Design of concrete structures – Procedure (Associação Brasileira de Normas Técnicas. NBR 6118: Projeto de estruturas de concreto – Procedimento), Rio de Janeiro, 2014 (in Portuguese).

[2]   American Concrete Institute ACI, Prediction of creep, shrinkage, and temperature effects in concrete structures. ACI-209R-08, ACI Committee 209, 2009.

[3]   European Standard. Eurocode 2: Design of concrete structures - Part 1: General rules and rules for buildings. EN 1992-1-1, European Committee for Standardisation, Brussels, 2004.

[4]   Gino D, Castaldo P, Giordano L and Mancini G. Model uncertainty in non-linear numerical analyses of slender reinforced concrete members, Struct Concr 2021; 22: 845-870. https://doi.org/10.1002/suco.202000600

[5]   Castaldo P, Gino D, Marano GC and Mancini G. Aleatory uncertainties with global resistance safety factors for non-linear analyses of slender reinforced concrete columns, Eng Struct 2022; 255:113920. https://doi.org/10.1016/j.engstruct.2022.113920

[6]   MacGregor JG and Breen JE. Design of slender concrete columns. J Proc, 67(1), 1970, p.6–28.

[7]   Head M and Aristizabal-Ochoa JD. Analysis of prismatic and linearly tapered reinforced concrete columns. J Struct Eng 1987; 113(3):575–589. https://doi.org/10.1061/(ASCE)0733-9445(1987)113:3(575)

[8]   Candappa D, Sanjayan J and Setunge S. Complete triaxial stress–strain curves of high-strength concrete. J Mater Civ Eng 2001; 13(3):209–215. https://doi.org/10.1061/(ASCE)0899-1561(2001)13:3(209).

[9]   Khuntia M and Ghosh SK. Flexural stiffness of reinforced concrete columns and beams: experimental verification. Struct J 2004; 101(3):364–374. https://doi.org/10.14359/13096

[10]   Li QS. A stability of non-uniform columns under the combined action of concentrated follower forces and variably distributed loads. J Construct Steel Res 2008; 64(3):367–376. https://doi.org/10.1016/j.jcsr.2007.07.006

[11]   Mutyalarao M, Bharathi D and Rao BN. Dynamic stability of cantilever columns under a tip-concentrated subtangential follower force. Math Mech Solids. 2013;18(5):449-463. https://doi.org/10.1177/1081286512442436

[12]   Alkloub A, Allouzi R and Naghawi H. Numerical Nonlinear Buckling Analysis of Tapered Slender Reinforced Concrete Columns. Int J Civ Eng 2019; 17, 1227–1240. https://doi.org/10.1007/s40999-019-00395-5

[13]   Zhao YP, Li L and Jin M. Stability of the neutral equilibrium of columns with a rotational end restraint by the generalized Fourier series. Math Mech Solids. 2020; 25(4):961-967. https://doi.org/10.1177/1081286519897110

[14]   Ye JB, Cai J, Chen QJ, Liu X, Tang XL and Zuo ZL. Experimental investigation of slender RC columns under horizontal static and impact loads. Structure. 2020; 24: 499-513. https://doi.org/10.1016/j.istruc.2020.01.034

[15]   Sadeghi K and Nouban F. Analysis of RC Beam-Columns Subjected to Monotonic and Cyclic Oblique Shear and Axial Loading. Int J Civ Eng 2021; 19, 733–748. https://doi.org/10.1007/s40999-021-00603-1

[16]   Gao M and Jin M. Stability of the critical equilibrium of a compressed column on a Winkler foundation. Math Mech Solids. 2022; 27(7):1222-1232. https://doi.org/10.1177/10812865211061593

[17]   Bingham EC. Rheology. I. The Nature of Fluid Flow, Vol.6, N.6. Lafayette College, Easton, Pennsylvania, USA, 1929. https://pubs.acs.org/doi/pdf/10.1021/ed006p1113

[18]   Davoli E, Roubček T and Stefanelli U. A note about hardening-free viscoelastic models in Maxwellian-type rheologies at large strains. Math Mech Solids. 2021; 26(10):1483-1497. https://doi.org/10.1177/1081286521990418

[19]   Faria R., Leitão L, Teixeira L, Azenha M and Cusson D. A structural experimental technique to characterize the viscoelastic behavior of concrete under restrained deformations. Strain 2017; 53(1), e12216. https://doi.org/10.1111/str.12216

[20]   Lapasin R and Pricl S. Rheology: Rheology of Industrial Polysaccharides: Theory and Applications. Springer, Boston, MA, 1995. https://doi.org/10.1007/978-1-4615-2185-3_3

[21]   Gilbert RI and Ranzi G. Time-dependent behaviour of concrete structures. 1st ed. CRC Press, p.443, 2010.

[22]   Kim JK and Lee SS. The behaviour of reinforced concrete columns subjected to axial force and biaxial bending. Eng. Struct 2000; 22: 11,1518–1528. https://doi.org/10.1016/S0141-0296(99)00090-5

[23]   Kwak GK and Kim JK. Ultimate resisting capacity of slender RC columns. Comput Struc 2004; 82: 11-12, 901–915. https://doi.org/10.1016/j.compstruc.2004.02.019

[24]   Bonet, JL, Romero ML, Miguel PF and Fernandez MA. A fast stress integration algorithm for reinforced concrete sections with axial loads and biaxial bending. Comput Struc 2004; 82: 2-3, 213–225. https://doi.org/10.1016/j.compstruc.2003.10.009

[25]   Pallarés L, Miguel PF and Fernández-Prada MA. A numerical method to design reinforced concrete sections subjected to axial forces and biaxial bending based on ultimate strain limits. Eng Struct 2009; 31: 12, 3065–3071. https://doi.org/10.1016/j.engstruct.2009.08.006

[26]   Kwak HG and Kwak JH. An improved design formula for biaxially loaded slender RC column. Eng Struct 2010; 2:(1) 226–237. https://doi.org/10.1016/j.engstruct.2009.09.009

[27]   Hamed E and Cynthia. Geometrically and materially nonlinear creep behaviour of reinforced concrete columns. Structures 2016; 5, 1-12. https://doi.org/10.1016/j.istruc.2015.07.001

[28]   Pires SDL and Silva MCATD. Optimization of slender reinforced concrete columns subjected to biaxial bending using genetic algorithms. Rev IBRACON Estrut Mater 2021; 14: e14610. https://doi.org/10.1590/S1983-41952021000600010

[29]   Mehta PK and Monteiro PJM. Concrete: Microstructure, Properties and Materials, McGraw-Hill, New York, 2017

[30]   Theiner Y, Drexel M, Neuner M and Hofstetter G. Comprehensive study of concrete creep, shrinkage, and water content evolution under sealed and drying conditions. Strain 2017; 53(2): e12223. https://doi.org/10.1111/str.12223

[31]   Liu R, Ye H, Liu Y, Zhao H, Correia JÁ and Xin H. Numerical simulation of concrete creep behaviour using integral creep algorithm with alternating stresses. Structures 2021; 29: 1979-1987. https://doi.org/10.1016/j.istruc.2020.11.081

[32]   Magalhães KMM, Brasil RMLRF, Wahrhaftig AM, Siqueira GH, Bondarenko I and Neduzha L. Influence of Atmospheric Humidity on the Critical Buckling Load of Reinforced Concrete Columns. Int. J Struct Stab Dyn 2022; 22: 2250011-1–225011–24. https://doi.org/10.1142/S0219455422500110

[33]   Gardner NJ and Zhao J-W. Creep and Shrinkage Revisited ACI Materials Journal 1993; 90(3):236-246. https://doi.org/10.14359/3875

[34]   Shenoi RA, Allen HG, and Clark SD. Cyclic creep and creep-fatigue interaction in sandwich beams. J Strain Anal Eng Des 1997;32: 1-18. https://doi.org/10.1243/0309324971513175

[35]   Fantilli AP and Vallini P. Strains in steel bars of reinforced concrete elements subjected to repeated loads. J Strain Anal Eng Des 2004; 39(5): 447–457. https://doi.org/10.1243/0309324041896489

[36]   Madureira EL, Siqueira TM and Rodrigues EC. Creep strains on reinforced concrete columns. Rev IBRACON Estrut Mater 2013; 06: 537–560. https://doi.org/10.1590/S1983-41952013000400003

[37]   Li P and Wu YF. Stress–strain behavior of actively and passively confined concrete under cyclic axial load. Compos Struct 2016; 149:369–384. https://doi.org/10.1016/j.compstruct.2016.04.033

[38]   Zhang S and Hamed E. Application of various creep analysis methods for estimating the time-dependent behavior of cracked concrete beams. Structures 2020; 25: 127-137. https://doi.org/10.1016/j.istruc.2020.02.029

[39]   Wahrhaftig AM, Magalhães KMM and Siqueira GH. Evaluation of limit state of stress and strain of free-fixed columns with variable geometry according to criteria from the Brazilian code for concrete structures. Lat Am J Solids Struct 2020; 17: 1–19. https://doi.org/10.1590/1679-78255780

[40]   Wahrhaftig AM, Silva MA and Brasil RMLRF. Analytical determination of the vibration frequencies and buckling loads of slender reinforced concrete towers. Lat Am J Solids Struct 2019; 16(05). https://doi.org/10.1590/1679-78255374

[41]   Hooke R. LECTURES De Potentia Restitutiva, OR OF SPRING Explaining the Power of Springing Bodies, Printed for John Martyn to the Royal Society, London, UK, 1678.

[42]   Kataoka LT, Marques AC, Machado MAS and Bittencourt TN. Acquisition control and health monitoring of creep in concrete specimens. Rev IBRACON Estrut Mater 2009, 2, 271-281. https://doi.org/10.1590/S1983-41952009000300005

[43]   Wahrhaftig AM. Time-dependent analysis of slender, tapered reinforced concrete column. Steel Compos Struct 2020; 36: 229–247. https://doi.org/10.12989/scs.2020.36.2.229

[44]   Pruchnicki E. On the homogenization of a nonlinear shell. Math Mech Solids. 2019; 24(4):1054-1064. https://doi.org/10.1177/1081286518768674

[45]   Wahrhaftig AM, Magalhães KMM; Silva, MA, Brasil RMLRF and J, Banerjee R. Buckling and free vibration analysis of non-prismatic columns using optimized shape functions and Rayleigh method, European Journal of Mechanics - A/Solids. (2022), 94, 104543. https://doi.org/10.1016/j.euromechsol.2022.104543

[46]   Wahrhaftig AM., Magalhães, KMM and Nascimento, LSMSC. Stress assessment in reinforcement for columns with concrete creep and shrinkage through

Brazilian technical normative. J Braz. Soc. Mech. Sci. Eng., 2021, 43, 6. https://doi.org/10.1007/s40430-020-02731-6

[47]   Kataoka LT and Bittencourt TN. Numerical and experimental analysis of time-dependent load transfer in reinforced concrete columns. Rev IBRACON Estrut Mater 2014; 07: 1–14. https://doi.org/10.1590/S1983-41952014000500003

4 PAPER 02

4.1 COMPLETE CITATION FORMAT

Magalhães KMM, Brasil RMLRF, Wahrhaftig AM, Siqueira GH, Bondarenko I and Neduzha L. Influence of Atmospheric Humidity on the Critical Buckling Load of Reinforced Concrete Columns. Int. J Struct Stab Dyn 2022; 22: 2250011-1–225011–24.

4.2 ABOUT THE JOUNAL AND IMPACT FACTOR

The aim of the International Journal of Structural Stability and Dynamics is to provide a unique forum for the publication and rapid dissemination of original research on stability and dynamics of structures. According to the journal site: papers devoted to all aspects of structural stability and dynamics (both transient and vibration response), ranging from mathematical formulations, novel methods of solutions, to experimental investigations and practical applications in civil, mechanical, aerospace, marine, bio- and nano-engineering will be considered to published. Its impact factor is 2.597.

4.3 TITLE

Influence of Atmospheric Humidity on the Critical Buckling Load of Reinforced Concrete Columns

4.4 ABSTRACT

In this paper, an evaluation of the influence of atmospheric humidity on the critical buckling load of reinforced concrete columns is performed. A particular case consisting of a real, extremely slender reinforced concrete pole was taken for the study. The

chosen mathematical procedure for calculating the critical load is based on the Mechanics of Deformable Solids due to variations of structure vibration frequency over time. The rheological behavior of concrete related to creep and shrinkage, which illustrates the time-dependent aspect of the problem, was also considered in the analysis following normative recommendations from the Brazilian Association of Technical Standards (ABNT). In order to evaluate value changes of critical buckling loads, different time instants after loading the structure as well as different relative humidity from 0% to 100%, in 10% increments were considered. According to the selected criteria, it was possible to verify that a higher atmospheric humidity decreases the water transport from the interior out to the exterior surfaces of concrete, hence positively influencing structure stiffness. Therefore, the lowest reduction on critical buckling was 41.9% at 100% relative atmospheric humidity, versus the highest 60.7% at 0% relative humidity. A period of 7500 days after loading the structure was considered in the analysis.

4.5 KEYWORDS

Critical buckling load; shrinkage; creep; relative humidity.

4.6 DIGITAL OBJECT IDENTIFIER (DOI)

4.7 INTRODUCTION

Reinforced concrete is a material formed by fragments of aggregates and a hydraulic binder (cement). The water that activates chemical reactions in the cement have a direct influence on the properties of the reinforced concrete, since it is essentially related to hardening and workability [1].

When reinforced concrete structures are exposed to the environment, they may be subjected to atmospheric humidity variations, thus affecting its rheological properties: creep and shrinkage. Creep is defined as increase in strain with time under constant stress level while shrinkage is defined as volume reduction in concrete specimens, even when no external loads are applied [2]. Since creep and shrinkage are related to water loss from a saturated cement paste, environment humidity becomes an essential factor for their determination [3]-[7].

Absorbed water diffusion and water held by capillary tensile stress in cement paste are time-dependent process that occur over long periods of time [8]. Troxell et al. [9] studied these phenomena through creep and drying shrinkage experiments, including long term analysis, different concrete mix proportioning as well as different types of aggregates, environment and load conditions. According to Troxel et al. [9] conclusions, an increase in the atmospheric humidity slows down the relative rate of water flow from the interior to the outer surfaces of concrete, i.e., a drier the environment produces a higher creep coefficient. Due to this matter, Madureira and Fontes [10] evaluated temperature influences on creep of reinforced concrete structural elements, particularly observing that temperature increments speed up creep effects and also steel yielding, since the increase in reinforcing bars stresses due load transfer from concrete may occur earlier. Besides, this effect may also initialize concrete's cracking process, endangering steel corrosion which could decrease durability and serviceability of the structure over its lifetime, according to conclusions obtained by Shaikh [11].

Although relative atmospheric humidity variation is a phenomenon that is difficult to predict in creep and shrinkage experiments, as postulates Wei et al. [12], there are several studies published in academic literature that seek to evaluate the relationship between environmental exposure and rheological behavior [13]-[18]. Following this same line of research, Nastic et al. [19] performed experimental investigations in which the concrete was exposed to a relative humidity percentage less than 20%, hence observing creep and shrinkage behaviors along 110 days and also comparing the obtained results with formulations suggested in reinforced concrete design codes. In the end of the study, it was possible to conclude that the relative humidity percentages from evaluated normative codes are generally underestimated. On the other hand, Zhang et al. [20] studied creep and shrinkage development, correlating internal relative humidity levels with global deformation of structures at time instants next the concrete placing period. Applications from evaluation of relative environmental humidity influences on creep effects on real structures, such as slender buildings, can be found in Chowdhary e Sharma [21].

Regarding integrity analysis of slender columns designed in reinforced concrete, a direct relationship is noticed between the composite's nonlinear behavior and its load capacity [22]. From that, Weng et al. [23] implemented investigations in which alternative methods were proposed, though simplified, to identify the instant when buckling of reinforced concrete columns occur. Although buckling studies began in Statics, in Rational Mechanics, this is a phenomenon with typically dynamic characteristics since it involves the equilibrium of mechanical systems. Particularly of reinforced concrete columns, stability determination, from Statics or Dynamics approaches, can be found in the work developed by Sharma et al. [24]-[25], respectively.

Concrete is a composite material. Therefore, concrete's properties depend on its components features, which may vary with time, temperature, environment conditions, and applied loads [26]. Specifically, reinforced concrete is a composite material that consists essentially of an association between concrete and a structural steel with low carbon content named reinforcement. The basic design hypothesis resides on the

perfect adherence between these materials. Design codes for reinforced concrete structures, e.g., ACI [27], Eurocode [28] and ABNT [29], present simplified formulations seeking to systematize the process of considering rheological behavior of concrete, also allowing calculations of load capacity of structural columns, or even contributing for strain prediction. In this context, comparisons among different mathematical procedures for determining the rheological behavior of concrete can be found in Goel et al. [30]. In general, mathematical models applied to predict creep can be represented by a time-dependent function associated with viscoelastic rheological models based on springs and dampers associations that seek to appropriately describe behavior over time, reliant to individual characteristics of the materials.

Seeking to evaluate critical buckling load variations in slender reinforced concrete columns, also considering concrete rheological behavior and different environment exposure conditions, i.e., different atmospheric humidities, in this paper a mathematical analysis by using Dynamics approach was developed in order to evaluate relative atmospheric humidity influences on the determination of critical buckling loads of a real slender column, made of reinforced concrete. The criteria for considering creep and shrinkage were in accordance with recommendations from ABNT NBR6118 [29]. The Brazilian Association of Technical Standards (Associação Brasileira de Normas Técnicas – ABNT) is internationally known for its high-quality level, being ISO 9000 certified as well. In the presented context, the study in this paper comes after two previous developed works [31]-[32]. In the first article, [31], the mathematical model established to calculate critical buckling loads was evaluated by comparison with Finite Element Method (FEM) results, using computer modelling. In the second article, [32], moment of inertia variations over time due homogenization of cross-sections subjected to creep were included to structural stiffness portions. In both cases, the relative humidity was considered constant. Thus, the present article brings an additional step in the investigation, since it includes several relative atmospheric humidity percentages in the analysis, as well as analysis of the column load capacity for different periods of time.

4.8 DETERMINATION OF CRITICAL BUCKLING LOAD

When developing a mathematical model that seeks to determinate critical buckling loads, it is crucial to define a theoretical model capable of representing, as accurately as possible, the actual behavior of the structure being analyzed. The developed model in this paper is based on the principle of virtual works and also generalized coordinates. The model allows the column to have properties varying along the length, such as geometry, elasticity or viscoelasticity, density, and reinforcement arrangement. Springs are applied to represent the lateral soil-structure interaction. With these conditions, the column is under the influence of gravitational forces originated from the distributed mass due to self-weight of the structure and other added masses; and of a concentrated mass at the top free end, to be defined at the event of loss of stability. It was adopted the hypothesis of free vibration mode, undamped, as well as small displacements condition, when the normal force direction does not change the implementation of the chosen function applied to describe the vibration (or buckling) mode. It is important to note that the analytical model is based on the frequency and natural mode of vibration, that is an intrinsic characteristic of the structure (column) [33]-[37].
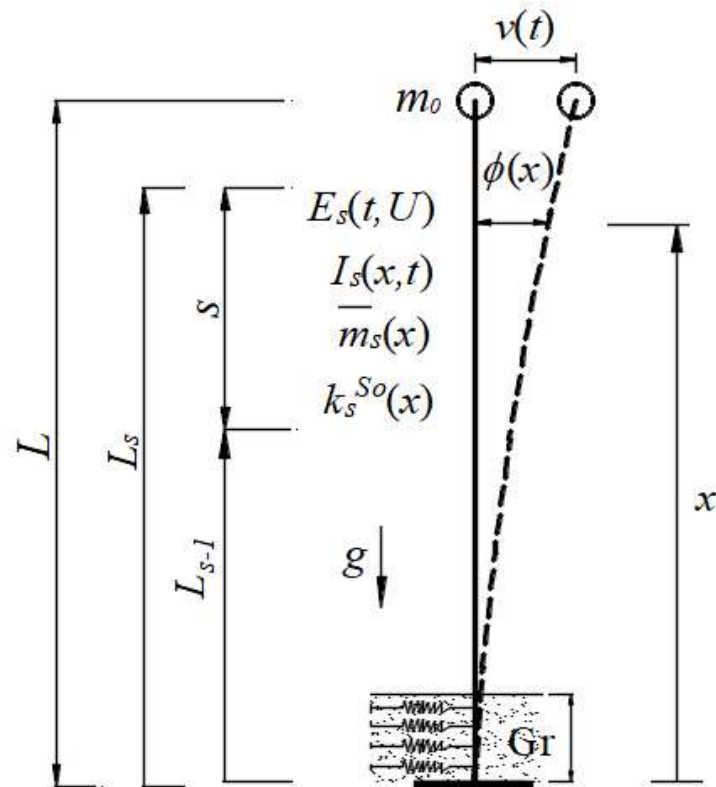
Figure 1 - Mathematical model

Figure 1 represents the proposed model, where: $\phi(x)$ is a function to approximate the shape of the vibratory movement or buckling, known as shape function – an important parameter to evaluate structures using a dynamic approach in "trial functions" method [38]-[39], t indicates time; L is the total length of the column; L_s and L_{s-1} are heights at the superior and inferior limits of a segment s, respectively; k_s^{So} represents soil stuffiness; E_s is the concrete elastic/viscoelastic module; $\bar{m}_s$ is the distributed mass along the length; I_s is the cross section inertia; g is the gravitational acceleration; Gr indicates the buried portion of the column and v is the generalized coordinate, which depends on the boundary conditions of the problem – in this case, the free end. The proposed formulation is based on dynamics principles, for which the first vibration frequency of the column is applied to determinate the event of loss of stability by bifurcation of equilibrium.

Applying the Principle of Virtual Work (PVW) and its derivatives, dynamic properties of the system can be obtained, i.e.: conventional elastic stiffness K_0, calculated using

Equation (1); geometric stiffness, K_g, obtained from Equation (3); and the portion regarding the effective soil stiffness, K_{Soil}, calculated with Equation (9). Therefore:

$$K_0(t,U) = \sum_{s=1}^{n} k_{0s}(t,U)'$$ (1)

where k_{0s} is the term that represents variations of stiffness over time, being calculated by Equation (2):

$$k_{0s}(t,U) = \int_{L_{s-1}}^{L_s} E_s(t,U) I_s(x,t) \left(\frac{d^2\phi(x)}{dx^2}\right)^2 dx$$ (2)

in which E_s is the concrete elastic/viscoelastic module, function of time t and relative environment humidity U; I_s is the moment of inertia of the section that varies along the segment, taken according to the considered movement, obtained by interpolation of subsequent sections, all homogenized in time for considering the presence of reinforcement; and K_g is the geometric stuffiness obtained by Equation (3):

$$K_g(m_0) = \sum_{s=1}^{n} k_{gs}(m_0)$$ (3)

where:

$$k_{gs}(m_0) = \int_{L_{s-1}}^{L_s} \left[N_0(m_0) + \sum_{s+1}^{n} N_s + \bar{m}_s(x)(L_s - x)g \right] \left(\frac{d\phi(x)}{dx}\right)^2 dx$$ (4)

in which the normal force at the column free end, N_0, becomes a variable that depends on the concentrated mass, m_0, also located at the free end, obtained by multiplying the mass by the gravitational acceleration g. N_s represents the normal force in the segments above the considered one, which can be obtained from Equation (5),

$$N_s = \int_{L_{s-1}}^{L_s} \bar{m}_s(x)g dx \qquad (5)$$

where $\bar{m}_s$ is the mass per unit length, defined by the product between material density and area of the considered section according to Equation (6),

$$\bar{m}_s(x) = A_s(x)\rho_s \qquad (6)$$

where A_s represents the cross-section, which can be the tapered or not, area and ρ_s is the material density for the respective segment s. Therefore, the generalized mass of the system, which includes both the lumped mass at the free extremity and the contribution of the column's self-weight, is obtained by observing Equation (7):

$$M(m_0) = m_0 + m, \qquad (7)$$

with

$$m = \sum_{s=1}^{n} m_s \quad \text{and} \quad m_s = \int_{L_{s-1}}^{L_s} \bar{m}_s(x)(\phi(x))^2 dx, \qquad (8)$$

In order to include the soil influence in the equilibrium of the system, it is necessary to represent it as a series of translational vertically distributed springs along the foundation. Thereby, the soil contribution to the structure stiffness can be defined as:

$$k_{soil} = \int_{L_{s-1}}^{L_s} k_s^{So}(x)\phi(x)^2 dx, \qquad (9)$$

in which the parameter k_s^{So} is an elastic property along the depth of the foundation. Considering positive the normal force, the total stiffness can be calculated by the expression:

$$K(m_0,t,U) = K_0(t,U) - K_g(m_0) + K_{Soil} \text{,}$$ (10)

and finally, Equation (11) allows the determination of the first natural vibration frequency as a time-dependent function, considering the generalized stiffness portion, *K*, and the concentrated mass at the free end, *M*:

$$f(m_0,t,U) = \frac{1}{2\pi} \sqrt{\frac{K(m_0,t,U)}{M(m_0)}} \text{.}$$ (11)

It is important to state that if some of the mentioned parameters, as functions of *x* and/or *t*, are constant over the segment length and time, these variables become known and assume constant values. In the previous equations, $\phi(x)$ is the shape function of the problem, established according to boundary conditions of the column. In the present study, Equation (12) refers to free-fixed columns,

$$\phi(x) = 1 - \cos\left(\frac{\pi x}{2L}\right) \text{,}$$ (12)

where *x* is the geometric variable of the problem, beginning at the base of the system. Other functions may be used, depending on particulars conditions for the case being analyzed. The previous equation represents the solution of the first buckling mode for columns with boundaries conditions as indicated in Figure 1, since when x = 0, $\phi(0) =$ 0 and x = v, $\phi(v) = 1$, as also shown in Figure 3(c). It is worth mentioning that results from frequencies or natural periods of vibration were applied by Reis et al. [40] when determining the susceptibility to second-order effects as well as when evaluating stability of reinforced concrete buildings.

Should be emphasized that the shape function choice regulates the approximation accuracy that must at least obey the essential boundary conditions of the problem (kinematic boundary conditions). For this paper, the chosen shape function respects the essential and natural boundary conditions (internal forces) in a certain way that no artificial stiffnesses are introduced in the generalized coordinate system. The

formulation presented above may be applied for calculating structural frequency as well as for defining critical buckling load. Specially in the latter case, the final force is obtained when the frequency of vibration becomes zero. More details of the mathematical procedure and its applications for the studied structure can be found in Ref. [41]-[44].

4.9 REOLOGICAL BEHAVIOR ACCORDING TO DESIGN CODES

A mathematical alternative for considering rheological behavior of concrete consists in adopting models for predicting creep and shrinkage as presented in ABNT NBR611829, approach that does not prevent the use of other design codes. Once included in the problem, the analysis of instability of reinforced concrete columns becomes time-dependent, since the modulus of elasticity is also time-dependent. According to ABNT NBR611829 proposal for calculating creep and shrinkage, when concrete stresses show no significant variations, the following simplifying assumptions are taken: creep deformation varies linearly with applied stress; for stress increments at different time instants, it is possible to superpose their effects, and initial deformations generate constant deformations over time. Therefore, deformations due creep can be calculated by using Equation (13):

$$\varepsilon_c(t,U) = \sigma_c(t_0)E_s(t,U) \text{,}$$ (13)

where εc is the strain at the particular time t (in days), σ_c is the compressive stress at t_0 when the structure is loaded, and E_s is the modulus of elasticity, defined by Equation (14):

$$E_s(t,U) = \cfrac{1}{\cfrac{1}{E_{c0}}} + \cfrac{1}{\cfrac{\varphi(t,U)}{E_{c28}}}$$ (14)

where E_{c0} is the modulus of elasticity of concrete when loading starts (taken in the direction of longitudinal bars); E_{c28} is the mean modulus of elasticity (at 28 days), and

φ is the creep coefficient at concrete age t due to load applied at the age t_0, as given by Equation (15):

$$\varphi(t,U) = \varphi_a + \varphi_{f\infty}[\beta_f(t,U) - \beta_f(t_0,U)] + \varphi_{d\infty}\beta_d(t) \text{,} \tag{15}$$

in which φ_a is the elastic creep coefficient (related to initial deformation), $\varphi_{f\infty}$, according to Equation (16), is the final value for creep coefficient (related to irreversible and slow strain), depending on relative environment humidity, U, concrete consistency at placing, notional thickness of the element, age of concrete at loading (t_0) and at a particular instant of time (t), for concretes with characteristic compressive strength less than 50 MPa. For concretes with characteristic compressive strength between 50 MPa and 90 MPa, as indicated by ABNT NBR5379;45 β_f at t and t_0 are coefficients related to the slow irreversible strain depending on the age of concrete. $\varphi_{d\infty}$ is the final value of creep coefficient related to initial and reversible strain, considered constant and equal to 0.4, while β_d is the coefficient related to slow and reversible deformation for a given age of concrete after loading. Thus:

$$\varphi_{f\infty}(U) = \varphi_{1c}(U)\varphi_{2c}(U) \text{,} \tag{16}$$

in which:

$$\varphi_{1c}(U) = 4.45 - 0.035U \text{,} \tag{17}$$

where U is expressed as percentage. It is worth mentioning that φ_{1c}, as given by Equation (17), is valid for slumps in the range of 5 cm to 9 cm (following criteria for slump testes from ABNT NBR 1688941) with $U \leq 90\%$. For ambient humidity equals to 100%, the Brazilian code suggests 0.8. The parameter φ_{2c} may be calculated using Equation (18),

$$\varphi_{2c}(U) = \frac{42 + h_{fic}(U)}{20 + h_{fic}(U)},$$ (18)

where h_{fic} is the element notional thickness (in centimeters), which is a parameter calculated according to dimensions and shape of the specimen, expressed in terms of theoretical or effective thickness. This thickness can be obtained by a dividing the area of concrete section, As, by the perimeter in contact with atmosphere, Ds, as shown in Equation (19):

$$h_{fic}(U) = \frac{2\gamma(U)A_s}{\pi D_s},$$ (19)

where γ is a constant depending on the relative environment humidity given by Equation (20):

$$\gamma(U) = 1 + e^{(-7.8 + 0.1U)}.$$ (20)

Importantly, there is a limit for using this constant, restricted to relative humidities between 40 and 90 percent (40% ≤ U ≤ 90%). When the relative humidity becomes greater than 100% (including U = 100%) the constant assumes a value of 30 (γ = 30). Another variable depending on relative humidity conditions is the coefficient β_f, determined by the following Equation (21):

$$\beta_f(t,U) = \frac{t^2 + At + B}{t^2 + Ct + D},$$ (21)

where the parameters A, B, C, D e E are given from Equation (22) through Equation (26):

$$A = 40,$$ (22)

$$B(U) = 116(h_{fic}(U))^3 - 282(h_{fic}(U))^2 + 220h_{fic}(U) - 4.8 \text{ ,} \tag{23}$$

$$C(U) = 2.5(h_{fic}(U))^3 - 8.8h_{fic}(U) + 40.7 \text{ ,} \tag{24}$$

$$D(U) = -75h_{fic}^3 + 585h_{fic}^2 + 496h_{fic}(U) - 6.8 \text{ ,} \tag{25}$$

$$E(U) = -169(h_{fic}(U))^4 + 88(h_{fic}(U))^3 + 584(h_{fic}(U))^2 - 39h_{fic}(U) + 0.8 \text{ ,} \tag{26}$$

Note that the parameters B, C, D, and E are dependent on the element notional thickness (h_{fic}) which has a reference interval between 5 and 160 centimeters (5 cm $\leq$ $h_{fic} \leq$ 160 cm). For values out of that range, the corresponding extremes are adopted.

Once all necessary parameters are obtained, the strain portion related to shrinkage can be calculated as:

$$\varepsilon_s^{cs}(t,U) = \varepsilon_s^{cs\infty}[\beta_s(t,U) - \beta_s(t_0,U)] \text{ ,} \tag{27}$$

where is the final value of shrinkage, associated with the consistency of concrete and ambient humidity, as written in Equation (28), and β_s is the coefficient related to shrinkage at concrete ages t and t_0, Equation (31). Hence,

$$\varepsilon_s^{cs\infty}(U) = \varepsilon_{1s}(U)\varepsilon_{2s}(U) \text{ ,} \tag{28}$$

in which ε_{1s} is a coefficient depending on the relative ambient humidity and consistency of concrete, calculated by Equation (29):

$$\varepsilon_{1s}(U) = \left(-8.09 + \frac{U}{15} - \frac{U^2}{2284} - \frac{U^3}{133765} + \frac{U^4}{7608150} \right) 10^{-4} \text{ ,} \tag{29}$$

It is worth to remind that ε_{1s}, as given by Equation (29), is valid for slumps between 5 to 9 cm, with relative humidity between 40 and 90. For relative humidity of 100%, the strain suggested by the Brazilian code is constant and equal to -1×10^4 cm. The coefficient ε_{2s} depends on the notional thickness, which also depends on the relative humidity, among other factors, and may be expressed as in Equation (30):

$$\varepsilon_{2s}(U) = \frac{32 + 2h_{fic}(U)}{28.8 + 3h_{fic}(U)}, \tag{30}$$

$$\beta_s(t,U) = \frac{\left(\dfrac{t}{100}\right)^3 + A\left(\dfrac{t}{100}\right)^2 + B(U)\left(\dfrac{t}{100}\right)}{\left(\dfrac{t}{100}\right)^3 + C(U)\left(\dfrac{t}{100}\right)^2 + D(U)\left(\dfrac{t}{100}\right) + E(U)}, \tag{31}$$

4.10 CASE STUDY

In order to investigate atmospheric humidity influences on the determination of critical buckling loads, a real slender reinforced concrete pole with geometry varying along the height was selected. The mathematical formulation main objective was to determinate the critical buckling load by using postulations from Mechanics of Deformable Solids, observing critical buckling load sensitivity to different relative environment humidity.

The selected column is 46 m height, including a 40 m superstructure, with hollow circular cross-section, and belled shaft foundation with 140 cm diameter and 20 cm length at the base, and shaft of 80 cm diameter and 580 cm length. The column can be interpreted as an extremely slender structural system, with slenderness ratio of 408. Table 1 presents the column geometry, where D is the external diameter; th is the wall thickness; d_b and n_b are the diameter and number of reinforcement bars, respectively; c' is the concrete cover; H is the height of a segment; and S indicates a specific cross-section.

Table 1 - Cross-sections and reinforcements details

	S1	S2	S3	S4	S5
D (cm)	140	80	80	70	70
th (cm)	-	-	15	13	13
d_b (mm)	12.5	12.5	12.5	12.5	12.5
n_b (Qty)	20	20	20	20	20
c' (mm)	25	25	25	25	25
H (cm)	0-20	20-600	600-1200	1200-1900	1900-4600

Note: D = external diameter; th = section wall thickness; db and n_b = diameter and number of reinforcement bars; c' = concrete cover; H = segment height; S = cross-section; Qty = quantity.

As can be seen in Figure 2, a set of antennas and a platform are installed on the top of the structure. There are cables and ladder along the height of the structure, adding up a distributed mass of 40 kg/m. Table 2 summarizes masses and densities of the structure.

Figure 2 - Pictures of the reinforced concrete pole

Table 2 - Masses and densities

Element	Length	Density
Foundation	0-6 m	2500 kg/m^3
Superstructure	6-46 m	2600 kg/m^3

| Distributed mass | 6-46 m | 40 kg/m |
| Concentrated mass | 46 m | To be determined |

Figure 3(a) and (b), show dimension details for each cross-section, including steel bars arrangement. For this case in particular, the shape function that defines the first buckling mode obeys Equation (12), as displayed in Figure 3(c), which represents the exact solution of the problem. It is important to mention that the application of Equation (12) for non-prismatic free-fixed columns was validated by Wahrhaftig et al. [31] in comparison with other mathematical models.   Evidently the selected case is a representative of a family of similar structures, since it is a pre-cast element that could be installed in any region of the globe with different atmospheric humidity.
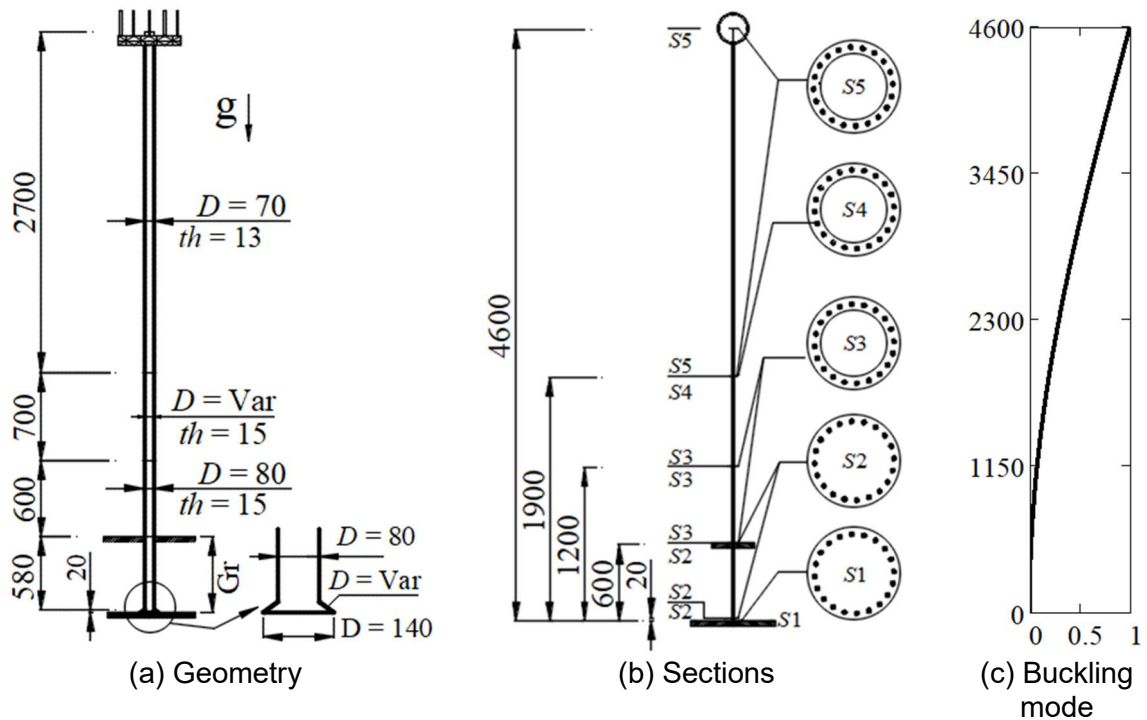

Figure 3 - Structural arrangement, in "cm".

Particularly in Brazil, a country of continental dimensions with a territory of 8.5 million square kilometers, which has pieces situated in both north and south hemispheres, climate conditions change substantially over different regions. Specially for relative humidity, the percentages may vary from 20% to 96%. Figure 4, sourced from the

National Institute of Meteorology (Instituto Nacional de Meteorologia – INMET) [47] of Brazil, shows the average annual relative humidity obtained for a period of 30 years (1981-2010) considering the state demarcation. However, as reveals the first National Assessment Report (RAN) presented in 2013 in the Brazil Panel on Climate Change (PBMC)48, the country's climate tends to become warmer and reduce relative humidity due to global climate changes.
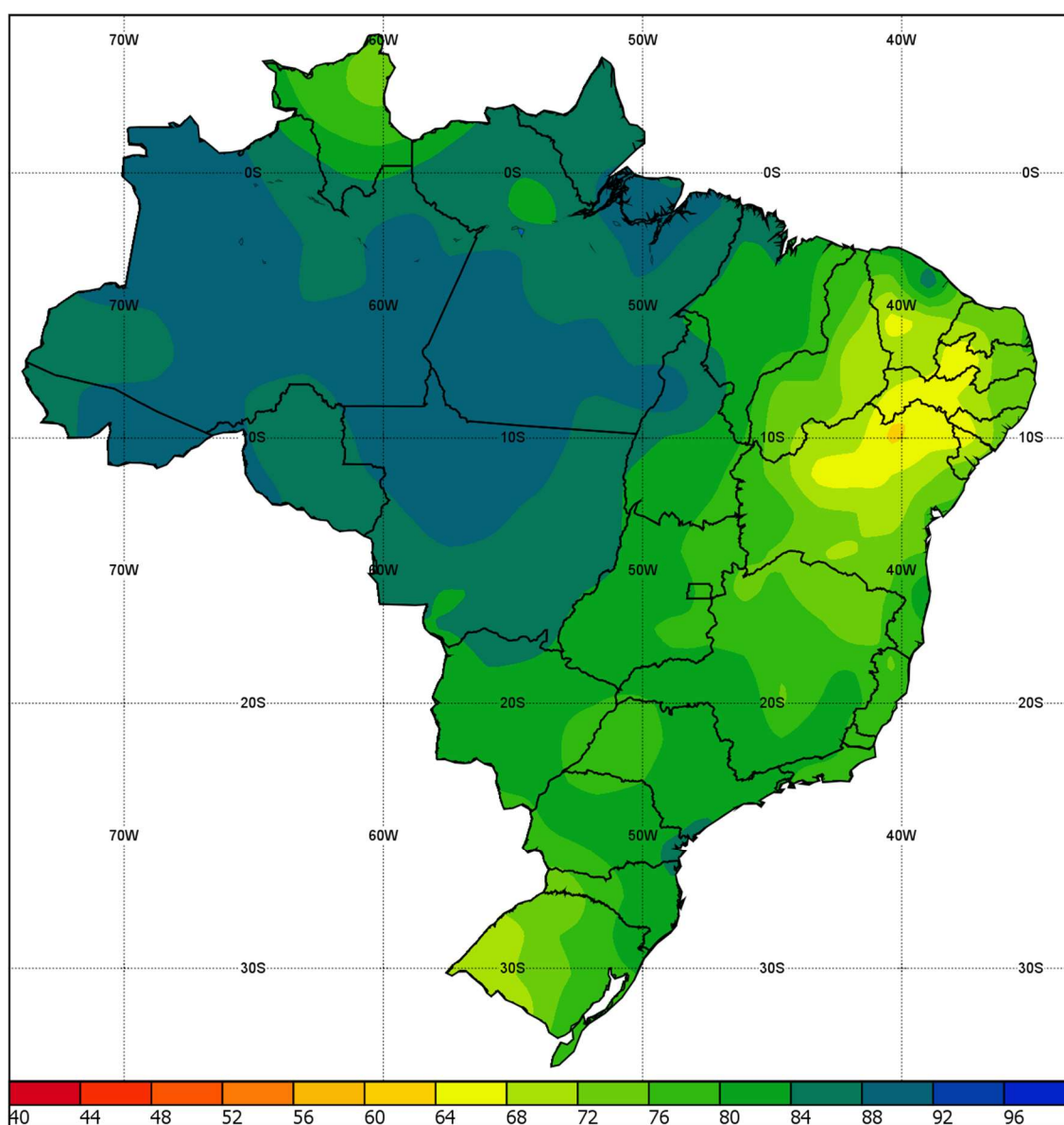

Figure 4 - Relative humidity in Brazilian regions. 30 years (1981-2010) states average [47]

Data of 2019 taken from INMET,42 Table 3, Figure 5, indicate the highest and lowest relative humidity in some Brazilian capitals.

Table 3 - Average relative humidity values of 2019 [47]

City (State Abb.)	Jan	Feb	Mar	Apr	May	Jun	Jul	Aug	Sep	Oct	Nov	Dec	Δ(%)
Aracajú (SE)	61.8	63.9	66.4	66.0	67.5	71.2	72.9	71.9	70.4	67.9	64.3	60.3	21
Belém (PA)	89.7	91.8	91.9	90.5	87.7	83.0	81.9	75.5	80.0	82.2	83.9	87.8	22
Belo Horizonte (MG)	55.5	65.5	66.4	66.6	65.8	60.2	51.8	54.4	51.8	51.8	67.8	67.3	31
Boa Vista (RR)	63.7	59.6	54.7	57.5	83.9	83.6	81.3	79.7	73.8	70.1	71.6	74.0	53
Brasília (DF)	63.2	74.5	79.2	78.4	70.3	62.1	51.9	44.2	38.2	49.1	68.8	72.6	107
Campo Grande (MT)	74.3	75.6	75.1	78.9	75.4	67.3	60.8	61.1	54.4	62.8	70.8	76.1	45
Cuiabá (PR)	74.2	80.9	82.0	81.5	85.2	80.2	75.8	77.5	-	-	-	-	15
Florianópolis (SC)	81.4	80.1	74.5	78.9	84.1	83.4	80.2	79.2	79.5	81.4	75.5	73.1	15
Fortaleza (CE)	81.6	84.7	90.1	87.1	84.4	80.1	78.2	73.0	73.4	71.9	72.6	-	25
Goiânia (GO)	59.5	71.6	70.2	70.2	63.5	51.2	45.6	39.1	*33.9	48.5	63.6	66.8	**111****
João Pessoa (PB)	72.9	78.6	79.5	80.0	77.4	81.6	82.6	79.4	76.7	73.2	70.7	73.0	17
Macapá (AP)	85.4	86.4	85.3	87.9	85.6	83.6	79.3	76.0	69.5	66.8	68.8	72.2	32
Maceió (AL)	80.9	78.3	77.0	78.5	79.8	84.6	83.2	85.0	82.5	76.4	73.0	73.3	16
Manaus (AM)	86.2	88.6	83.9	82.8	82.5	75.6	71.0	66.5	68.3	76.0	78.4	82.5	33
Natal (RN)	74.5	78.1	80.6	81.8	79.0	80.2	80.4	78.0	78.0	76.1	76.2	76.1	10
Palmas (TO)	78.5	81.0	81.8	78.8	71.8	54.9	48.1	38.8	41.3	71.3	74.3	74.7	**111****
Porto Alegre (RS)	73.3	71.2	73.8	81.0	86.1	80.9	81.6	76.0	76.1	78.8	72.5	60.5	42
Recife (PE)	77.2	80.5	81.9	85.5	86.9	83.8	88.3	84.5	82.2	78.5	68.8	67.4	31
Rio Branco (AC)	**92.4	91.0	89.7	87.4	87.0	86.1	87.6	72.8	77.1	84.3	86.6	87.7	27
Salvador (BA)	75.9	75.2	-	-	-	85.1	87.0	73.5	82.6	79.3	77.8	76.8	18
São Paulo (SP)	74.0	75.4	76.8	74.6	74.8	69.0	66.9	70.2	72.7	70.6	75.8	75.1	15
Vitória (ES)	-	75.5	74.9	77.8	-	78.4	74.5	78.0	75.7	75.1	81.0	78.2	**9***

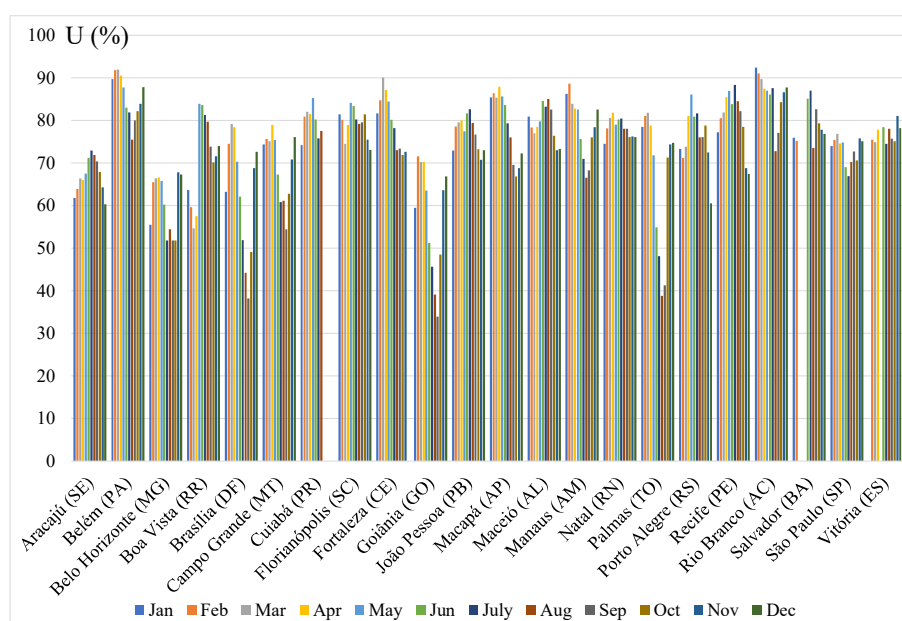Abb.= Abbreviation; *minimum; **maximum; Δ = variation

Figure 5 - Average relative humidity values for month of the year of 2019.

Figure 7, adapted from the Brazilian Institute of Geography and Statistics (Instituto Brasileiro de Geografia e Estatística – IBGE), in association with Table 4 from INMET, offers an overview of relative humidity variations over that year in the most important cities of the country, which allows the comparison with other metropolises in countries of similar characteristics. It is important to consider that what really exists in Figure 7 are localized points (cities) in a plan (map). The colored regions in there represent an approximation of possible real values. The observation of the existing data, which are depicted in Figure 6, reveals an average variation of 37% among the considered cities, with some variation occurrences reaching 111% as in Goiânia (state of Goiás) and Palmas (state of Tocantins). The minimum variation for the year of 2019, by 8%, happened in Vitória (ES). The standard deviation for that year was 32%.
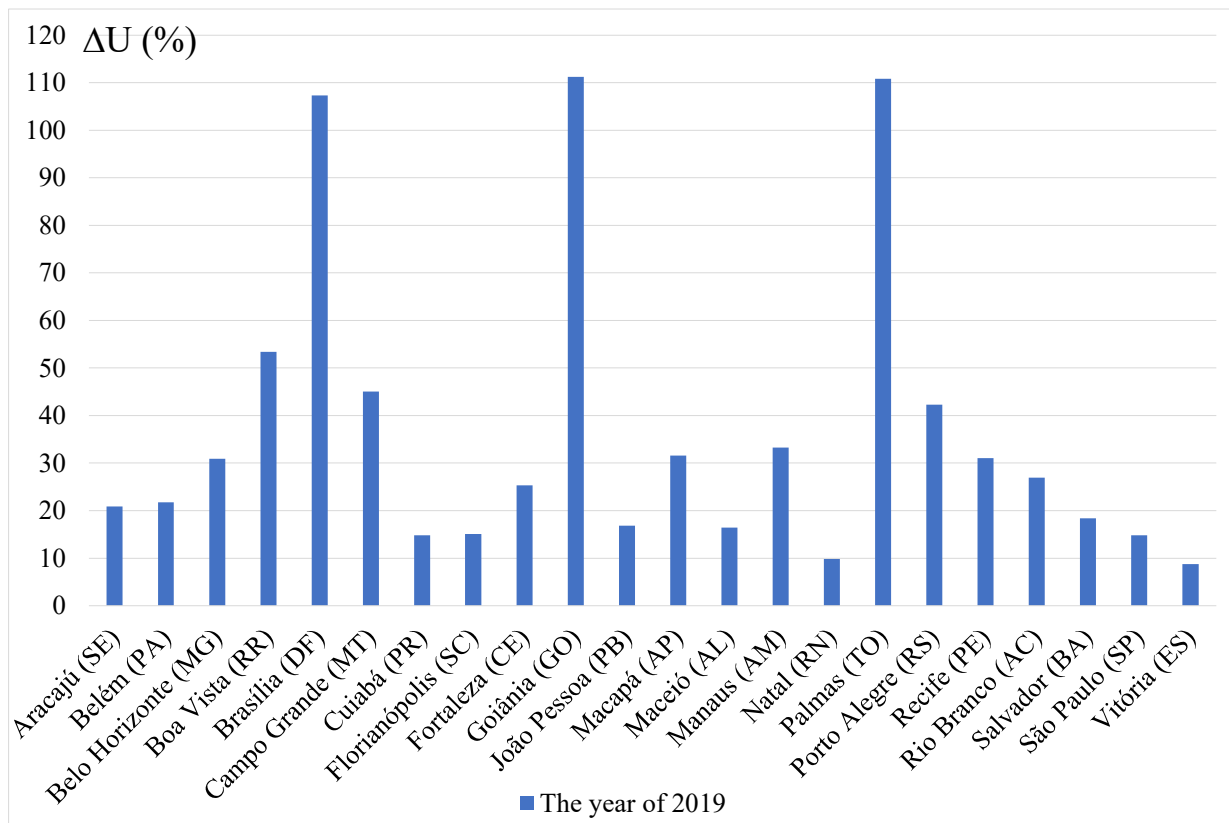

Figure 6 - Humidity variation for the year of 2019 for Brazilian capital cities.

Table 4 - Two-Letter State Abbreviations (in alphabetical order).

| State name	Abbreviation	State name	Abbreviation	State name	Abbreviation
Acre	AC	Mato Grosso	MT	Rio Grande do Norte	RN
Alagoas	AL	Mato Grosso do Sul	MS	Rio Grande do Sul	RS
Amapá	AP	Minas Gerais	MG	Rondônia	RO
Amazonas	AM	Pará	PA	Roraima	RR
Bahia	BA	Paraíba	PB	Santa Catarina	SC
Ceará	CE	Paraná	PR	São Paulo	SP
Espírito Santo	ES	Pernambuco	PE	Sergipe	SE
Goiás	GO	Piauí	PI	Tocantins	TO
Maranhão	MA	Rio de Janeiro	RJ	Distrito Federal	DF
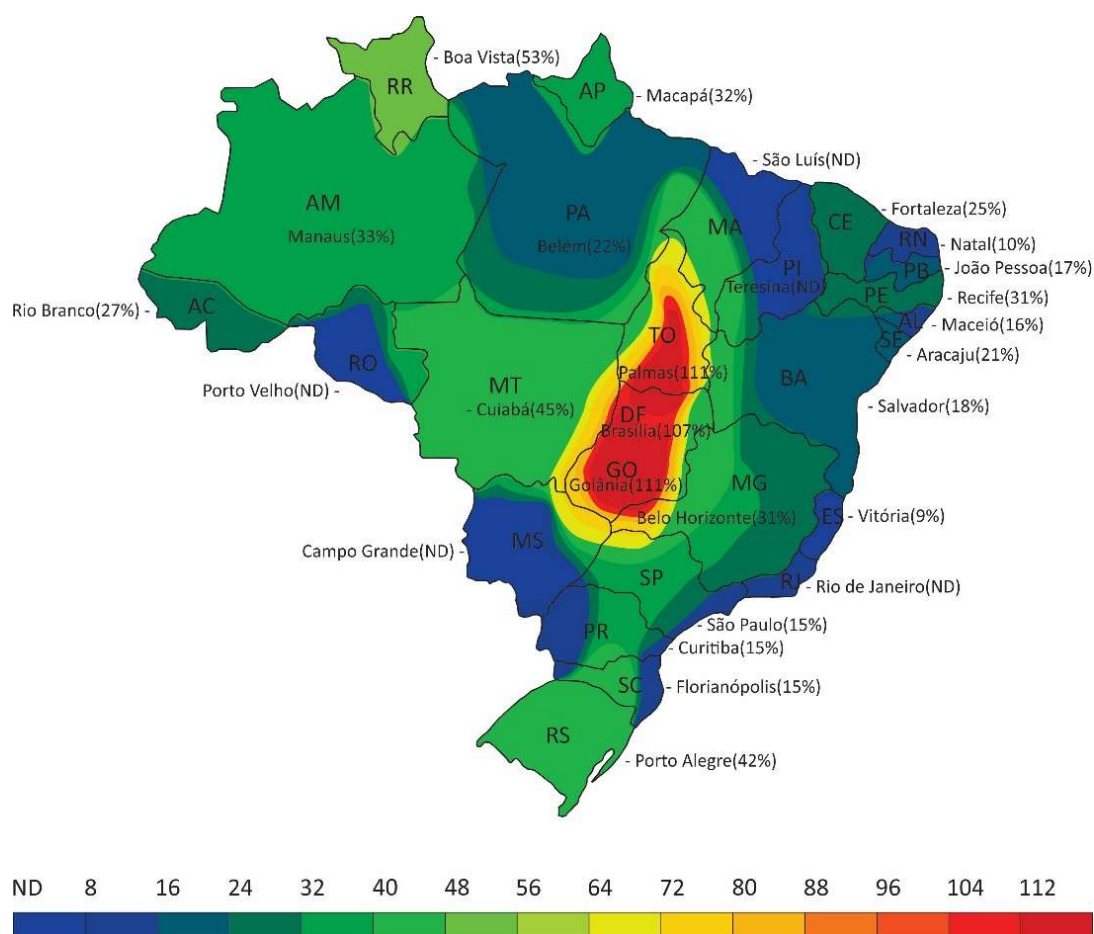
Figure 7 - Brazilian states and capitals with its respective variation of humidity in 2019.

4.11 RESULTS AND DISCUSSIONS

For the analyzed case, the relative environment humidity variations were adopted considering U in the interval of 0% ≤ U ≤ 100%, with increments of 10%, and following criteria from ABNT NBR611829 to consider creep and shrinkage. Figure 8(a) shows the over-time variation of the parameter γ, as can be calculated by Equation (20).

When the relative humidity was lower than 40%, it was assumed γ = 1.022; when U = 100%, γ was considered equal to 30.0, as recommended by the Brazilian code. The ε_{1s} coefficient, taken in order to determine shrinkage, is also dependent on the relative humidity. Figure 8(b) presents ε_{1s} variations for different environment conditions.
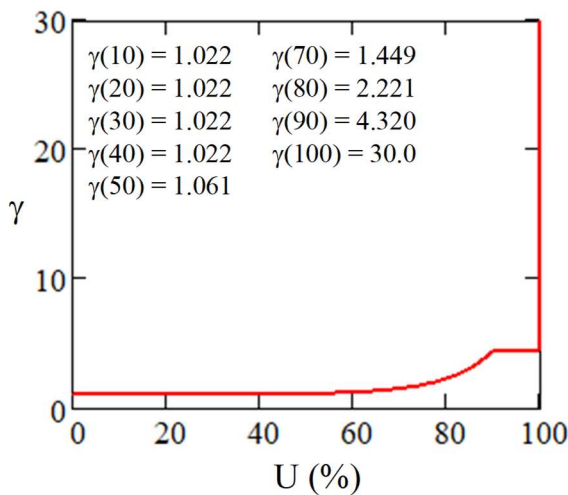
$$\gamma(U) = 1 + e^{(-7.8+0.1U)}$$

(a) Parameter γ Eq.(20)
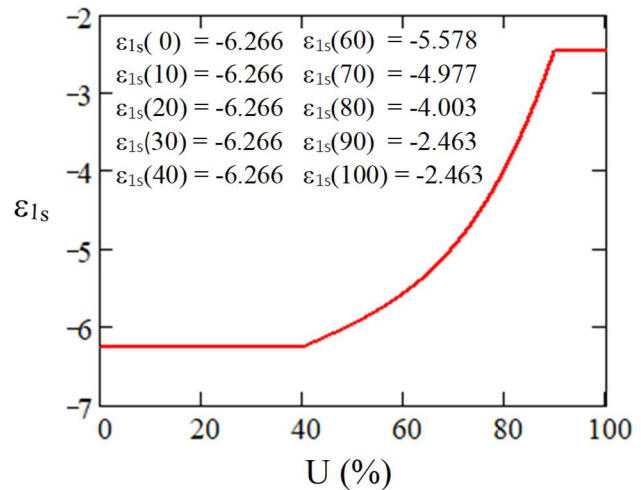
$$\varepsilon_{1s}(U) = \left(-8.09 + \frac{U}{15} - \frac{U^2}{2284} - \frac{U^3}{133765} + \frac{U^4}{7608150} \right) 10^{-4}$$

(b) Coefficient ε_{1s} (29)

Figure 8 - Results of the parameter γ and coefficient e_{1s} by different environment conditions.

The frequency of the structure first vibration mode and its variation with time was computed for relative humidity from 0% to 100%, as can be seen in Figure 9. Frequency variations were investigated considering a time interval of 7500 days, counted from t_0 = 28 days after concrete production, when the structure is initially loaded. In this context, the critical load is determined imposing a null value for the

frequency at different time instants in the structure lifetime. It was possible to observe that a convergency in the load capacity tends to occur around 7500 days, regardless the relative environment humidity. Once the load capacity of the column is found as a function of expected service life of the structure, the parameters for the evaluation of limit states, such as stress and strain, can be analyzed at the desired time instant, considering the suggested safety factors for engineering practical applications.
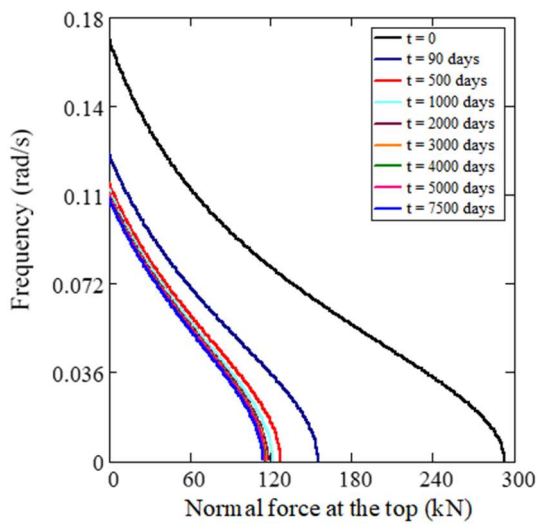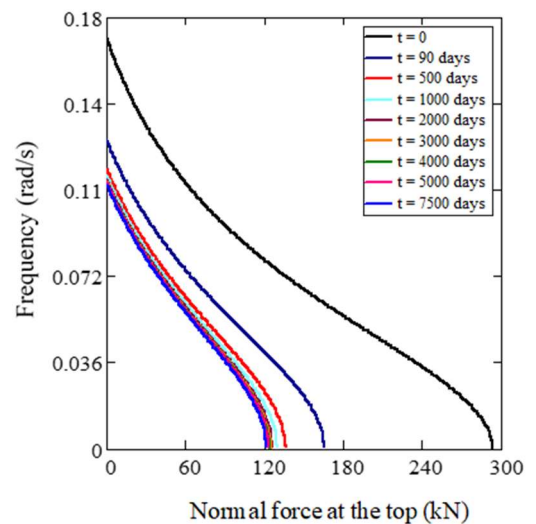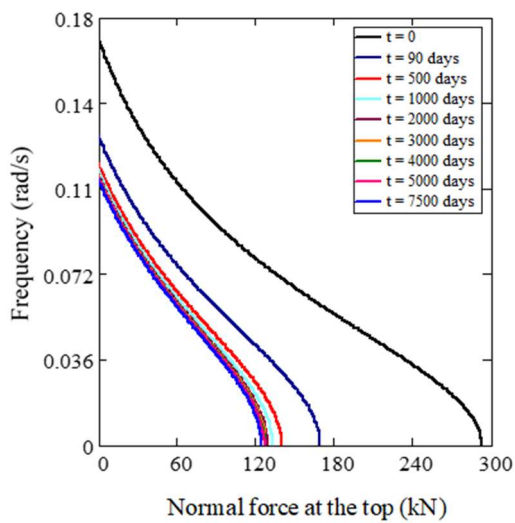

(a) U= 0%
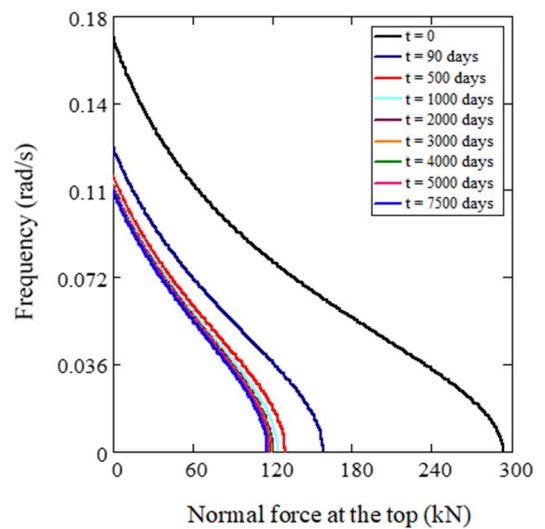
(b) U= 10%
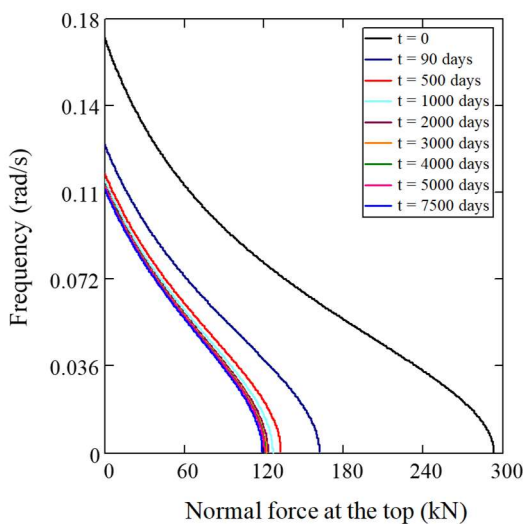
(c) U= 20%

(d) U= 30%

(e) U= 40%
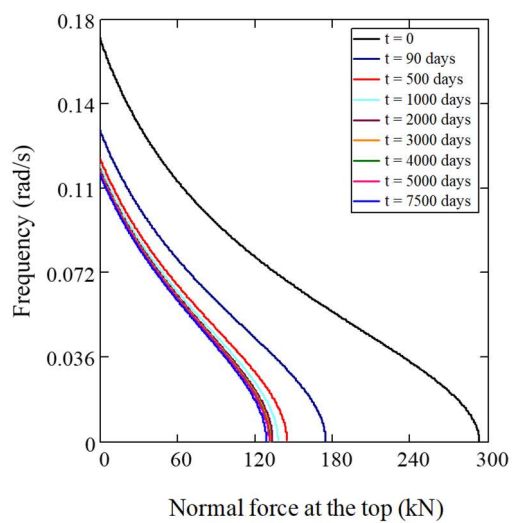
(f) U= 50%
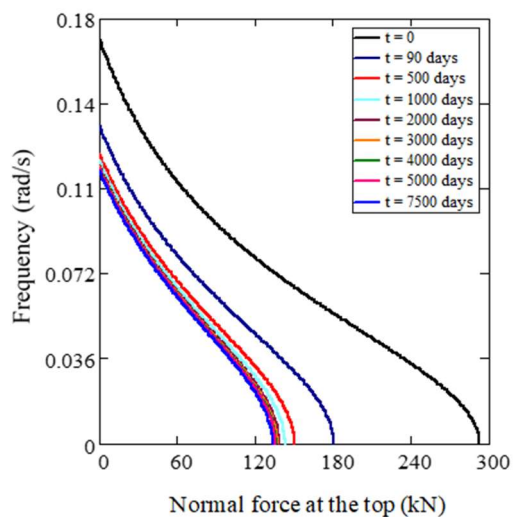
(g) U= 60%
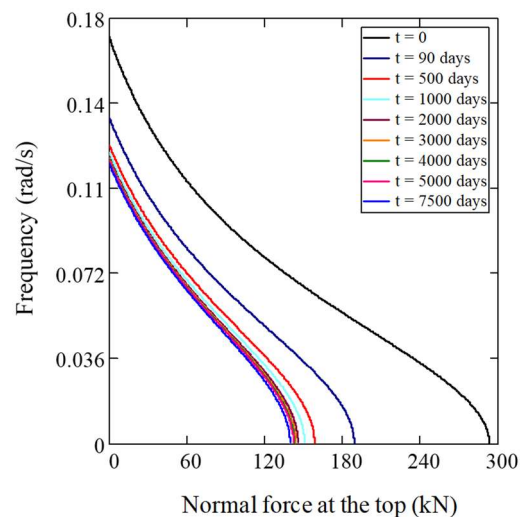
(h) U= 70%
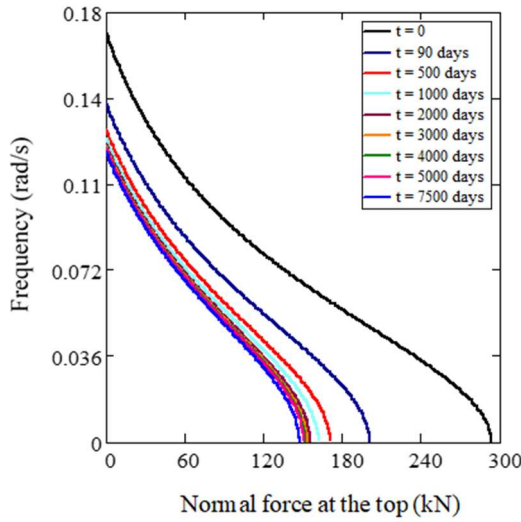
(i) U= 80%
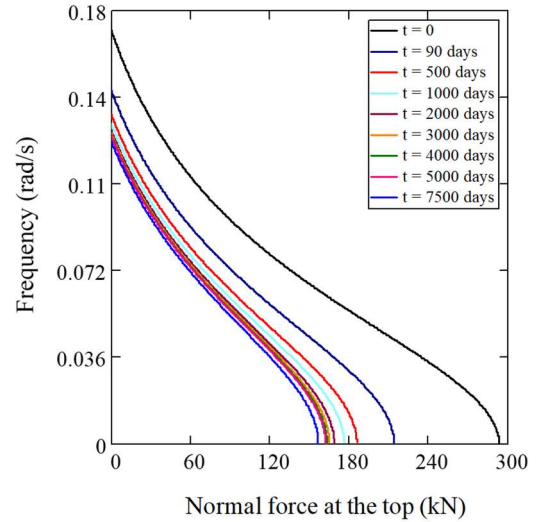
(j) U= 90%
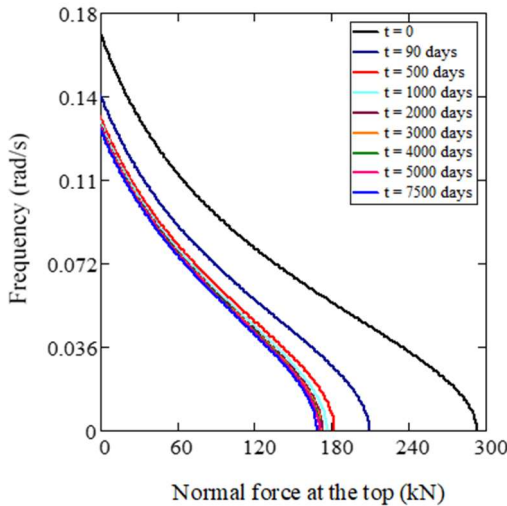
(k) U= 100%

Figure 9 - Structural frequency variation over-time

Critical buckling load variations for different adopted relative humidities can be seen in Table 5, where N_{cr} is the critical buckling load e ΔNcr indicates its variation. Figure 10 presents a bar diagram to visualize the trend of the results. According to the results, it is possible to conclude that as the relative humidity increases, the critical buckling load decreases, after 7500 days of service life of the structure. The greatest variation found in this study happened when the relative environment humidity was 0%, resulting in 60.7% reduction. In parallel, as the relative atmospheric humidity increased, the

critical buckling load variation for t = 0 and t = 7500 days decreased to 42.1%, when U = 100%. The results found in this analysis corroborate previous studies developed by [50]-[51]. For more humid environments, there is a reduction in rheological effects of the material, resulting in a greater load capacity when compared to drier environments.

Table 5 - Obtained results.

t	U = 0%		U = 10%		U = 20%		U = 30%		U = 40%		U = 50%	
	N_{cr}	ΔN_{cr}	N_{cr}	ΔN_{cr}	N_{cr}	ΔN_{cr}	N_{cr}	ΔN_{cr}	N_{cr}	ΔN_{cr}	N_{cr}	ΔN_{cr}
(day)	(kN)	(%)	(kN)	(%)	(kN)	(%)	(kN)	(%)	(kN)	(%)	(kN)	(%)
0	293.4	-	293.4	-	293.4	-	293.4	-	293.4	-	293.4	-
90	155.7	46.9	158.8	45.9	161.9	44.8	165.6	43.6	169.8	42.1	174.8	40.4
500	127.6	18.1	130.2	18.0	132.9	17.9	136.3	17.7	140.1	17.5	144.7	17.2
1000	121.8	4.6	124.3	4.5	126.8	4.6	130.0	4.6	133.6	4.6	137.9	4.7
2000	118.3	2.9	120.6	2.9	123.1	2.9	126.2	2.9	129.7	2.9	133.8	2.9
3000	117.0	1.1	119.3	1.1	121.8	1.1	124.8	1.1	128.2	1.2	132.3	1.1
4000	116.3	0.6	118.6	0.6	121.1	0.6	124.0	0.6	127.4	0.6	131.4	0.7
5000	115.9	0.3	118.2	0.3	120.7	0.3	123.6	0.3	126.9	0.4	130.9	0.4
7500	115.3	0.5	117.6	0.5	120.1	0.5	122.9	0.6	126.3	0.5	130.2	0.5
D (%)		60.7		59.9		59.1		58.1		56.9		55.6

t	U = 60%		U = 70%		U = 80%		U = 90%		U = 100%	
	N_{cr}	ΔN_{cr}	N_{cr}	ΔN_{cr}	N_{cr}	ΔN_{cr}	N_{cr}	ΔN_{cr}	N_{cr}	ΔN_{cr}
(day)	(kN)	(%)	(kN)	(%)	(kN)	(%)	(kN)	(%)	(kN)	(%)
0	293.4	-	293.4	-	293.4	-	293.4	-	293.4	-
90	180.9	38.3	189.2	35.5	200.7	31.6	214.8	26.8	221.1	24.6
500	150.5	16.8	158.6	16.2	170.5	15.0	187.2	12.8	195.2	11.7
1000	143.4	4.7	150.9	4.8	161.8	5.1	177.8	5.0	186.2	4.6
2000	138.9	3.1	145.8	3.4	155.7	3.8	170.2	4.3	178.7	4.0
3000	137.3	1.1	143.9	1.3	153.2	1.6	166.8	2.0	175.3	1.9
4000	136.4	0.7	142.8	0.8	151.8	0.9	164.9	1.1	173.4	1.1
5000	135.9	0.4	142.2	0.4	150.9	0.6	163.7	0.7	172.2	0.7
7500	135.1	0.6	141.3	0.6	149.7	0.8	161.9	1.1	170.3	1.1
D (%)		53.9		51.8		48.9		44.8		41.9

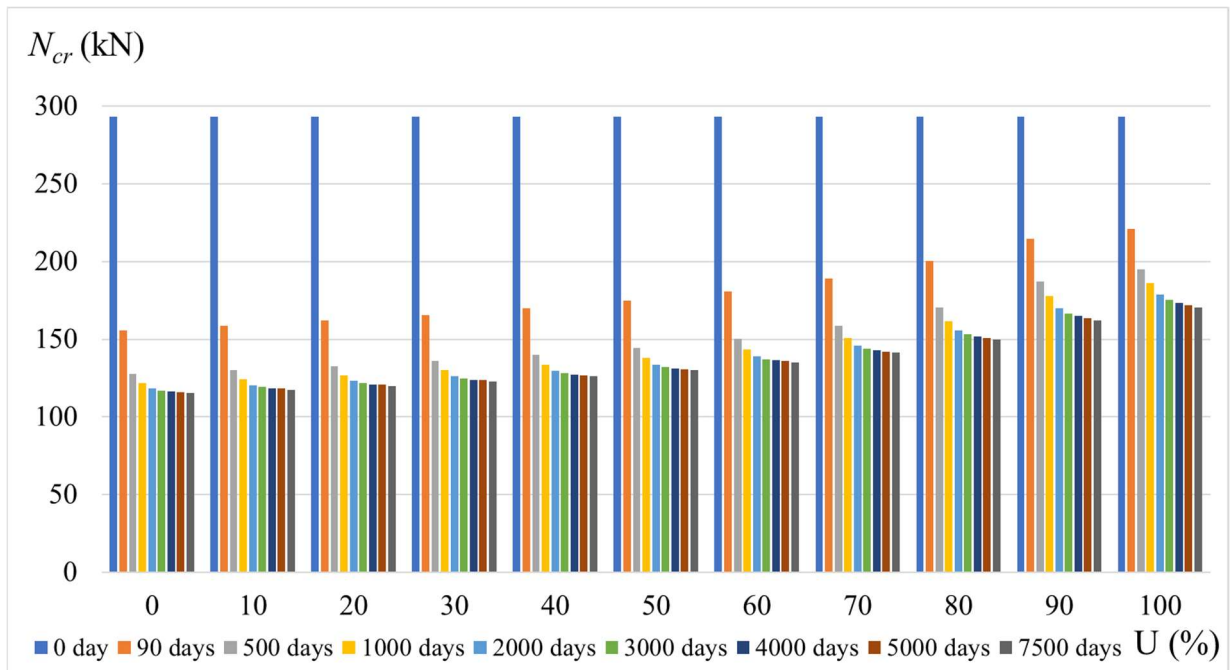Note: N_{cr} = critical buckling load; D = variation

Figure 10 - Critical buckling load for relative humidity and time.

Figure 11 presents critical load variations as a function of relative humidity for different time instants selected for this study.
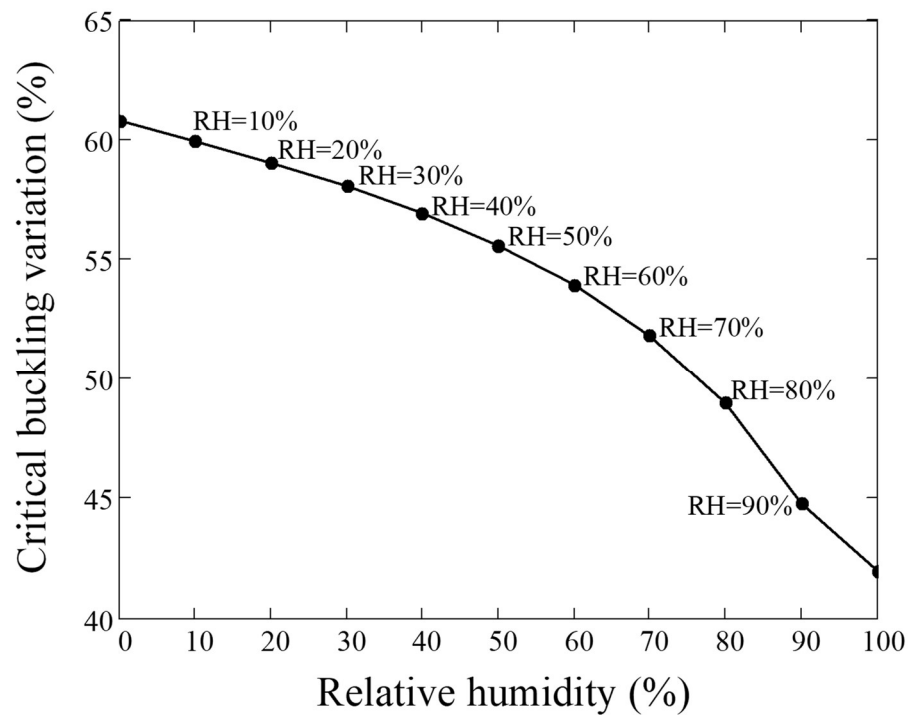

Figure 11 - Critical buckling load variation

It can be noted through Figure 11 that as the atmospheric humidity increases, the critical buckling load of the structure presents a smaller variation over time. In other words, in places with humidity rates greater, the vertical capacity of loading of the system tends to variate less over time than in locals with smaller rates. This result is related to the rheological behavior of concrete, which is caused by the water movement inside the hardened mass. That aspect is potentialized by an environment with low atmospheric humidity because it allows a greater exchangeability of moisture from the concrete to the environment [52]-[56].

4.12 CONCLUSIONS

In this paper, the influence of relative environment humidity on the determination of critical buckling loads was evaluated for a slender column, with cross-section varying along the height, made from reinforced concrete. The analysis took into account all parameters necessary for the calculation, such as: geometric imperfections, material nonlinearity, and rheological properties of concrete. The main conclusions follow:

- Due rheology of concrete, the evaluation of instability of concrete columns must be assessed considering a time-dependent approach. Taking the loading moment as 28 days of concrete production, there are still no creep and shrinkage effects. Therefore, the critical buckling load does not depend on atmospheric humidity.
- For 0% relative humidity, a 60.7% critical buckling load variation occurred after 7500 days, in which the result for this time instant is 32.3% lower than results for 100% relative humidity.
- It is worth mentioning that the failure to comply with the previous conclusion may cause the system to collapse, whether during design stage or when updating the vertical load capacity of the structure, since the critical load increase cannot be bearded by load safety factors.
- The maximum force that could be applied to the column (170.3 kN) refers to 100% relative humidity condition. With the same percentage, the column

presented the lowest load capacity variation after 7500 days in service, i.e., 42.9%.

- According to this study, the most unfavorable condition for the critical buckling load occurs when the relative humidity is near zero. Therefore, when designing the element, this condition should be considered for the location where the structure will be installed.

- Assuming Brazil as a reference, it was possible to verify that two urban centers presented an annual relative humidity variation that reached up to 111%. In a case, this variation was found between a minimum of 34% and a maximum of 72%, and between 39% and 82% for another case. For Brazil, the maximum and minimum relative humidity registered in 2019 were 33.9% and 92.4%.

- Based on the developed analysis, when assessing pre-cast structures that can be installed in any location in a country, it is recommended to adopt the lowest relative environment humidity as a precautionary measure.

- Lastly, it was possible to conclude that the higher the relative humidity, the greater the load capacity of the structure and the lower its variation over time. This outcome happens due to the fact that a low relative environment humidity favors water transport inside the column, affecting concrete creep and shrinkage phenomena, which already was experimentally proven.

- For future studies, a comparison among the results found in this paper and results considering other design codes is suggested. The application of the mathematical model to other structural systems, such as buildings, could also complement the present study.

4.13 REFERENCES

[1]   Mehta PK, and Monteiro PJM. *Concrete microstructure, properties and materials*. 5th ed. McGraw-Hill, New York, 2017.

[2]   Husni R, Benítez A, Manzelli A, Macchi C, Charreau G, Risetto J, Luco LF, Guittelman FN and Morris W. Ações sobre as estruturas de concreto. In: HELENE, P. Manual de reparo, proteção e reforço de estruturas de concreto. (Red Rehabilitar, 2005) p.37-104.

[3]   Benboudjema F, Meftah F and Torrenti JM. Interaction between drying, shrinkage, creep and cracking phenomena in concrete, *Eng. Struct.* 2005, 22, 239-250.

[4]   Acker P and Ulm FJ. Creep and shrinkage of concrete: physical origins and practical measurements, *Nucl. Eng. Des*. 2001,203, 143-158.

[5]   Yuan Y and Wan ZL. Prediction of cracking within early-age concrete due to thermal, drying and creep behavior, *Cem. Concr. Res.* 2002, 32(7),1053-1059.

[6]   Cagnon H, Vidal T, Sellier A, Bourbon X and Camps G. Drying creep in cyclic humidity conditions, *Cem. Concr. Res.* 2015, 76, 91-97.

[7]   Liu W, Zhang S, Sun B and Chen L. Creep characteristics and time-dependent creep model of tunnel lining structure concrete. *Mech. Time-Depend Mater.* 2020, 1-18.

[8]   Marques C, Bittencourt TN and Barbosa MP. Influence of the environment and loading age on SCC drying creep. *Rev. IBRACON Estrut. Mater.* 2013, 6(2), 227-245.

[9]   Troxell GE, Davis RE and Raphael JM. Long–Term Creep and Shrinkage Tests of Plain and RC. In: *Proceedings ASTM*. 1958, 1101-1120.

[10]   Madureira EL and Fontes BVC. Temperature influence on creep of reinforced concrete. *Rev. IBRACON Estrut. Mater.*, 2020, 13(6).

[11]   Shaikh FUA. Effect of cracking on corrosion of steel in concrete. *Int. J. Concr. Struct. M.* 2018,12(1), 3-15.

[12]   Wei Y, Huang J and Liang S. Measurement and modeling concrete creep considering relative humidity effect. *Mech. Time-Depend Mater.*2020, 24, 161–177.

[13]   Rüsch H, Junqwirth D and Hilsdorf HK. *Creep and shrinkage: theirs effect on the behavior of concrete structures*. 1st ed., Springer-Verlag, New York, 1983.

[14]   Bažant ZP and Wang TS. Practical prediction of cyclic humidity effect in creep and shrinkage of concrete. *Mater. Struct.* 1985, 18(1), 247–252.

[15]   Bažant ZP. Prediction of concrete creep and shrinkage: past, present and future. *Nucl. Eng. Des.* 2001, 203(1), 27–38.

[16]   Havlásek P. Creep and shrinkage of concrete subjected to variable environmental conditions. (Thesis, Fakulta stavební, Praha, Tchéquia, 2014).

[17]   Lluka D, Guri M and Cullufi H. Effect of Relative Humidity on Creep and Shrinkage of Concrete According to the European Code for Calculation of Slender Columns. *Int. J. Eng. Res.* 2015, 04(10), 1-7.

[18]   Li P and He S. Effects of Variable Humidity on the Creep Behavior of Concrete and the Long-Term Deflection of RC Beams. *Adv. Civ. Eng.* 2018, 1–12.

[19]   Nastic M, Bentz EC, Kwon OS, Papanikolaou V and Tcherner J. Shrinkage and creep strains of concrete exposed to low relative humidity and high temperature environments, *Nucl. Eng. Des.* 2019, 352(1), 110-154.

[20]   Zhang J, Dongwei H and Wei S. Experimental study on the relationship between shrinkage and interior humidity of concrete at early age. *Cem. Conc. Res.* 2010, 62(3), 191-199.

[21]   Chowdhary P and Sharma RK. Effect of relative humidity on creep-shrinkage behaviour of composite tall buildings. *Lat. Am. J. Sol. Struct.* 2013, 10(3), 571-584.

[22]   Fenollosa E, Cabrera I and Almerich CA. Non-Linear Analysis of Rheological Effects in Slender Composite Columns. *Appl. Mech. Mater.* 2014, 389–395.

[23]   Weng J, Tan KH and Lee CK. Identifying buckling resistance of reinforced concrete columns during inelastic deformation. *Int. J. Struct. Stab. Dyn.* 2020, 20(3), 2050029.

[24]   Sharma MR, Singh AK and Benipal GS. Elastic Stability of Concrete Beam-Columns Part I: Static Stability. *Int. J. Struct. Stab. Dyn.* 2017, 17(01), 1750095.

[25]   Sharma MR, Singh AK and Benipal GS. Elastic Stability of Concrete Beam-Columns Part II: Dynamic Stability. *Int. J. Struct. Stab. Dyn.* 2017, 17(01), 1750095.

[26]   Neville M. *Properties of Concrete*, 5th edition, (Prentice Hall, New Jersey, 2012) American Concrete Institute, Prediction of creep, shrinkage, and temperature effects in concrete structures.

[27]   American Concrete Institute ACI, Prediction of creep, shrinkage, and temperature effects in concrete structures. ACI-209R-08, ACI Committee 209, 2009.

[28]   European Standard. *Eurocode 2: Design of concrete structures - Part 1: General rules and rules for buildings*. EN 1992-1-1, European Committee for Standardisation, Brussels, 2004.

[29]   Brazilian Association of Technical Standards. *NBR 6118: Design of concrete structures – Procedure.* Rio de Janeiro, 2014 (in Portuguese).

[30]   Goel R, Kumar R and Paul DK, Comparative Study of Various Creep and Shrinkage Prediction Models for Concrete. *J. Mater. Civ.* 2007, 19(3), 249–260.

[31]   Wahrhaftig AM, Silva MA and Brasil RMLRF. Analytical determination of the vibration frequencies and buckling loads of slender reinforced concrete towers. *Lat. Am. J. Sol. Struct*. 2019, 16(5), 1–31.

[32]   Wahrhaftig AM, Magalhães KMM and Siqueira GH. Evaluation of limit state of stress and strain of free-fixed columns with variable geometry according to criteria from the Brazilian code for concrete structures. *Lat. Am. J. Sol. Struct*. 2020, 17(1), 1-19.

[33]   Carrion R, Mesquita E and Ansoni JL. Dynamic response of a frame-foundation-soil system: a coupled BEM–FEM procedure and a GPU implementation. *J Braz. Soc. Mech. Sci. Eng*. 2015, 37, 1055–1063.

[34]   Dai K, Lu D, Zhang S, Shi Y, Meng J and Huang Z. Study on the damping ratios of reinforced concrete structures from seismic response records. *Eng. Struct.* 2020, 223, 111-143.

[35]   Tamura Y and Suganuma S. Evaluation of amplitude-dependent damping and natural frequency of buildings during strong winds. *J. Wind. Eng. Ind. Aerod.* 1996, 59(2-3), 115–130.

[36]   Chen MC, Astroza R, Restrepo JI, Conte JP, Hutchinson T and Bock Y. Predominant period and equivalent viscous damping ratio identification for a full-scale building shake table test. *Earthq. Eng. Struct. Dyn.* 2017, 46(14), 2459–2477.

[37]   Miranda CE. Evaluation of Damping Ratios for the Seismic Analysis of Tall Buildings. *J. Struct. Eng.* 2017, 143(1), 04016144.

[38]   Bajurko P and Czarnocki P. Numerical and experimental investigations of embedded delamination growth caused by compressive loading, *J. Theor. App. Mech-Pol.* 2014*,* 52(2), 301–312.

[39]   Calio and Elishakoff I. Closed-Form Trigonometric Solutions for Inhomogeneous Beam-Columns on Elastic Foundation, *Int. J. Struct. Stab. Dyn*. 2004, (4)1, 139–146.

[40]   Reis G, Siqueira GH, Vieira LCM and Ziemian RD. Simplified Approach Based on the Natural Period of Vibration for Considering Second-Order Effects on Reinforced Concrete Frames. *Int. J. Struct. Stab. Dyn.* 2018, 18(5), 1850074.

[41]   Wahrhaftig AM and Brasil RMLRF. Initial undamped resonant frequency of slender structures considering nonlinear geometric effects: The case of a 60.8 m-high mobile phone mast. *J. Braz. Soc. Mech. Sci. Eng.* 2017, 39(3), 725–35.

[42]   Wahrhaftig AM and Brasil RMLRF. Vibration analysis of mobile phone mast system by Rayleigh method. *Appl. Math. Model.* 2017, 42(1), 330–345.

[43]   Wahrhaftig AM, Magalhães KMM and Brasil RMLRF. Updating the bearing capacity, stresses, and strain for retrofitting reinforced concrete towers of the cellular and internet system. *Mech. Based Des. Struc.* 2020, 1–17.

[44]   Wahrhaftig AM, Magalhães KMM and Nascimento LSMSC. Stress assessment in reinforcement for columns with concrete creep and shrinkage through Brazilian technical normative. *J. Braz. Soc. Mech. Sci. Eng.* 2021, 43(6),1-14.

[45]   Brazilian Association of Technical Standards. *NBR 5739: Compression test of cylindrical specimens*, Rio de Janeiro, 2018.

[46]   Brazilian Association of Technical Standards. NBR 16889: Fresh concrete — Slump test. Rio de Janeiro, 2020.

[47]   Instituto Nacional de Meteorologia, Ministério da Agricultura, Pecuária e Abastecimento, INMET, 2019, http://www.inmet.gov.br/portal/.

[48]   Brazilian Panel on Climate Change (PBMC), Scientific basis for climate change, Vol. 1 - First national assessment report, Rio de Janeiro, 2013.

[49]   Instituto Brasileiro de Geografia e Estatística (IBGE), Mapas, Rio de Janeiro, 2020.

[50]   Vandewalle L. Concrete creep and shrinkage at cyclic ambient conditions. *Cem. Concr. Res.* 2000, 22(3), 201–208.

[51]   Nguyen B, Lin WS and Liao WC. Long-Term Creep and Shrinkage Behavior of Concrete-Filled Steel Tube. *Materials* 2021, 14(1).

[52]   Pickett G. The effect of change in moisture content on the creep of concrete under a sustained load. *J. Am. Concr. Inst*. 1942, 38, 333–355.

[53]   Adam I and Taha MMR. Identifying the Significance of Factors Affecting Creep of Concrete: A Probabilistic Analysis of RILEM Database, *Int. J. Concr. Struct. Mater.* 2011, 5(2), 97–111.

[54]   Rossi P, Tailhan JL, Maou FL. Comparison of concrete creep in tension and in compression: influence of concrete age at loading and drying conditions. *Cem. Concr. Res*. 2013, 51(9), 78–84.

[55]   Gao Y, Zhang J, Luosun Y. Shrinkage stress in concrete under dry–wet cycles: an example with concrete column. *Mech. Time-Depend. Mater.* 2013, 18(1), 229–252.

[56]   Cagnon H, Vidal T, Sellier A, Bourbon X and Camps G. Drying creep in cyclic humidity conditions. *Cem. Concr. Res.* 2015, 76, 91–97.

5 GENERAL CONCLUSIONS AND FUTURE WORKS

This study conducted an analytical-mathematical analysis with the purpose of accurately evaluating the load-carrying capacity and deformation behavior of extremely slender reinforced concrete columns. The approach adopted was based on the fundamental principles of the dynamics of deformable solids. The analysis was carried out with careful consideration of the time-dependent rheological behavior of concrete and taking into account various environmental exposure conditions following the application of loads. To achieve this, the analytical model employed incorporated the physical nonlinearity of the material by reducing the flexural stiffness of the concrete and mathematically representing its viscoelastic behavior, strictly following the normative guidelines prescribed by ABNT NBR6118:2014 [12] to accurately predict this phenomenon.

Based on the advancements achieved throughout the research, it was possible to develop and publish two scientific articles in respectable international journals. The first article evaluated, through two distinct analytical-mathematical approaches, the total deformations induced by axial loading to confirm the premise that, within the considered range, Hooke's law is valid and, therefore, there should be no difference between the final deformations obtained by both methods. In the second article, the formulation was applied to a real practical case, assessing the influence of ambient relative humidity on the determination of the critical buckling load over a period of 7500 days following the initiation of loading. In conclusion, important findings were obtained within the context of the two published articles, as described below:

- As evidenced in the publication titled "Strain regime induced by axial compression in slender reinforced concrete columns using different mathematical approaches," it was found that the application of Hooke's Law as an assumption for the linear behavior of deformations is valid in the context of determining the critical buckling load in slender reinforced concrete columns. This validity encompasses the temporal behavior of concrete, taking into account the variation of properties over time.

- The analytical development presented in this research, using the concepts of solid mechanics, has proven to be effective in analyzing elements whose mathematical model can be represented in a one-dimensional manner, such as slender reinforced concrete columns, buildings etc.,

- The maximum difference in total deformations of the investigated structure using the two distinct mathematical approaches, namely the stress-strain curve (normative) of concrete and the method of integrating the differential displacement equations along the length of the structure, was found to be 1.07%. This comparative study of the results indicates a good agreement, thus confirming the validity of Hooke's law for the linear deformation region of the material.

- Despite the minimal difference observed in the comparison of the proposed mathematical methods in this study, it was noted that the equation suggested to describe the relationship between deformation and stress would be more suitable to characterize it as a smooth curve rather than a linear straight line.

- After 3000 days since the structure was put into service, a convergence of deformation results was observed, validating the proposed time period in the conducted analyses, which corresponds to 7500 days. During this interval, it was found that the relative humidity of the environment has a significant impact on the load-carrying capacity of slender reinforced concrete columns. A maximum reduction of 60.7% in load capacity was observed when the relative humidity was 0%, and a reduction of 59.9% was observed when the relative humidity was 10%.

- The results obtained in this research clearly highlight the importance of considering the rheological behavior of concrete when making design predictions for the load-carrying capacity of extremely slender reinforced concrete columns. The structure investigated in this study consisted of a precast reinforced concrete element with potential application in different regions. It was demonstrated that in areas with predominantly humid climates, such as the southern and southeastern regions of Brazil, the analysis becomes more critical due to the effects of the environment.

As suggestions for future work, it would be interesting to incorporate the formulation presented in this study into analyses of buildings, evaluating their behavior in a one-dimensional manner. Additionally, adimensionalizing the analysis in terms of slenderness would be beneficial in order to broaden the applicability of the study. Comparisons with other calculation methods for slender reinforced concrete columns could be included to assess their effectiveness and accuracy. Another improvement would be to conduct experimental tests on slender reinforced concrete columns using strain gauges to compare the numerical results obtained in this investigation with empirical data. This would contribute to validating and enhancing the proposed mathematical analysis.

6 GENERAL REFERENCES

[1]   Euler L. De Curvis Elasticis, Additamentum I to his Methodus Inveniendi Lineas Curvas Maximi Minimive Proprietate Gaudentes. Lausanne and Geneva, 1744.

[2]   Greenhill AG. Determination of the greatest height consistent with stability that a vertical pole or mast can be made, and the greatest height to which a tree of given proportions can grow, Proc Cambridge Philos Soc 1881, 4:65–73.

[3]   Timoshenko SP, Gere JM. Theory of elastic stability, 2nd ed, McGraw-Hill Book Company. New York, 1961.

[4]   Wahrhaftig AM, Magalhães KMM, Brasil RMLRF and Krzysztof M. Evaluation of Mathematical Solutions for the Determination of Buckling of Columns Under Self-weight. J. Vib. Eng. Technol. 2021, 9, 733–749.

[5]   Rayleigh. Theory of Sound. Dover Publications, New York, re-issued, 1877.

[6]   Wahrhaftig AM, Magalhães KMM and Brasil RMLRF. Updating the bearing capacity, stresses, and strain for retrofitting reinforced concrete towers of the cellular and internet system. Mech. Based Des. Struc. 2020, 1–17.

[7]   Wahrhaftig AM, Magalhães KMM and Siqueira GH. Evaluation of limit state of stress and strain of free-fixed columns with variable geometry according to criteria from the Brazilian code for concrete structures. Lat. Am. J. Sol. Struct. 2020, 17(1),1-19.

[8]   Wahrhaftig AM, Magalhães KMM and Nascimento LSMSC. Stress assessment in reinforcement for columns with concrete creep and shrinkage through Brazilian technical normative. J Braz. Soc. Mech. Sci. Eng. 2021, 43, 6.

[9]   Magalhães KMM, Wahrhaftig AM and Brasil RMLRF. Strain regime induced by axial compression in slender reinforced concrete columns using different mathematical approaches. Structures 2023,49,655-665.

[10]   Magalhães KMM, Wahrhaftig AM and Brasil RMLRF. Strain regime induced by axial compression in slender reinforced concrete columns using different mathematical approaches. Structures 2023,49,655-665.

[11]   Wahrhaftig AM, Magalhães KMM, SilvaMA, Brasil RMLRF and J, Banerjee RJ. Buckling and free vibration analysis of non-prismatic columns using optimized shape

functions and Rayleigh method, European Journal of Mechanics - A/Solids. 2022, 94, 104543.

[12]   Brazilian Association of Technical Standards. NBR 6118: Design of concrete structures – Procedure. Rio de Janeiro, 2014 (in Portuguese).

[13]   Brazilian Association of Technical Standards. NBR 16889: Concrete determination of consistency by slump test. Rio de Janeiro, 2014 (in Portuguese).

[14]   Hooke R. LECTURES De Potentia Restitutiva, OR OF SPRING Explaining the Power of Springing Bodies, Printed for John Martyn to the Royal Society, London, UK, 1678.